POLITECNICO DI MILANO

Department of Physics

Physics Engineering

INTEGRATED OPTICS SET-UP FOR PHOTODYNAMIC THERAPY

Supervisors:
Antonio Pifferi
Stefan Andersson-Engels

Co-supervisors:
Johan Axelsson
Johannes Swartling

Master degree work by
Cristina PANTALEONE
Matr. N. 750637

Academic Year 2011-2012

Abstract

Interstitial photodynamic therapy is a local treatment technique for solid cancer, which relies on the simultaneous presence of light, photosensitizer and oxygen. SpectraCure AB has been developing a light delivery system for prostate cancer therapy. The use of this instrument is meant to be extended to other solid tumor treatments such as cancer in the pancreas or the ear, nose and throat tract. The connection between the eighteen light sources and the patient is based on a mechanical switch that enables the system to alternate between treatment mode and monitoring mode. The aim of the project is the development of an all optical passive circuit aimed at replacing the complex mechanical switch. The core part of this alternative system is the possibility to perform measurements on all the eighteen channels during the treatment times, with clear advantages in terms of robustness of the measurements and positive treatment outcome. This feature has been obtained introducing a frequency encoding of each channel. Briefly, each channel is tagged with a characteristic modulation frequency, therefore distinguishable at each detection point from the other channels and from the treatment light. The latter is filtered out to prevent the photodiode saturation. The effective attenuation coefficient μ_{eff} is calculated from the Fourier transform of the signal collected by each channel. The reduction of the fibers core diameter from 400μm to 200μm has been suggested to reduce the costs and the invasiveness of the technique. This aspect has been regarded as plausible according to some tests but it requires further investigation. Satisfying results have been obtained with a test version of the new design, in terms of reliability for the evaluation of μ_{eff}, repeatability of the results and costs. In fact, the system has proved to be able to estimate the value of μ_{eff} with an error of about 6% and a RSD of less than 4%. As conclusion of the work, a set of specifications has been proposed, to be used in the next generation of IPDT instruments.

Abstract

La terapia fotodinamica interstiziale (IPDT) è una tecnica di trattamento locale di masse tumorali. La terapia si basa sulla presenza simultanea di luce, farmaco fotosensibile e ossigeno. SpectraCure AB ha sviluppato un sistema di somministrazione e dosaggio della luce per il trattamento dell'adenocarcinoma prostatico. L'utilizzo di questo macchinario sarà esteso al trattamento di altri tipi di cancro. La connessione tra le diciotto sorgenti laser e il paziente avviene tramite uno switch meccanico che consente di alternare il trattamento alla misura delle proprietà ottiche della ghiandola. Lo scopo di questo lavoro è lo sviluppo di un circuito passivo ottico per rimpiazzare lo switch meccanico. Il cuore di questo sistema alternativo è la possibilità di usare simultaneamente tutti i diciotto canali del sistema sia per le misure che per il trattamento. Questo approccio ha evidenti vantaggi in termini di robustezza della stima dei parametri ed esito positivo della terapia. Questa caratteristica è ottenuta introducendo un sistema di codificazione dei canali. Ogni canale è etichettato mediante una frequenza di modulazione caratteristica che consente di riconoscere il canale di provenienza del segnale in ogni punto del tessuto e di distinguere la luce di monitoraggio da quella di terapia, la quale è eliminata mediante filtraggio per evitare la saturazione del fotodiodo. Il valore del coefficiente effettivo di attenuazione μ_{eff} è ottenuto calcolando la trasformata di Fourier del segnale ad ogni canale. Ho suggerito di ridurre il diametro delle fibre ottiche da 400 μm a 200 μm in modo da ridurre costi e invasività del trattamento. Test indicano che questa scelta è plausibile, andrebbe tuttavia indagata ulteriormente. Con questo design, sono stati ottenuti risultati soddisfacenti in termini di affidabilità della stima di μ_{eff}, ripetibilità delle misure e costi. Infatti il sistema ha dimostrato di essere in grado di stimare il valore di μ_{eff} con un errore relativo medio del 6% e una RSD media di circa 4%. A conclusione del lavoro, è stata proposta una serie di specifiche che potrà essere utilizzata per la nuova generazione di strumentazione per IPDT.

Populärvetenskaplig sammanfattning

Cancer är en av de vanligaste dödsorsakerna hos västerlänningar. Prostatacancer i sig utgör den näst vanligaste tumören hos män över hela världen. I två tredjedelar av fallen är prostatacancer inte livshotande. Den sista tredjedelen kan botas fullständigt förutom om metastaserna sprids för långt ifrån körteln till resten av kroppen. Den här formen av tumörer är lämplig för fotodynamisk terapi (PDT).

PDT är en lokal behandlingsmetod som förlitar sig på att ljus och läkemedel är närvarande samtidigt. Läkemedlet, som kallas fotosensibiliserare, är ljuskänsligt och aktiveras genom interaktion med ljus i en specifik våglängd. Ifall denna metod används för cancerbehandling, angriper läkermedlet nästan aldrig tumörcellerna direkt, utan den överför energin till molekylärt syre, vilket skapar syreradikaler. Syreradikalerna, i sin tur, dödar cellerna.

Interstitiell fotodynamisk terapi (IPDT) används för att behandla solida tumörer, såsom prostatacancer. De optiska fibrerna placeras inne i tumörmassan, dit läkemedlet tidigare har levererats, och på så vis kureras cancern utan invasiv kirurgi. Det finns många fördelar med IPDT: den är selektiv på grund av den selektiva upptagningen av fotosensibiliseraren och ljusets lokala administrering, den är minimalt invasiv och joniserande strålningar behövs inte. Därmed kan den användas i alla de fall där klassisk strålbehandling inte längre är applicerbar.

PDT kan kanske komma att vara den primära cancerbehandlingsmetoden tack vare sin selektivitet och effektivitet.

SpectraCure AB har utvecklat ett system för att administrera ljus till prostatacancerbehandling och har påvisats vara effektiv mot tumörer. Detta har påvisats både med ultraljud och genom övervakning av PSA-värden (Prostate Specific Antigen) hos patienterna. Systemet ska användas för behandling av andra solida tumörer inom en snar framtid.

Kopplingen mellan ljuskällorna och patienten grundas i en mekanisk switch som gör det möjlig att växla mellan behandling och övervakning. Den mekaniska switchen är komplex, stor och väldigt dyr; för att inte tala om att den kan råka ut för allvarliga mekaniska problem på grund av

sin komplicerade mekanik. Därför är designen av en optisk passiv bana, som syftar till att ersätta den mekaniska switchen, det första och viktigaste steget mot utvecklingen av en ny generation IPDT-instrument.

Kärnan i detta alternativa system är att det möljgör för att genomföra mätningarna och behandlingen genom alla optiska kanalerna samtidigt. Denna funktionalitet har uppnåtts med hjälp av frekvenskodning för varje kanal. Enkelt beskrivet märks varje kanal med en karaktäristisk modulationsfrekvens, så att de kan skiljas både från behandlingsljuset och de andra kanalerna i varje mätpunkt. Fördelen är så klart att mätningarna av ljusets attenuering är robustare. Därmed kan terapin kontrolleras bättre, både med avseende på ljusdosimetri och övervakning av behandlingsprocessen, vilket hjälper till att förbättra behandlingsresultaten.

Riassunto

Scopo del progetto

Lo scopo del lavoro è lo sviluppo di un circuito passivo interamente ottico per la sostituzione di uno switch meccanico che attualmente costituisce il cuore di un macchinario per la terapia fotodinamica interstiziale dell'azienda SpectraCure AB. Il design è stato realizzato con l'ulteriore obbiettivo di migliorare la qualità delle misure effettuabili dalla strumentazione rispetto a quelle ottenibili dal set-up attuale, tenendo inoltre presenti gli aspetti di funzionalità e flessibilità rispetto a possibili cambiamenti futuri del circuito nonché economici di realizzazione.

Introduzione

L'utilizzo delle sorgenti di luce per il trattamento di alcune malattie, soprattutto cutanee, è una tendenza sempre più diffusa in medicina. È possibile pensare per esempio al trattamento dell'ittero neonatale, che è curato stimolando l'eliminazione della bilirubina in eccesso mediante l'esposizione del bambino ad una sorgente di luce blu; a quello della psoriasi, in cui l'eccessiva produzione di cellule epiteliali è bloccata tramite l'interazione di un farmaco a somministrazione topica con luce ultravioletta; o a quello del distacco della retina, il quale è trattato utilizzando luce laser nella parte verde dello spettro che agisce da coagulante. Come in ogni altro campo, i laser costituiscono una categoria speciale di sorgenti luminose grazie alle loro peculiari caratteristiche di controllo e precisione. Infatti, regolando il fascio laser termini di potenza, localizzazione del punto di fuoco e lunghezza d'onda è possibile utilizzare questi dispositivi in molti modi, ad esempio per tagliare i tessuti in sostituzione del bisturi, bruciarli al posto dell'azoto liquido oppure come agenti coagulanti. Per merito di questa grande versatilità, l'utilizzo dei laser è attualmente diffuso nella maggior parte dei campi medici: angioplastica, estetica, chirurgia, imaging, dermatologia e molti altri. In oncologia, i laser sono utilizzati principalmente per la localizzazione e il trattamento dei tessuti tumorali con tecniche quali, ad esempio, la terapia fotodinamica (PDT). Questo tipo di terapia, allo stato dell'arte, è in uso come normale pratica clinica soprattutto per la cura dei tumori cutanei e subcutanei non estesi; l'applicazione di questa tecnica per il trattamento di altri tipi di cancro quali tumori al cervello, alla vescica o al seno, è in via di sviluppo e, in alcuni casi, anche in stadio avanzato di test clinici su persone.

La terapia fotodinamica, come tutte le altre tecniche ottiche, si basa sull'interazione della luce

con i tessuti biologici. In questo tipo di tessuti, la propagazione della luce è determinata principalmente dalle proprietà di assorbimento e diffusione dei materiali biologici, i quali sono classificati come materiali altamente diffusivi. Questa caratteristica consente, da un lato, di utilizzare la luce come sonda per la determinazione delle caratteristiche del tessuto e dall'altro di modificare i tessuti stessi. Infatti, grazie a questa forte interazione i tessuti e le caratteristiche del fascio di luce si modificano vicendevolmente. Le tecniche ottiche possono essere utilizzate, quindi, sia come strumento di diagnosi, utilizzando laser a bassa potenza, che come strumento di terapia, con laser a potenza relativamente alta. Entrambe queste opzioni sono generalmente utilizzate durante una sessione di trattamento mediante PDT. Queste tecniche risultano particolarmente attraenti in quanto sono in grado di ottenere risultati soddisfacenti in termini di capacità diagnostiche, guarigione, estetica delle ferite nonché sicurezza del paziente sia durante la diagnosi che durante la terapia. Le tecniche ottiche, infatti, sono non-mutagene in quanto non utilizzano radiazioni ionizzanti ma luce principalmente nello spettro del visibile e dell'infrarosso.

Terapia fotodinamica (PDT)

La terapia fotodinamica è una tecnica ottica utilizzata per il trattamento locale di alcune patologie, tra cui il cancro. Questo tipo di terapia è basato sull'attivazione di un farmaco fotosensibile mediante luce alla lunghezza d'onda d'eccitazione caratteristica del tipo specifico di farmaco. Questo, precedentemente somministrato per via orale o endovenosa, è generalmente assorbito in modo selettivo dal tessuto obiettivo ed è inerte qualora il tessuto non sia illuminato da luce alla giusta lunghezza d'onda. La terapia fotodinamica risulta così un metodo altamente selettivo in quanto la zona trattata è controllata sia mediante l'assorbimento del farmaco che mediante la somministrazione locale della radiazione. La morte cellulare non è, in generale, causata direttamente dal fotosensibilizzante. Al contrario, lo stato eccitato di quest'ultimo trasferisce energia all'ossigeno molecolare il quale è capace di formare radicali liberi, in particolare specie reattive dell'ossigeno (ROS), le quali uccidono le cellule all'interno del tessuto. I fattori principali per il successo della terapia sono quindi un'adeguata ossigenazione del tessuto obiettivo e un'appropriata dosimetria sia del farmaco che della luce. Per questo motivo, il monitoraggio della terapia e delle proprietà ottiche del tessuto sono di fondamentale importanza per la riuscita del trattamento e per proteggere l'integrità dei tessuti circostanti la zona da trattare, in particolare se localizzata in un punto delicato del corpo e di volume consistente, dell'ordine di qualche centimetro quadro.

Un tipo particolare di PDT è la terapia fotodinamica interstiziale (IPDT) che consente il trattamento di tumori subcutanei, anche voluminosi. La luce è somministrata mediante fibre ottiche posizionate direttamente all'interno del tessuto tumorale utilizzando aghi per la biopsia. Alcuni esempi di tumori trattabili con questa tecnica sono il cancro al seno, che è stato causa durante il 2007 della morte di 12050 donne solo in Italia, e quello alla prostata, che è tra i tumori più diffusi

tra la popolazione maschile mondiale. Quest'ultimo, che si sviluppa direttamente nella ghiandola, è pericoloso per la vita del paziente solo in un terzo dei casi ed è inoltre quasi sempre completamente curabile qualora diagnosticato in tempo, il che significa a meno che le metastasi non siano già diffuse in tutto il corpo.

In Svezia, l'azienda SpectraCure AB ha sviluppato un macchinario per il trattamento del cancro alla prostata con questo tipo di terapia. Durante questa terapia la prostata viene totalmente trattata adattando il dosaggio della luce durante il trattamento stesso facendo attenzione a non danneggiare gli organi sensibili circostanti, quali il retto, l'uretra e la vescica. La somministrazione della luce avviene mediante un complesso switch meccanico che consente di alternare la terapia al monitoraggio delle proprietà ottiche della ghiandola, in modo da avere la possibilità di modificare, eventualmente, il dosaggio della luce in base ai risultati delle misure. In pratica, durante la terapia lo switch accoppia le sorgenti laser a tutte le fibre ottiche connesse al paziente, mentre durante monitoraggio un solo canale è utilizzato come sorgente e i sei canali adiacenti sono usati come ricevitori per effettuare misure a diverse distanze dal punto sorgente. Il monitoraggio termina quando ognuno dei diciotto canali è stato utilizzato come sorgente. Questo approccio è limitato, da un lato, dalla natura meccanica dello switch che potrebbe ad esempio non essere allineato correttamente per l'accoppiamento, e dall'altro dai ristretti tempi in cui è possiblie effettuare le misure. Infatti, il tempo totale in cui il paziente può essere sottoposto a questo tipo di terapia è di circa quattro ore, il che implica che i tempi utili per il monitoraggio sono estremamente ristretti in quanto il tempo effettivo di trattamento non può essere ridotto. Il lavoro di questa tesi ha come obiettivo la sostituzione di tale switch mediante il design di un circuito ottico passivo che, tra le altre cose, compensi queste inefficienze dello switch meccanico.

Modello dell'interazione della luce con i tessuti

Il modello che è generalmente adottato per descrivere l'interazione della luce con i materiali altamente diffusivi è il trasferimento radiativo. Questo modello particolare considera la radiazione come un insieme di particelle che si muovono all'interno del mezzo. Matematicamente, la teoria del trasporto è basata sull'equazione del trasporto radiativo, secondo cui la propagazione della luce può essere descritta in termini di bilancio energetico. Se si assume di avere una sorgente di luce monocromatica, l'equazione risulta

$$\frac{1}{v}\frac{\partial}{\partial t}L(\mathbf{r},\mathbf{\Omega},t) \; + \; \mathbf{\Omega}\cdot\nabla L(\mathbf{r},\mathbf{\Omega},t) \; + \; [\mu_a(\mathbf{r}) \; + \; \mu_s(\mathbf{r})]L(\mathbf{r},\mathbf{\Omega},t)$$
$$= \int_{4\pi} L(\mathbf{r},\mathbf{\Omega}',t)\mu_s(\mathbf{r},\mathbf{\Omega}'\rightarrow\mathbf{\Omega},t)d\mathbf{\Omega}' \; + \; S(\mathbf{r},\mathbf{\Omega},t)$$

dove $L(\mathbf{r},\mathbf{\Omega},t)$ è la radianza [$Wm^{-2}sr^{-1}$], μ_a e μ_S sono rispettivamente i coefficienti di assorbimento e scattering, v la velocità di propagazione della luce nel mezzo e $\mathbf{r}$, $\mathbf{\Omega}$ e t sono rispettivamente la posizione, la direzione del fotone e il tempo. Introducendo alcune ipotesi, questa equazione può essere risolta analiticamente o numericamente in alcuni casi specifici.

L'approccio più semplice è quello di adottare l'approssimazione di diffusione in cui si assume che il coefficiente di scattering sia molto maggiore di quello di assorbimento, $\mu_s \gg \mu_a$, ossia che il mezzo sia altamente diffusivo. Sotto questa ipotesi, l'equazione del trasporto radiativo diventa l'equazione di diffusione in cui il trasferimento radiativo è espresso in termini di fluenza

$$\Phi(\mathbf{r}, t) \; = \; \int_{4\pi} L(\mathbf{r}, \mathbf{\Omega}', t) d\mathbf{\Omega}'$$

L'equazione di diffusione può essere risolta analiticamente assumendo che il mezzo sia otticamente omogeneo, altrimenti è necessario ricorrere a metodi numerici, come ad esempio il metodo degli elementi finiti. Questi metodi sono in grado di modellizzare materiali otticamente non omogenei. La soluzione dell'equazione di diffusione utilizzata in questo progetto è ottenuta assumendo di avere una sorgente puntiforme modulata a una frequenza molto pù piccola della frequenza degli eventi di scattering, in un mezzo infinito e in stato stazionario

$$\Phi(r) = \frac{P_0}{4\pi D r} \exp(-\mu_{eff} r)$$

dove $\mu_{eff} \; = \; \sqrt{3\mu_a(\mu_a + \mu_s')}$ è il coefficiente effettivo di attenuazione, P_0 è la potenza della sorgente e $D = 1/\mu_{eff}$ è il coefficiente di diffusione. L'espressione utilizzata per la valutazione della capacità del sistema di stimare il valore di μ_{eff} secondo il modello qui presentato è il logaritmo dell'equazione precedente

$$-ln(r\Phi(r)) \; = \; \mu_{eff} r - ln\left(\frac{P_0}{4\pi D}\right)$$

in quanto più facilmente valutabile in termini di comportamento, in particolare di linearità delle misure rispetto ai parametri ottici dei campioni e alla distanza del punto di misurazione dalla sorgente.

Un modo alternativo per risolvere l'equazione del trasporto radiativo è quello di utilizzare i metodi Monte Carlo. Questi sono metodi statistici che prevedono la simulazione della propagazione di un numero statisticamente significativo di fotoni in modo da seguirne idealmente il percorso ed ottenere mappe di statistiche riguardanti il loro comportamento in termini di assorbimento e scattering. Nella realtà, queste simulazioni non seguono il percorso di ogni singolo fotone ma di un pacchetto di fotoni in modo da ottimizzare la computazione in termini di tempo. A ciascun pacchetto è assegnato un determinato peso, parte del quale è perso ad ogni evento di scattering, a rappresentare l'assorbimento di un certo numero di fotoni del pacchetto nella posizione del punto di scattering. Le proprietà ottiche del mezzo sono espresse in termini di probabilità di assorbimento e scattering in ogni punto della mappa. Il programma Monte Carlo for Multi-Layered media (MCML) di Jacques *et al.* è stato leggermente modificato in modo da adattare le simulazioni allo scopo per cui sono state usate in questo progetto. In particolare, è stata introdotta una condizione per considerare l'effetto dell'apertura numerica della fibra alla superficie di separazione tra lo strato rappresentante la prostata, generico materiale diffusivo con le stesse proprietà ottiche, e il materiale all'esterno, cioè la fibra.

Entrambe queste rappresentazioni sono state utilizzate per valutare diversi aspetti del circuito ottico proposto in sostituzione dello switch meccanico.

Circuito ottico

Il circuito ottico è basato su un singolo modulo, il canale, il quale è ripetuto diciotto volte in modo da avere diciotto diverse sorgenti, analogamente a come avviene nel sistema attuale. La connessione tra le sorgenti, i detector e il paziente è completamente passiva, il che significa, tra le altre cose, che non sono richiesti né calibrazione né driver per il collegamento.

Il singolo canale è costituito da tre parti: una di sorgenti, una di rilevazione e una di collegamento. Il collegamento è costituito da un semplice splitter ottico 1x2 con efficienza di accoppiamento 1:99 per massimizzare l'efficienza di accoppiamento verso i detector, e un core di 200 μm di diametro. La riduzione del core della fibra da 400 μm a 200 μm è una delle novità introdotte da me con questo design. Data la semplicità di questo componente, il principio di funzionamento è relativamente elementare: la somministrazione della radiazione avviene lanciando la luce in uno dei rami dello splitter ottico, quello con più bassa efficienza di accoppiamento, mentre la rilevazione del segnale dal lato del paziente avviene raccogliendo la luce dalla terminazione comune verso l'altro ramo dello splitter a cui è collegato il fotodiodo.

Le sorgenti laser sono due diodi laser. Questi tipi di laser sono infatti facili da modulare, adatti all'ambiente clinico, economici e compatti. Il primo laser, quello per la terapia, ha una lunghezza d'onda di 690 nm e una potenza di 150 mW mentre il secondo, utilizzato per il monitoraggio del coefficiente effettivo di attenuazione, ha una lunghezza d'onda di 730 nm e una potenza tale da somministrare nel tessuto luce con una potenza di picco di 30 mW. Il motivo dietro la scelta di questa specifica lunghezza d'onda è, da un lato, la separazione spettrale dalla componente a 690 nm dei laser di terapia, per consentire un buon filtraggio ottico del segnale, dall'altro la sufficiente vicinanza alla lunghezza d'onda di emissione di fluorescenza del farmaco, 710 nm, in modo che la luce di monitoraggio e quella di emissione abbiano approssimativamente le stesse proprietà ottiche. L'idea iniziale era quella di avere un laser di monitoraggio ad una lunghezza d'onda che fosse esattamente la stessa di quella di emissione del farmaco ma per limitazioni tecniche dovute all'incertezza nella lunghezza d'onda d'emissione reale del diodo, si è preferito adottare una soluzione di questo genere. La sorgente di monitoraggio è modulata in frequenza in modo da etichettare ogni singolo canale mediante una frequenza di modulazione caratteristica, la quale consente di distinguere la luce proveniente da ogni singolo laser, e quindi da ogni canale, in ciascun punto del campione. La modulazione è ottenuta con un'unica PCI DAQ a 32 uscite analogiche, e permette inoltre di distinguere il segnale utilizzabile per il monitoraggio delle proprietà ottiche da quello proveniente dai laser per la terapia. Questo sistema di etichettatura consente di misurare le proprietà ottiche del tessuto durante il trattamento, usando contemporaneamente tutti i canali sia come sorgenti che come punti di rilevazione, permettendo quindi

misure più veloci e robuste in quanto queste risultano effettuabili durante tutto il tempo della sessione di terapia, senza interruzioni non necessarie del trattamento stesso. Le due sorgenti laser sono connesse allo splitter principale da un normale splitter 1x2 bilanciato con diametro del core standard 65, 100 o 125 μm a seconda della fibra accoppiata all'uscita dei laser e delle disponibilità sul mercato. La connessione dello splitter principale con le sorgenti è anch'essa modulare. Qualora fosse necessario aggiungere altre sorgenti per effettuare altri tipi di misure, come ad esempio il monitoraggio del livello di ossigenazione dei tessuti, è sufficiente sostituire lo splitter 1x2 con uno 1xM, dove M è il numero di sorgenti necessarie alla specifica applicazione, o con una semplice cascata di splitter 1x2 a patto di regolare la potenza in uscita dai laser in modo da compensare per le ulteriori perdite introdotte. Inoltre sono da considerare eventuali complicanze nella parte di rilevazione, che saranno spiegate in seguito.

La parte di rilevazione è ottenuta concatenando un filtro passa alto con lunghezza d'onda di cut-off di 700 nm e trasmissione in banda superiore all'80% in banda e approssimativamente nulla fuori banda, e un fotodiodo con ampia area sensibile, un tempo di salita dell'ordine di qualche decina di nanosecondi e range dinamico di circa 0.3 μW alla lunghezza d'onda di 730 nm. Il filtro è necessario per eliminare la componente di luce di terapia in modo da evitare la saturazione del fotodiodo. I diciotto fotodiodi, uno per ciascun canale, sono connessi ad altre tre PCI DAQ, ciascuna a otto entrate analogiche differenziali. Una volta registrato il segnale, il suo spettro è calcolato in ogni punto in modo da ottenere dati a diverse distanze per ogni canale e calcolare il valore di μ_{eff} interpolando la serie di misure ottenute per ciascuna frequenza di modulazione. L'interpolazione è lineare e il coefficiente effettivo di attenuazione corrisponde al coefficiente angolare della retta. Qualora un numero maggiore di sorgenti di monitoraggio siano introdotte, è necessario apportare alcune modifiche a questa parte del sistema. Una possibilità sarebbe avere più di una frequenza di modulazione associata ad ogni canale in modo da poter distinguere le diverse sorgenti utilizzando gli stessi fotodiodi, altrimenti questi andrebbero sostituiti con spettrometri, come nel sistema attualmente in uso, a scapito ovviamente dei costi.

Per motivi di tempo ed economici è stato deciso di utilizzare un set-up modificato per la validazione del sistema. La differenza principali consiste nel fatto di aver diviso gli esperimenti riguardati il filtraggio ottico da quelli per valutare l'efficienza di estimazione del valore di μ_{eff} utilizzando contemporaneamente più di un canale sorgente. Questi ultimi sono stati effettuati rimuovendo le sorgenti sul canale usato per la rilevazione in modo da ridurre il rumore dovuto alle riflessioni della luce di terapia nel canale stesso e riducendo la potenza delle altre due sorgenti di terapia a 3 mW. Inoltre è stato utilizzato un filtro passa banda. Questo filtro ha una lunghezza d'onda centrale di 730 nm e trasmissione di picco del solo 60%, al posto del filtro passa alto proposto in quanto era disponibile in laboratorio. Questi cambiamenti non sono stati ritenuti sostanziali rispetto alle quantità da misurare quindi i risultati che sono stati ottenuti sono stati ritenuti completamente validi e trasferibili al sistema qui descritto. Ovviamente, tale sistema dovrà essere

propriamente testato quando fondi e tempo lo consentiranno.
Le DAQ utilizzate in questo progetto, diverse da quelle proposte nel design finale, sono state interfacciate mediante un programma Labview in grado, da un lato di generare il segnale di modulazione e dall'altro di registrare e analizzare spettralmente il segnale ricevuto.
Oltre a queste misure principali, alcuni semplici esperimenti secondari e simulazioni sono stati effettuati per valutare la possibilità di ridurre il diametro del core dello splitter principale da 400μm, diametro del core delle fibre utilizzate nel sistema attuale, a 200μm.

Risultati

Le diverse parti del circuito sono state testate in modo da verificarne il corretto funzionamento. Nel complesso, il sistema si è rivelato affidabile, efficace e robusto nella stima del coefficiente effettivo di attenuazione nonché relativamente economico. Infatti, la stima dei costi per la realizzazione di un circuito completo di questo tipo è di circa 31000 €, quindi approssimativamente 1800 € per canale, includendo tutte le componenti suggerite nel capitolo conclusivo.
Gli esperimenti per valutare qualora potesse essere vantaggioso ridurre il diametro del core dello switch ottico principale non hanno dato risultati rilevanti. L'ipotesi iniziale era che fibre con diametri di 400 μm e 200 μm potessero avere approssimativamente la stessa efficienza di collezione in quanto si era supposto che fibre con diametro comparabile avessero approssimativamente lo stesso cono di raccolta. Questa ipotesi è stata provata soltanto in parte. Infatti, si è rivelata vera nel caso in cui la luce si propaghi in un mezzo con proprietà ottiche simili all'aria ma non nel caso in cui la propagazione avvenga in un mezzo torbido con una profondità di penetrazione della luce limitata, come nel caso dei tessuti biologici. Nonostante questo risultato, la scelta di avere fibre più piccole è stata mantenuta in quanto, nel caso le misure siano invasive, c'è da considerare l'effetto dell'accumulo del sangue alla punta della fibra dovuto alla presenza dell'ago nel tessuto. Questo effetto è meno marcato nel caso si usino fibre più piccole e può arrivare anche a più che compensare l'effetto della ridotta efficienza di raccolta. Questo aspetto non è stato ulteriormente indagato per motivi di tempo. Data la sua importanza secondaria nel complesso del sistema, si è deciso di includere semplicemente una piccola verifica di utilizzabilità negli esperimenti che seguono. Maggiori dettagli e una discussione più approfondita del problema sono stati forniti nel testo della tesi.
Nonostante siano state usate componenti di gran lunga peggiori di quelle proposte nelle conclusioni, risultati riguardanti la valutazione del circuito vero e proprio hanno dato risultati estremamente positivi. Il sistema è stato testato su cinque phantom diversi con un livello di attenuazione progressivamente crescente in modo da poter valutare il comportamento dei dati ottenuti rispetto alle caratteristiche ottiche dei campioni. Entrambe le parti dell'esperimento hanno dimostrato che il sistema è efficiente e affidabile per quanto riguarda la stima del coefficiente effettivo di attenuazione. In molti casi, le stime sono state ottenute con errori inferiori al 4%, relativamente

al valore predetto dal modello . Questo parametro è risultato in media intorno al 10% a causa di grosse sovrastime ottenute dalle misure sul campione a più basso assorbimento. Sono state individuate alcune possibili cause, come ad esempio effetti di bordo che potrebbero aver causato perdite aggiuntive di luce, o errori nella preparazione dei phantom e quindi errori nella predizione delle proprietà ottiche. Purtroppo non è stato possibile verificare alcuna di queste cause in quanto non è stato possibile accertare le proprietà ottiche dei phantom con un metodo alternativo a quello sotto osservazione. Se si escludono i risultati ottenuti con questo campione, l'errore relativo medio scende al 6%, che è un risultato migliore di quello ottenuto durante i test effettuati per la valutazione del sistema attualmente in uso nell'azienda. Questa osservazione ha portato a concludere che gli errori commessi sul campione a basso assorbimento siano dovuti a cause esterne al circuito stesso. Per limitare ulteriormente l'influenza di errori esterni al sistema nella valutazione della bontà delle misurazioni effettuate utilizzando il circuito, sono stati considerati altri parametri e caratteristiche delle misure, scelti in modo da essere indipendenti dai valori delle proprietà ottiche derivati dal modello teorico. I valori calcolati considerando la deviazione standard relativa (RSD) sono stati particolarmente soddisfacenti, una RSD media compresa tra il 3% e il 4% è stata ottenuta dal complesso delle misure. Valori così bassi della RSD sono indice di misure ripetibili nel senso che diversi set di misure danno risultati simili su campioni simili. Inoltre sono state ottenute RSD così piccole anche dalle misure sul campione a più basso assorbimento a conferma del fatto che le discrepanze tra il valore previsto e quelli misurati sono dovute a fattori esterni al circuito stesso. É stato ritenuto opportuno valutare il comportamento dei dati relativamente al comportamento previsto dal modello teorico riportato precedentemente. Ciascun set di dati è risultato lineare, quindi interpolabile mediante una retta con scarti quadratici medi molto piccoli. Inoltre i dati relativi a misure effettuate su campioni con un valore del coefficiente effettivo di attenuazione più alto sono risultati interpolabili mediante rette con coefficienti angolari più alti, come previsto dalla teoria della diffusione.

Conclusioni

Lo scopo di questo lavoro di tesi è stato pienamente raggiunto in quanto il circuito ottico passivo proposto corrisponde ai criteri di funzionalità richiesti dall'azienda. Gli esperimenti e le misure effettuate dal circuito ottico hanno fornito risultati soddisfacenti per quanto riguarda le prestazioni del sistema stesso.

Effettuando una stima dei costi, basata in gran parte su quotazioni ottenute da me direttamente dalle aziende manifatturiere, si è concluso che il sistema non è solo affidabile in termini di misure ma risponde anche alle esigenze economiche messe alla luce dalla compagnia durante lo sviluppo di questo progetto.

Il design si è inoltre dimostrato flessibile ed adattabile a future esigenze di misura, anche diverse da quelle per cui è stato progettato, in risposta all'obiettivo aggiuntivo che mi ero posta

autonomamente all'inizio della progettazione.

Acknowledgments

I would like to give the greatest thanks of all to my family for their infinite support and patient, especially my mum and dad to always try to do their best to give me the greatest opportunities in life and to always be on my side no matter what. My friends from all over the world have been the most wonderful part of my life and my adopted family in the university years, always ready to cheer me up even when I didn't needed, to give me all those great memories, the big boxes of ice-cream and the opportunity to be interviewed with a chicken tight as microphone. You're great! So a really special thanks goes to all of you.

My appreciation goes to my Swedish supervisors Prof. Stefan Andersson-Engels, PhD Johan Axelsson and Johannes Swartling for giving me the opportunity to do this project and develop my ideas, and my Italian Prof. Antonio Pifferi for following my work in Sweden. I would also like to thank the people from the office for their support and great welcoming during these six months.

I would like to show my gratitude to Doctor Massimo D'Amore from the Urology and Radiology department of "Ospedale Renzetti" (Lanciano, Italy) for his precious information on some of the medical aspects.

Contents

Introduction **19**

1 Biomedical Optics **21**

1.1 Light propagation in biological tissues 22

1.1.1 Absorption 23

1.1.2 Scattering 25

1.1.3 Optical properties in prostate 26

1.2 Fluorescence 27

1.3 Modeling light propagation in biological tissues 28

1.3.1 Standard Diffusion Equation 28

1.3.2 Monte Carlo method 30

1.3.3 Differences between the two approaches 32

1.4 Optical parameters estimation 33

1.4.1 Interstitial measurements 34

2 Photodynamic therapy **38**

2.1 Insight into Photodynamic therapy 39

2.2 Photodynamic action and biological targets in PDT 40

2.3 Monitoring for real-time assessment and dosimetry 42

2.4 PDT for prostate cancer 44

3 PDT system development and characterization **47**

3.1 Global description of the systems 48

3.2 Light sources 52

3.2.1 Modulation frequency encoding 53

3.3 Delivery fibers 54

3.3.1 Channel module 54

3.4 Detection and signal processing 56

3.4.1 Optical filtering 56

3.4.2 Detection 58

3.4.3 Acquisition and processing 59

4 System validation **62**

4.1 Evaluation methods and measurement set-ups 63

4.1.1 Evaluation of the effect of the fiber core diameter on the detected light . . . 63

4.1.2 Measurements for μ_{eff} evaluation with modulation frequency encoding . . 67

4.2 Results and discussion 73

4.2.1 Effect of the fiber core diameter on the detected light 73

4.2.2 Modulation frequency encoding 77

Conclusions and future work **87**

Proposed set-up for the new generation of IPDT machines 87

A Abbreviations **91**

B Modifications to the MCML code and Matlab script for the evaluation **93**

C μ_{eff} estimation in Matlab **96**

D Labview graphic code **99**

Bibliography **101**

List of Figures

1.1 Spectra of the main absorbers in biological tissues. 24
1.2 MRI image of prostatic tissue showing the difference between tumor and normal tissue structures. 27
1.3 Flow chart of the Monte Carlo algorithm. 31
1.4 Measurement geometries. 34
1.5 Fiber positioning in interstitial measurements. 35
1.6 Spectra of oxyhemoglobin and hemoglobin in the range 650-850 nm. 36

2.1 Energy-level diagram of the type I and type II reactions for a general photosensitizer. 41
2.2 Two possible measurement set-ups for real-time monitoring of IPDT. 43

3.1 Sketch of the section of the body during treatment, with fiber positioning and TRUS and a flow chart of the treatment procedure of the SpectraCure AB IPDT system. 49
3.2 Block scheme of the current SpectraCure AB PDT set-up and a sketch of the fibers during the monitoring mode. 50
3.3 Overview of the proposed set-up. A block scheme of the interaction between the module and sketches of the single channel and detection modules. 51
3.4 Spectrum of the 730 nm LD output, being modulated at 30 Hz. 54
3.5 Design of the channel module. 55
3.6 Schematics of the detection part. 57
3.7 Transmission curve of the interference filter Thorlabs FEL0700. 57
3.8 Typical DET100A spectral responsivity curve. 58
3.9 Photodiode response at different wavelengths. 59
3.10 Labview program interface. 61

4.1 Flow chart of the modifications introduced in the MCML code to introduce the effect of the numerical aperture. 65
4.2 Schematics of the measurement set-ups used for the evaluation of the effect of the fiber core diameter on the collected light. 67

4.3 Schematics of the measurement set-up for the evaluation of the effective attenuation coefficient. 68
4.4 NI USB-6009. 69
4.5 Transmission curve of the filter Thorlabs FB730-10. 70
4.6 Spectra of the signal at the detector with and without the effect of the back-reflection. 70
4.7 Configurations for the fiber positioning. 72
4.8 Spectra of the light collected by the fibers from an integrating sphere. 74
4.9 Image of the geometrical argument to explain the differences in the collection efficiency in the case of propagation in air and in a biological tissue. 75
4.10 Spectra of the light collected by the fibers during the reflectance measurements. . 75
4.11 Plot of the measurements from channel 1 on the five different phantoms. 79
4.12 Plots of the measurements from channel 1 and 2 on Phantom D in the two different configurations. 80
4.13 Plots of the measurements from channel 1 and 2 on Phantom A using a 200 μm core fiber for the detection. 81
4.14 Plots of the measurements on Phantom A' and Phantom B during the filtering experiments. 82
4.15 Plot of a measurement on a really low absorbing phantom with a fluctuation in the laser power. 85

List of Tables

3.1 Conversion factor from output voltage to light power of the photodiode Thorlabs DET100A. 59

4.1 Parameters for the MCML simulations. 66
4.2 Main characteristics of the analog ports of the NI DAQ-6009. 69
4.3 Hardware settings used in the measurements. 71
4.4 Composition and optical properties of the phantoms used for the measurements . 73
4.5 Results for the estimation of the effective attenuation coefficient. 84
5.1 Hardware characteristics of the proposed system. 89

Introduction

The progress made in the field of medicine by science and engineering can be considered common knowledge. Not many, though, know the outstanding role that the use of light sources, like lamps and lasers, are having in this process. The use of light applied to medicine is nothing new, there are many examples of diseases treated with light, even sunlight. One can think for example to neonatal jaundice, an increase in the bilirubin level in newborns that shows itself as a yellow pigmentation of the skin. This disease is cured nowadays by exposing the newborn child to blue light, the so called Bili lamp. This lamp stimulates the conversion of the bilirubin and its elimination from the body. In older times, instead, doctors were able to cure the jaundice exposing the children to sunlight, when exposed to such a light, the yellowish pigmentation tended to disappear from the newborn skin. However, what made the role of light exponentially important is the invention of laser. This influence is so important that a whole new branch name in the field of medicine have been coined, Laser medicine, to group all this diverse applications. Among the others, one can list fields like angioplasty, dermatology, cosmetics, surgery, tomography, medical imaging, mammography and cancer diagnosis and treatment.

Cancer treatment is one of the main goals for the western medicine since it is among the most diffuse causes of death in the developed countries. In particular, skin and solid tumors, whose carrier has actual chances of complete recover, have major complications in the treatment because of the side effects that mutilating surgery has, like infections, long recovery times and, sometimes, anti-cosmetics results.

Photodynamic therapy finds its application to cancer treatment in these fields. It is a local and targeted phototherapy that is based on the interaction of light with a photosensitizer and oxygen. This technique has some major advantages: it is minimally invasive, so it avoids infections and wounds as much as possible, it is able to reach, virtually, every organ thanks to the fiber optics technology and it is believed to stimulate the immune response against cancer. For solid tumors, in particular, interstitial photodynamic therapy is used. This technique is so flexible that it is applicable for the treatment of whatever solid tumor at the only expense of modifying the light dose software.

SpectraCure AB has developed a system for interstitial photodynamic therapy to cure prostate cancer. This system will be applied, in the future, to the treatment of cancer in pancreas ans the

ear, nose and throat tract. The light delivery system, from the hardware point of view, is based on a complex switch that enables to alternate the therapy with the optical properties assessment, i.e. calculation of the effective attenuation coefficient, in order to control the state of the tissue and adapt the light dose to the optical properties of the tissue.

The objective of this project presented herein has been to develop an all optical passive circuit to replace the switch in order to have a system that is simpler and more compact. The use of a passive circuit instead of a mechanical switch has, among the others, the advantage of eliminate the need for mechanical instrument calibration since no parts need to be moved.

This work has been concluded proposing a passive optical circuit that shown itself as compact, cheap, effective, flexible to changes and, more important, reliable. In fact, the designed system have been able to predict the effective attenuation coefficient within few percentage points from the value predicted by the model. The proposed circuit bases the calculations, as the previous one, on multi-distance measurements. Unlike the previous, it is able to perform the measurements along with the therapy, simultaneously on all the channels. This feature is obtained using a modulation frequency encoding of the monitoring sources. This approach makes it possible to enhance the dosimetry calculations and to make the optical properties assessment more robust, at the advantage of the therapy outcome and so of the patient recovery.

Chapter 1

Biomedical Optics

The study of the propagation of light in biomedical tissues is the basis for the photodynamic therapy (PDT) since the interaction between light and tissues is the way through which the treatment is achieved. This chapter presents an overview of how the light interacts with biological materials and how its propagation can be described in terms of optical properties. A discussion about the differences between normal and tumoral tissues in terms of optical properties is presented, and some specific data about the prostatic gland are given. The Diffusion Equation and the Monte Carlo methods are illustrated in section 1.3 as models of the light propagation in highly diffusive materials. An overview on the different possible measurement configurations, in particular for interstitial measurements, is presented in section 1.4.

There are many ways to deal with diagnosis and treatment of cancer and other diseases that are treated with optical techniques: ordinary mutilating surgery, radiotherapy, cryotherapy and many others. What makes optical applications so interesting and attractive is the ability to achieve clinically satisfying results in a wide range of fields related to biology and medicine. These results are satisfactory, for instance, in terms of safety of the diagnostic measurements, in fact optical techniques are non-mutagenic, recovery from the disease or cosmetics. The price to pay for this versatility is the complexity of the interactions between light and tissue. A good knowledge of these interactions and all the phenomena that lie behind it is the keystone for the understanding necessary for further development of these techniques. The branch of physics and engineering that deals with this field is called Biomedical Optics.

The interaction between light and biological tissues are different at different wavelengths. Depending on the optical characteristics of the medium, mainly the absorption, the light has diverse

penetration depths. For for instance, the tissue can undergo heating because of the presence of water, if wavelengths in the infra-red are used. Another example is protein denaturation due to tissue exposure to ultra-violet light. Of particular importance is the range of wavelengths between 600 nm and 1200 nm. In this interval, the absorption of the main chromophores in tissue, such as hemoglobin and water, is at its minimum, so the light can penetrate deeper into the tissue. Biological tissues are turbid media, so the light that travels through those tissues is highly affected by the tissue optical properties because of such strong interaction. These characteristics are exploited both for diagnosis and treatment. At low powers, the light does not condition the tissue, so it can be used as a diagnostic tool to measure the optical properties of the materials; these can give useful information for diagnostics since they are affected by the status of the tissue; for instance, differences in the blood absorption coefficient are indicators of differences in the tissue oxygenation, or changes in the optical properties in a specific site within a bulk tissue can be used to identify carcinomas. Treatment techniques use relatively high power levels. In fact, these methods take advantage of the light-tissue interaction to modify the tissue itself. This can be achieved following different paths, the greatest majority of them rely on the absorption to induce changes in the tissue by heating, one example is wrinkles removal, or by photoactivation of a light sensitive drug, as in photodynamic therapy.

As any other phenomenon, a deep investigation of light-tissue interaction requires a model. The most successful so far has been the radiative transport theory. Its approximation, the diffusion equation, is the most adopted model to describe photon propagation due to its simplicity and the possibility to obtain an analytical solution. Another algorithm to solve the radiative equation is the Monte Carlo method. This latter provides a statistical solution to the problem.

An overview of these models and the main parameters used in this field are presented in this chapter.

1.1 Light propagation in biological tissues

Biological tissues can be defined as a set of cells, not necessarily identical, that perform the same function. As for any other medium, light propagating through these tissues is affected by their composition and structure, in a fashion that depends on the properties of the light itself.

There are four main phenomena that affect light propagation: reflection, refraction, absorption and scattering. Reflection and refraction determine the light propagation at the boundary with different refractive index and they can be assessed as the cause for scattering, if seen on a microscopic level. They are described by Fresnel's and Snell's laws.

More interesting for present work are the absorption and scattering properties of biological tissues. These are the cause for the attenuation of light during propagation, so they are two of the key parameters in light dosimetry for medical applications, as they can affect both the distribution of the light intensity and the propagation depth, and, as a consequence, the position and volume of tissue affected by the therapy. When the attenuation is due to a loss of the photon from the beam, it is referred to as absorption, while when it is due to a deviation of the photon trajectory from the cone of detection, it is referred to as scattering.[1]

Because of their structure, biological tissues are considered highly scattering media. This property is linked to the size and distribution of the different components of the tissue, scatterers, at the cellular and sub-cellular level,[2] while the absorption is affected by the concentration of different kind of chromophores, i.e. light-absorbing elements, such as hemoglobin, water and fat.[3]

Distinct type of tissue have various characteristic structures and chromophores so they can be discriminated by means of their optical properties. Histological applications can take advantage of these properties of the light-tissue interaction. In particular, normal and malignant tissue have different physiological properties so they can be discriminated using optical techniques.[4] These techniques are generally referred to as optical biopsy, since they analyze how the light intensity is affected by traveling through the tissue.[5]

1.1.1 Absorption

Absorption is described by the absorption coefficient μ_a, and can be expressed in terms of chromophores concentration as:

$$\mu_a \;=\; \sum_k C_k \sigma_k \tag{1.1}$$

where σ_k is the absorption cross-section and C_k is the molecular concentration. The absorption is related to the light intensity by means of the Lambert-Beer law, that states that the intensity of the light that propagates through an absorbing, but not scattering, medium has an exponential decay, the further the detection point is from the source. The decay constant is given by the absorption coefficient μ_a:

$$I(r) \;=\; I_0 \exp(-\mu_a r) \tag{1.2}$$

where $\mu_a r$ is referred to as the attenuation A; as explained in section 1.1.2, this statement is valid only if the absorption is strongly larger than the scattering, namely $\mu_a \gg \mu_s$, where μ_s is the scattering coefficient.[1]

Absorbers in biological tissues can be endogenous or exogenous. Among the exogenous, the most common are specific kinds of drugs and tattoo inks.

The most important endogenous chromophore is water, because of its high concentration in the body. Along with water, there are heme proteins, lipids and some pigments like bilirubin and melanin,[6,1] that are important absorbers, especially in the NIR region. Hemoglobin plays a significant role in absorption in blood perfused tissues,[7] such as in soft tissues, and its absorption properties depend on the oxygenation state and therefore on the metabolic functions.[1]

The wavelength dependence of the absorption coefficient of a specific tissue is affected both by the concentration and the wavelength dependence of the absorption coefficient of each chromophore. The absorption spectra of the main absorbers is shown in Figure.1.1 As it is

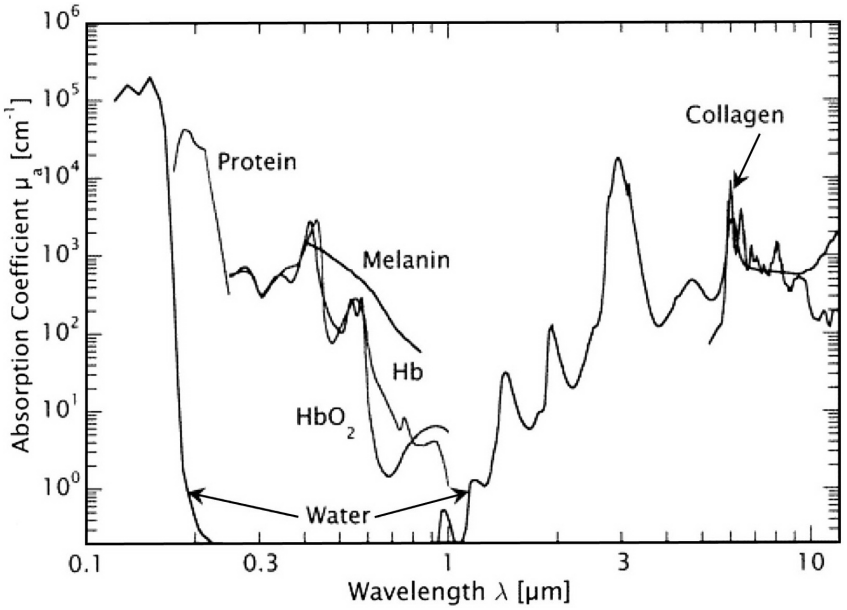

Figure 1.1: *Spectra of the main absorbers in biological tissues.*[8]

possible to notice from the spectra in the figure, the absorption of these chromophores, so of biological tissues, is at its minimum in the wavelength interval 600-1200 nm. This part of the spectrum is called Diagnostic Window.[9] In fact, the relative transparency of biological tissues in this range makes it possible to use light at these wavelength to perform measurements of the diffused light in biological samples; this property is exploited in section 3.2 to choose a proper source for the development of the system in this work.

The absorption coefficients dependence of the wavelength can be used to determine some important parameters such as tissue oxygenation, oxygen saturation level and water and lipid concentrations.

Normal and malignant tissue differ consistently in absorption behavior at all wavelengths.[4] In general, the absorption values that are obtained from measurements over malignant tissue are significantly higher than for normal tissue.[5] This is due to the fact that tumor-containing tissues

are strongly pigmented[10] and have higher oxygenation and total hemoglobin levels. The oxygen saturation is higher in malignant melanomas because of their worsened capacity to extract oxygen from oxyhemoglobin as well as their higher blood flow, due to a higher metabolism, and perfusion.[5] In fact, the blood vessels in tumoral volumes are not properly developed or hierarchically structured.[11] The inability to extract oxygen from blood is used to distinguish malignant melanomas from benign fibrotic and cystic tumors since it is a unique characteristic of these tissue formations.[5]

1.1.2 Scattering

When dealing with scattering media, as biological tissues are, Eq. (1.2) is not valid anymore because it holds true only for non-scattering media. In fact, for these materials, the attenuation A does not depend linearly on the absorption coefficient μ_a and the degree of non-linearity depends on the scattering coefficient μ_s. Multi-scattered light is subject to an increased total pathlength from the source to the detector, so the probability for the photon to be absorbed before reaching the detector is higher. The Lambert-Beer law can be modified to include this effect, so it can be applied to the cases where $\mu_a \gg \mu_s$ does not hold anymore. The attenuation A is calculated by introducing a term related to the scattering losses, expressed as the scattering coefficient μ_s. This description in terms of average scattering is possible since the single scattering event is not relevant if the light has experienced enough scattering events. This condition is true for turbid materials, such as biological tissues.

The scattering coefficient μ_s can have an angular dependence, meaning that the scattering of the photons is anisotropic. Since it is easier to describe isotropic than anisotropic scattering,[12] this effect is modeled introducing the anisotropy factor g, defined as the averaged cosine of the scattering angle. The scattering in tissues is directed forward, so the anisotropy factor generally falls in the range 0.7-0.95.[13] The scattering coefficient is then replaced by the transport (or reduced) scattering coefficient $\mu_s' = \mu_s(1-g)$. The transportation mean-free-path is then defined as:

$$mfp' = \frac{1}{\mu_a + \mu_s'} \tag{1.3}$$

Biological tissues results to be highly scattering media manly as a result of the presence of mitochondria and lipid vesicles in the cells. In fact, scattering is caused by cell structures, such as separation membranes, since they introduce a variation in the refractive index, and thus a deviation of the photon trajectory. The wavelength dependence of the reduced scattering coefficient μ_s' can be described by an empirical power law derived by simulation on Mie scattering. It decreases gradually with increasing wavelength, following:

$$\mu_s' = a \cdot \lambda^{-b} \tag{1.4}$$

where b is generally smaller than few units.[14]

As it happens for absorption, the tumor and the normal tissue have different scattering properties because of the differences in structure and composition. A change in the scattering coefficient can be due to a loss of the cellular structure and to the presence and changes in concentration of different kind of components, in particular proteins, in the tissue. The differences are not as significant as for absorption, but changes in μ_s' are expected to be more substantial in early-stage highly cellular tumors.[4] In addition, there is not a main trend in how the scattering coefficient is affected by tumoral structures because an increase or a decrease in the reduced scattering coefficient μ_s' depends strongly on the kind of tissue involved, meaning in which substrate the cancer lies. If the presence of a tumor implies a loss of cellularity and an increase of the water content, which usually happens in solid tumors, fluid-filled cysts and in presence of necrotic areas, the reduced scattering coefficient tends to be lower; while in case of fibroadenoma, i.e. fibrotic tissue, the value of μ_s' tends to increase.[5]

1.1.3 Optical properties in prostate

Typical optical properties in prostate are 3.7$\pm$0.24 cm^{-1} for the attenuation coefficient and 14$\pm$11 cm^{-1} at 732 nm, wavelength close to the one used in the system object of this work.[15] These values are given only as a reference since the biological variations, even in the same subject, are extremely significant so these values cannot be said to be representative of the whole population.

An MRI image of a prostate showing the difference in the structure of a tumoral tissue in respect of the normal tissue is shown in figure 1.2. The difference in the structure affect the optical properties as assessed in the previous paragraphs.

The main absorbers in the prostate gland are hemoglobin, water and lipids. The last two can be considered to be approximately 70% and 10% of the whole volume, respectively.[17] Even if prostate have a high water and lipid content, the hemoglobin is the chromophore that account for most of the absorption in this gland because of the relatively low absorption of water and lipids in the wavelength range that is used for the measurements (600-800 nm).
The wavelength dependence of the scattering coefficient can be assumed to be $\mu_s' = \lambda^{-1.1}$.[18]

The prostate has, in general, a percentage of oxy- and deoxyhemoglobin calculated in respect of the total blood content that has been assessed to be around 75% and 25% respectively.[19]

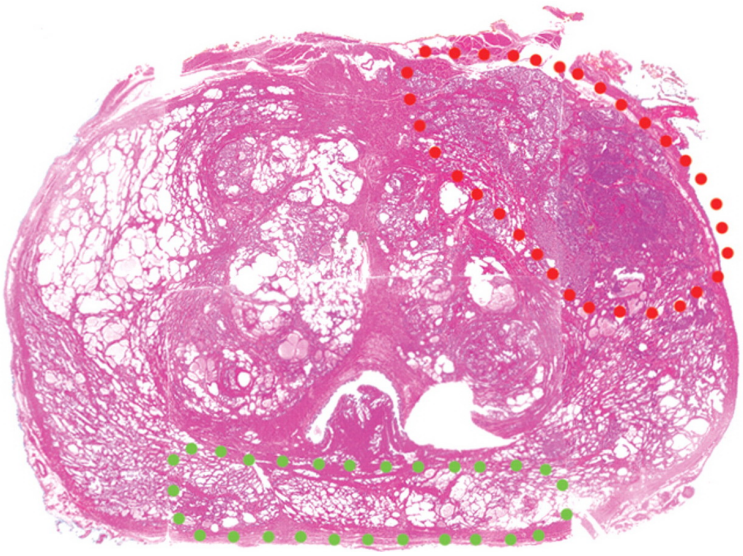

Figure 1.2: *MRI image of prostatic tissue showing the difference between tumor and normal tissue structures.*[16]
Tumoral (red) and normal (green) peripheral tissue.

1.2 Fluorescence

Fluorescence is an important property in most of the applications that involve biological tissues since it constitutes an important metric both for specific tissue characteristics and for certain kind of drugs.

The intrinsic fluorescence of a material is defined as autofluorescence. Autofluorescence occurs in tissue due to the presence of fluorescent molecules in the medium. The main cause of autofluorescence in biological tissues is the presence of the coenzyme NADPH, along with certain proteins, as collagen or elastin, and particular sub-cellular structures such as mitochondria or lysosomes.[20] Autofluorescence constitutes a bright background in fluorescence measurements, which can make it impossible to use certain drugs as markers, if these have the same emission wavelength as the endogenous molecules. On the other hand, it can be used as a diagnosis parameter, for example in cytotoxicity measurements, instead of other exogenous fluorescent markers.[20]

Specific photosensitizers are present among other fluorescent agents. These have peculiar fluorescent characteristics that, in principle, allow them to be used as diagnostics or monitoring indicators during specific kinds of treatments. The use of fluorescence in applications such as PDT is not clearly defined as the state of art. There are suggestions, for example, to monitor the photosensitizer photobleaching as a measure of the progress of the therapy and as a dosimetry parameter during the treatment, since a higher light-dose delivered to the tissue induces a higher degree of photobleaching.[21]

1.3 Modeling light propagation in biological tissues

The light propagation in turbid media has to be described by a model that includes the multiple-scattering effect. The transport theory provides such a model, since it solves the radiative transport equation. By means of this equation, the light propagation is expressed in terms of energy balance. In this theory, scattering is described by means of a phase function that models how much of the photon flux is deviated from one direction to another, at each scatter position.[22]

The radiative transport equation requires approximations to be solved analytically or numerically. The most common one, which is one used in the the present work, is the diffusion approximation, which assumes that the light is diffused in the medium. This approach leads to the diffusion equation.

An alternative way to solve the radiative transport equation is to use Monte Carlo methods. These are computational algorithms that follow the path of each photon package in the scattering material. With this approach, optical properties are described in terms of probabilities for the photon to be absorbed or scattered at each randomly distributed scattering event.[23] Therefore, they provide a statistical solution to the problem.

These approaches and their solutions are described in further details in the following sections.

1.3.1 Standard Diffusion Equation

The standard diffusion equation (SDE) is an important model in the field of light propagation in turbid media. Among the other parameters that can be derived from it, the fluence rate, i.e. the photon density within the tissue, is a relevant quantity in applications such as PDT since it states how much of the light is available for the interaction between light and tissue. As a matter of fact, the fluence rate is the sole parameter that can be controlled during the therapy process, therefore its good estimation is relevant for the light dose plan.

The diffusion equation is derived from the Radiative Transport Equation (RTE). The same is also used in applications like heat induction or modeling of neutrons in nuclear reactions. The RTE for monochromatic light propagating in turbid media is[6]

$$\begin{aligned} \frac{1}{v}\frac{\partial}{\partial t}L(\mathbf{r},\mathbf{\Omega},t) \;+\; \mathbf{\Omega}\cdot\nabla L(\mathbf{r},\mathbf{\Omega},t) \;+\; [\mu_a(\mathbf{r}) \;+\; \mu_s(\mathbf{r})]L(\mathbf{r},\mathbf{\Omega},t) \\ = \int_{4\pi} L(\mathbf{r},\mathbf{\Omega}',t)\mu_s(\mathbf{r},\mathbf{\Omega}'\rightarrow\mathbf{\Omega},t)d\mathbf{\Omega}' \;+\; S(\mathbf{r},\mathbf{\Omega},t) \end{aligned} \tag{1.5}$$

where v is speed of light in the medium, $L(\mathbf{r},\mathbf{\Omega},t)$ is the radiance [$Wm^{-2}sr^{-1}$], defined as the radiant power transported at the location $\mathbf{r}$ in a given direction $\mathbf{\Omega}$ per unit solid angle per unit area normal to that direction, and $S(\mathbf{r},\mathbf{\Omega},t)$ is the energy radiance of a light source. The RTE

describes the light in terms of a stream of photons, i.e. particles that transport energy. It is based on the energy conservation principle so it is a balance equation; the different terms can be physically described as, from the left, the change of photon distribution over time, the losses due to photons crossing the surface boundaries and due to absorption and scattering, the gain due to photons scattered in the direction $\mathbf{\Omega}$ from other directions and due to the presence of an internal light source.

The RTE can be solved analytically or numerically, for specific cases, making a number of assumptions. The simplest approach is the diffusion approximation that assumes that the light is diffused, $\mu_s' \gg \mu_a$. To find an analytical solution a further assumption must be introduced: the medium has homogeneous optical properties.
Under the diffusion approximation, the radiative transfer is expressed in terms of fluence by

$$\Phi(\mathbf{r}, t) \; = \; \int_{4\pi} L(\mathbf{r}, \mathbf{\Omega}', t) d\mathbf{\Omega}' \tag{1.6}$$

In the steady-state, the fluence rate can be calculated as[24]

$$\nabla^2 \Phi(\mathbf{r}) - \mu_{eff}^2 \Phi(\mathbf{r}) \; = \; \sum_i S(\mathbf{r_i}) \tag{1.7}$$

where $\sum_i S(\mathbf{r_i})$ is an isotropic point source and the effective attenuation coefficient is defined as

$$\mu_{eff} \; = \; \sqrt{3\mu_a(\mu_a + \mu_s')} \tag{1.8}$$

For a point source in an infinite medium, the solution has the form

$$\Phi(r) = \frac{P_0}{4\pi D r} \exp(-\mu_{eff} r) \tag{1.9}$$

where P_0 is the power of the source and $D = 1/\mu_{eff}$ is the diffusion coefficient; the penetration depth of collimated light, and so the pathlength can be estimated from the diffusion coefficient as its square root.
This approach can be used in modeling turbid media, whose dimensions are larger than the mean pathlength, i.e. media that can be considered infinite. This approximation is not valid for distances from the source smaller than $1/(\mu_a + \mu_s')$ and near the boundaries.
The diffusion equation is also applicable in case where the light source is modulated, with the limitation that the modulation frequency should be smaller than few GHz.[4]

As stated, the RTE can be also solved numerically. In particular Finite Elements Methods (FEM) can be used when the optical properties are position dependent. An alternative is to estimate the radiance as a series of spherical harmonics and solve the resulting system of equations. The lowest-order solution is the diffusion equation.

In this work, the diffusion equation is used to estimate the value of μ_{eff} from the reflectance measurements, since this model is applicable to model the light propagation in soft homogeneous tissue such as the prostate.

1.3.2 Monte Carlo method

Monte Carlo methods simulate and follow the photon path through the medium. The output of the algorithm is a series of maps that represent the recording of the scattering and absorption behavior of each photon. The accuracy of this method depends only on the number of photons tracked.

The flow chart of the algorithm is presented in Figure 1.3. Each photon is initialized at a chosen set of coordinates, identical for each photon. The direction can be either chosen randomly within the downwards solid angle, if a diffused radiance source is to be simulated, or downwards, if the source is a collimated beam normally incident on the surface.

The propagation distance at each step is calculated from a probability density that follows the Lambert-Beer's law, so the stepsize results:

$$\Delta s = \frac{-ln\xi}{\mu_a + \mu_s} \tag{1.10}$$

where ξ is a random variable uniformly distributed in [0,1].

At each step a scattering and an absorption event occur. The absorption events are based on the concept of packets of photons. Each photon, which is rather a packet of photons, has been assigned a weight w. When an absorption event occurs, the photon weight is updated. Part of its weight is recorded in the local position and the rest is scattered away. The absorbed part is proportional to the albedo

$$a = \frac{\mu_s}{\mu_a + \mu_s} \tag{1.11}$$

so the new photon weight results to be $w_{new} = aw_{old}$ and the amount of light recorded in the absorption matrix at the given location is $(1-a)w_{old}$.

The parameter w is bounded to never reach zero. This fact causes an issue in the computation since it is highly inefficient to keep on tracking a photon that has a really small weight. On the other hand, removing the package biases the calculations, so the removal must be done in an unbiased way. The technique used in Monte Carlo simulations is called roulette: each photon that has a weight under a predefined threshold, has a survival probability of $1/m$. If it survives, its weight is updated and becomes mw, otherwise it is set to zero and the photon is killed.

The scattering event determines the direction of the next step. This direction is modeled by a probability density function for the azimuthal and longitudinal angle. For biological tissues, the scattering direction has axial symmetry so the probability density function is entirely described

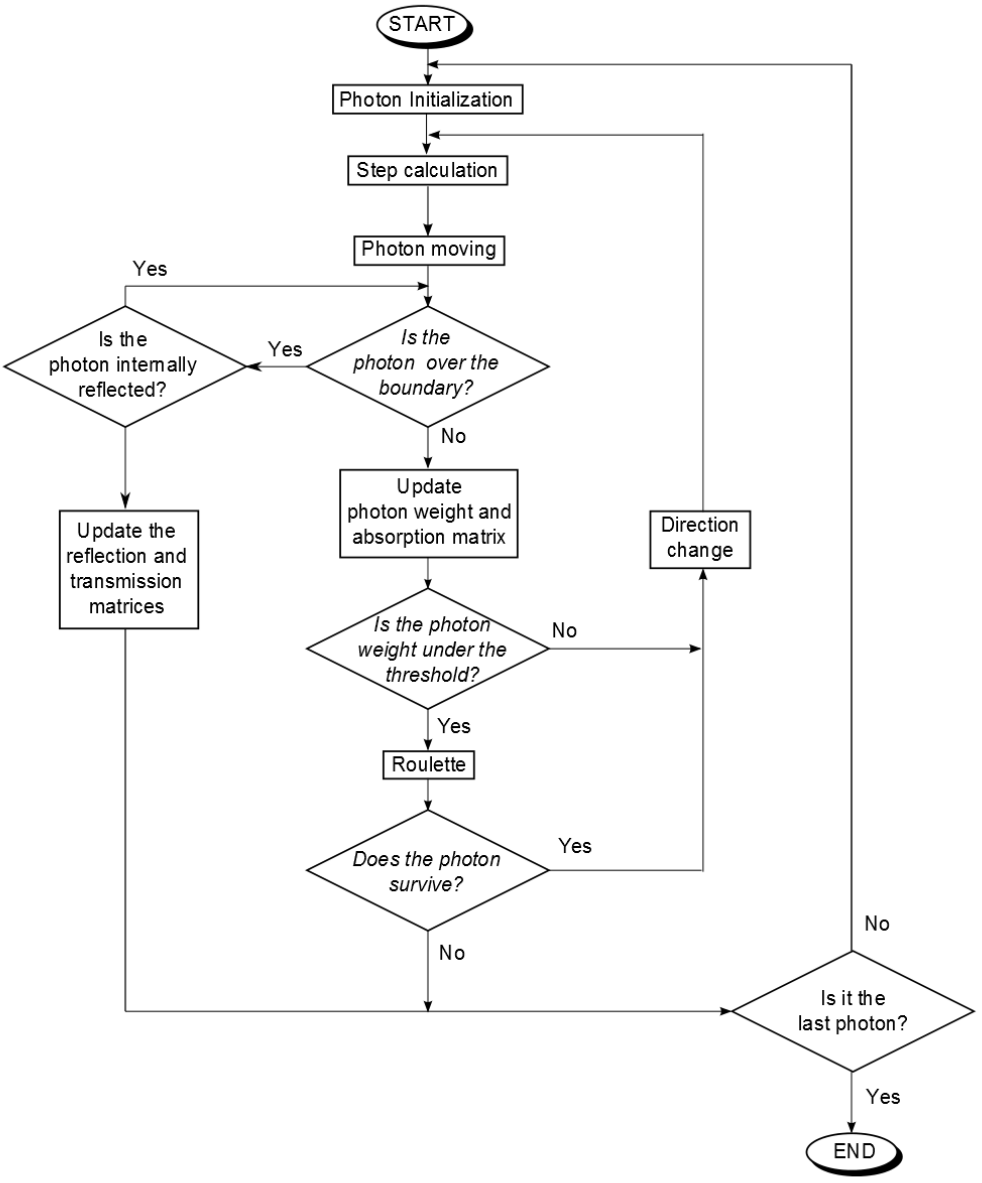

Figure 1.3: *Flow chart of the Monte Carlo algorithm.*[25]

by the cosine of the azimuthal angle θ, that follows the Henyey-Greenstain function[26]

$$\cos\theta \;=\; \frac{1}{2g}\left[1+g^2-\left(\frac{1-g^2}{1-g+2g\xi}\right)^2\right] \tag{1.12}$$

where g is the anisotropy coefficient and ξ is defined as above. So, when the photon is moved along the direction defined by the cosine of the azimuthal angle, each coordinate is updated by a value corresponding to the stepsize Eq. (1.10) multiplied by the angle that the photon's direction makes with each axis. These calculations are performed only if the photon has a weight larger than the threshold weight or if it survives to the roulette.

The internal reflections and the propagation across the boundaries between different media are determined by Fresnel's reflection coefficient and Snell's law.

The photon launching is independent of the depth z, so it is possible to simulate different irradiation profiles convolving the beam profile with the results obtained simulating a point source, as above. This approach is highly efficient because it is possible to calculate the effect of different source profiles from one single output of the Monte Carlo simulation, assuming that the rest of the parameters do not change. If a Gaussian beam is used as a source, the equation for the fluence is[25]

$$\Phi(r,z) \;=\; \frac{2P}{\pi R^2}e^{-2(r'/R)^2}\int_0^\infty G(r',z)e^{-2(r'/R)^2}I_0(4rr'/R^2)dr' \tag{1.13}$$

where P and R are the total power and the $1/e^2$ radius of the beam, $G(r,z)$ is the Green's function for the medium, i.e. the fluence given a point source, and $I_0(r)$ is the zero order modified Bessel function of the first kind.

In this work, Monte Carlo simulations have been used to estimate the effect of the fiber core diameter on the detected light.

1.3.3 Differences between the two approaches

The two models presented in the previous sections have different characteristics and limitations that make them suitable for certain applications rather than others. The differences lie on the very nature of the solution and how they are calculated. As explained, Monte Carlo methods are models based on the calculation of probability densities, so their complexity requires high computational power and times compared to the ones needed by applying the solution of the diffusion equation.

For the same reason, the error on the solutions obtained from Monte Carlo simulations is statistical. That is not the same for the diffusion theory, which provides an analytical or a numerical solution.

On the other hand, to obtain an analytical expression, a number of approximation are needed. This implies a limitation in the applicability of the solution; a limit that Monte Carlo simulations do not have, even though each Monte Carlo simulation is specific for a particular set of parameters, so the simulations must be repeated each time the set is changed.

1.4 Optical parameters estimation

Optical parameters can be estimated using different techniques depending on the kind of application and the required accuracy. The common problem in all these techniques is the limit on the measurable quantities. In fact, the transmitted or back-reflected light is the only directly measurable one.

Given the detected light at different points of the tissue, the parameters can be calculated by applying the diffusion theory, given that the source-detector separation is big enough for the diffusion approximation to be valid. This kind of measurement is called multi-distance measurements and it is the kind of measurements performed in this work.

Steady-state measurements at a fixed wavelength do not allow to discriminate between absorption and scattering coefficients, so the only assessable parameter is the inverse of the penetration depth μ_{eff}. This parameter represents a mean value of the optical properties since biological tissues are not homogeneous media, even if the diffusion model assumes that they are. Absorption and scattering coefficients can be separated performing time-resolved measurements, both in time or frequency domain. These two techniques use pulsed[27] and sinusoidally modulated[1,4] light sources, respectively. Furthermore, it is possible to calculate the different chromophores concentrations performing multi-spectral measurements, by solving Eq. (1.1). This knowledge is essential to obtain important information such as tissue oxygenation or blood and water volumes.[4,5]

The light is measured using two or more fibers: one fiber is used as a source to shine light in the sample, the other ones are used as a detectors to collect the diffused light.
Two possible measurement geometries, reflectance and transmittance configurations, are shown in Figure 1.4.
The detected light carries information on the optical properties of the probed medium. As previously stated, in the case of steady-state measurements, the information is carried by the detected intensity. If homogeneous optical properties are assumed, it is possible to perform multi-distance measurements since the absorption and scattering coefficients are independent from the position and the source-detector separation. The μ_{eff} is then calculated from the fluence rate in Eq. (1.9), calculating the slope of the line:

$$-ln(r\Phi(r)) \;=\; \mu_{eff}r - ln\left(\frac{P_0}{4\pi D}\right) \tag{1.14}$$

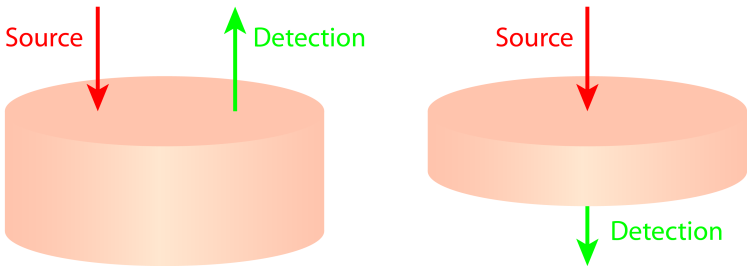

Figure 1.4: *Measurement geometries.*
Reflectance (left) and transmittance (right) configuration.

In case an heterogeneous region is probed, the measured value of μ_{eff} represents an average of the optical properties of the different parts of the sample. If the measurements are performed over phantoms with known optical properties, this value is compared to the theoretical one in Eq. (1.8) to asses the reliability and the performance of the method.

The optical method to provide tissue functional information presents several advantages in respect of other techniques such as MRI or CT. They do not make use of ionizing radiation so they permit repeated and continuous exposure; they are non carcinogenic, since they do not affect the DNA, noninvasive, relatively portable and inexpensive.[4,28,29] In fact, for example, light-screening techniques could constitute a valid alternative to conventional hazardous x-ray imaging to obtain information on benign or malignant lesions.[30]

1.4.1 Interstitial measurements

Interstitial measurements are performed in situations where the tissue is not optically accessible from the body surface or when the skin is not involved and would only be of encumbrance, mainly because of the poor light penetration due to the absorption.[31] This technique is of course more invasive than the non-interstitial ones and of other imaging techniques.

Interstitial measurements are performed placing the optical fibers directly into the tissue using biopsy needles or other probes. The positioning is done by means of imaging techniques such as ultrasonography. An example of the positioning of the fibers and of the ultrasound image of a needle in the prostate is shown in Figure 1.5. In general, for measurements on tissues that can be assumed homogeneous, one fiber is used to carry the light into the sample and a number of other fibers are positioned at different distances from the source for light collection.

In measurements that need to be carried out during the therapy over a small target volume, such as the prostate, it is important to not perturb the treatment. Optical techniques are the only ones able to take measurements in the tissue without influencing the treatment since the fibers used as probes are only minimally invasive, and so is the perturbation they cause.[29] As it will be

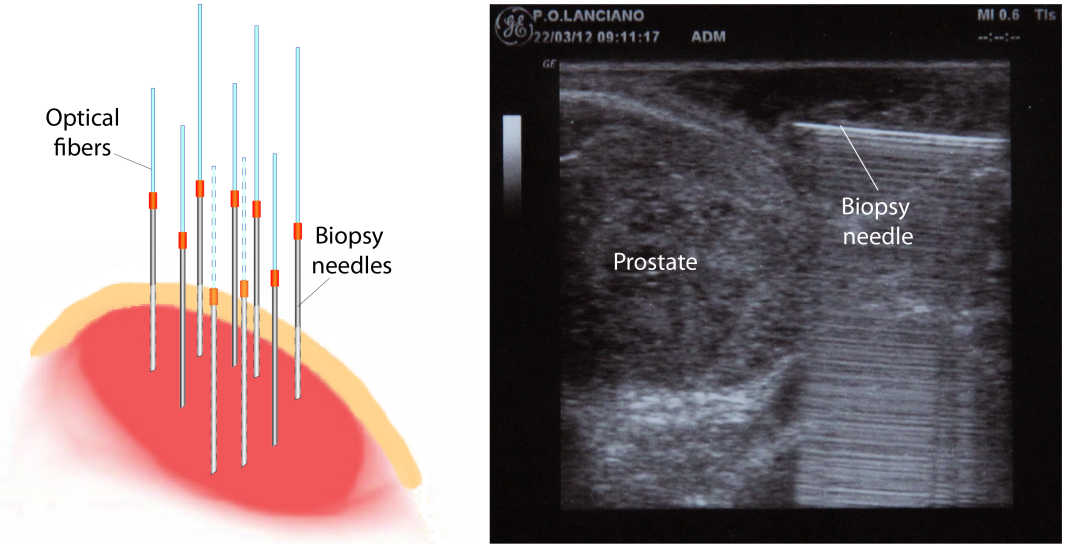

Figure 1.5: *Fiber positioning in interstitial measurements.*
Example of fiber geometry (left) and Ultrasonography image of a biopsy needle in the prostate (right). Courtesy of Dott. M. D'Amore, Medical Director Urology Department, Ospedale "F. Renzetti", Lanciano, Italy.

presented in chapter 3, the system for interstitial measurements developed in this work does not introduce any additional fiber-probes to the treatment ones, so the measurements do not induce any perturbation during the therapy. The major problems with interstitial measurements are the formation of blood pools at the tip of the fibers and an additional decrease of the fluence rate with the distance. This latter one is mainly caused by the absorption and the spreading of the light in all directions due to the geometric setup.[6]

Blood pools

Optical parameters of blood deviate considerably from those of soft tissues. Therefore the blood content can significantly affect the optical behavior of blood perfused tissue, which soft tissues are. In fact, the optical response of this kind of tissues is heavily dependent on the presence of blood, the oxygen saturation and the hematocrit, i.e. the concentration of red blood cells in the total blood volume.[7]

The major increase in absorption in blood is caused by the highly anisotropic scattering that characterizes the whole blood. Scattering in blood is due to the significant change in refractive index introduced by the presence of erythrocytes. The scattering, in turn, leads to an increased optical pathlength that increases the overall probability for the photon to be absorbed before reaching the detector, and thus the absorption coefficient μ_a. The spectra of oxy- and deoxyhemoglobin in the range of interest are shown in Figure 1.6.

The significant effect of the blood and its changes on the optical properties of soft tissues, induces the need to take it explicitly into account in absorption measurements.

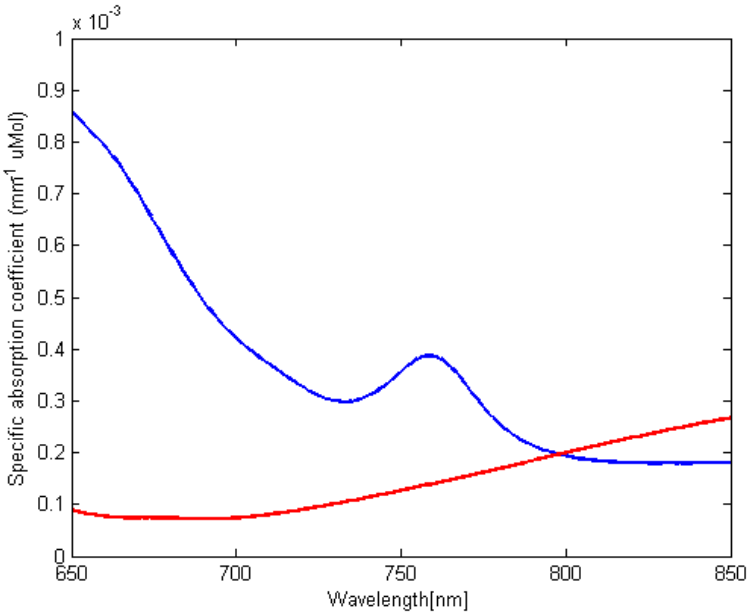

Figure 1.6: *Spectra of oxyhemoglobin and hemoglobin in the range 650-850 nm.*[32]
O_2Hb (red), Hb (blue)

For dose calculations and monitoring measurements, in particular, calcifications and blood occlusions close to the source, i.e. at the fiber tip, can largely decrease both the power delivered to the tissue and the detected power,[33] as much as 20 times attenuation each 1 mm of blood.[34] The effect of the blood pools, however, is merely a scale factor, and does not affect the value of the measured optical properties, if differential measurements are performed, like multi-distance measurements can be considered as. Nonetheless, this can have significant effects on both the real-time measurements and the therapy itself, as much as it can obscure the measurements and increase the treatment times as a consequence of the less light that is actually delivered to the tissue. If the real-time measurements are not performed simultaneously with the treatment, this can contribute to further extend the total therapy time.

Conclusions

In this chapter, a brief description of what a biological tissue is and how it can be modeled as a highly diffusive medium has been given. Some of the phenomena that affect the propagation of light in these tissues have been listed.The focus has been kept primarily on the description of the effect of absorption and scattering since these have the highest influence on the light-tissue interaction. These are described by means of the absorption and scattering coefficients, whose values are affected by the structure and composition of the tissue itself. For this dependence

of the optical properties on the characteristics of the tissue, tumoral formations in tissues can be discriminated by means of optical techniques, such as the optical biopsy or optical imaging, since neoplasic tissues have a different structure and composition in respect of the healthy surroundings.

Two of the models that are commonly used to describe the propagation of light in biological tissues, the Diffusion and the Monte Carlo models, have been analyzed along with the possible experimental set-ups for the optical properties assessment. In particular, the Standard Diffusion Equation is a model of fundamental importance in PDT since it is the one that is used to retrieve the value of the effective attenuation coefficient from multi-distance measurements, which are the kind of measurements performed by the system presented in this work.

Chapter 2

Photodynamic therapy

The optical circuit developed in this work is part of a PDT system for prostate cancer treatment. Therefore, the technique is introduced and the basic concepts behind it are explained in this chapter. In particular, some emphasis is put on the importance of on-line dosimetry and interstitial photodynamic therapy (IPDT) since this specific technique is the one used for solid tumors, like prostate cancer. PDT applied to prostate cancer and some details about the principles of functioning of the current SpectraCure AB system to be upgraded, are given in section 2.4.

Photodynamic therapy (PDT) is an optical technique that can be used for the local treatment of a number of diseases. The most noble and investigated application of PDT is cancer treatment. This technique was used for the first time in oncology during 1903 for the treatment of skin cancer.[35] Since then, many progresses have been made. From the treatment of topical malignancies, the applicability of PDT has been extended to the treatment of solid and infiltrated tumors, such as pancreatic,[36] brain[37] or bladder tumors.[38]

To induce cell death, PDT action requires the concomitance of light, photosensitizer and oxygen in the treatment site; this characteristic makes PDT a highly selective technique. The cell death occurs through direct or indirect pathways, all mediated by the presence of oxygen radicals. In particular, it is worth specifying that, in many cases, photodynamic therapy has been proved to induce an anti-tumor immunity that provides long-term tumor control,[39] so enhances the chances of recovering and survival of the carrier.

Light dosimetry pays an important role in this technique. Since the optical properties of the tissue change significantly during the therapy,[40] the light dose must be adapted to those changes in order to optimize the treatment, so on-line monitoring and dosimetry are fundamental to im-

prove the treatment outcome.[29] These techniques are being developed in modern system since they are a prerequisite when dealing with tumors grafted into sensitive surroundings.

Interstitial photodynamic therapy (IPDT), a technique that allows the treatment of embedded tumors by means of optical fibers, has found its successful way to the treatment of both breast and prostate cancer. These two are, in fact, the most common kinds of tumor among the world population.
Prostate cancer treatment is introduced in this chapter.

2.1 Insight into Photodynamic therapy

Photodynamic therapy relies on the possibility to activate specific kinds of drugs using light. This particular drugs, called photosensitizers, are inert in the tissues, but, if irradiated, they are able to produce cytotoxic radicals, in particular reactive oxygen species (ROS), such as the singlet oxygen.[41] These are able to cause lethal damage to both tumor cells and the surrounding malignant tissue. This damage can be caused directly or indirectly, as it will be discussed in 2.2. The activation of the photosensitizer is induced by matching its excitation spectrum with the light source wavelength. On the other hand, the kind of drug that is used depends on the treatment site and the pharmacokinetics. The delivery of the drug can be topic, by spreading an ointment on the skin, or systemic, by drinking or injection of a solution.

Photodynamic therapy can be potentially used to treat all kinds of tumor and malignancies: solid tumors, dysplasias and papillomas in a growing number of organs such as brain, bladder, prostate, esophagus and skin. In addition to these, PDT is used to treat basal cells carcinomas.[6] At the state of art, some of the systems are still at clinical trial stages while some others are already an ambulatory practice, like PDT for malignant skin melanomas removal.
PDT is also used to treat formations that are not related to tumors, such as acne,[42] psoriasis, rheumatoid arthritis, localized bacterial and fungal infections and age-related macular degeneration, being able to stop or slow down the progression of the disease.[6]

As showed, the main advantage of this technique is the wide range of applicability to the treatment of a number of diseases. Besides that, PDT exhibits a number of even more pragmatic advantages, such as the relative portability and inexpensiveness. The pros that make this technique extremely attractive are even more important when the outlook is taken over the strictly treatment aspects. It is minimally invasive: in case the tumor is not reachable from the skin, the light can be delivered to the tissue by optical fibers inserted in inspection probes or needles (Interstitial Photodynamic therapy IPDT), so it minimizes, if not avoids, mutilating surgery,

as the death tissue is eliminated by the body itself. It provides a selective cytotoxicity if proper photosensitizer and dose plan are used.[43] In addition, it has a low systemic toxicity so it can be repeated[44] and it can be applied to recurrent tumors that cannot be treated with radiation therapy or other techniques anymore because it is compatible with them and does not make use of ionizing radiation.[6,43] Moreover, in many occasions, it is effective at the first treatment, since it triggers a number of biological reactions that concur to cell death and presents minimal hazard for tumor cell migration.[45] In some cases, the tissue response can be detectable even before the end of the treatment. The flexibility in the dosimetry plan makes it possible to attack big tumor masses, even if, in some cases, the effect can result only palliative.[6] It has been proved, by tests on animals, that PDT enhances the probability of survival for the tumor carrier.[44]

Along with the many advantages, PDT presents some side effects. The major ones are those experienced by the patient; namely the cutaneous photosensitivity, due to the relatively slow clearance of the photosensitizer from the body, and the discomfort and pain after the treatment, caused by the tumor necrosis, manly if deeply infiltrated tumors are treated.[43]

2.2 Photodynamic action and biological targets in PDT

The aim of photodynamic therapy is to induce cell death into tumoral tissues. This is obtained exciting a photosensitizer with light. The excited photosensitizer interacts with the tissue to form cytotoxic radicals, i.e. reactive oxygen species, that induce cell death. The ROS formation can occur by photooxydative reactions in two ways, as shown in Figure 2.1. The type I modality involves the surrounding substrate: the excited photosensitizer accepts or looses an electron, transferring it from or to molecules in the tissue, to form radicals, which, in turn, react with oxygen to form cytotoxic ROS. The type II reaction does not involve any mediator molecule; the excited state of the photosensitizer reacts directly with ground state molecular oxygen exciting it to its singlet state $^1O_2$ that is highly reactive with the substrate, so it is able to attack cells. The type II reaction is regarded to be the most effective pathway for cell death during PDT. In fact, single oxygen radical is considered to be the main cytotoxic agent since it is the cause for most of the damage to the biological tissues during this kind of therapy.[46] The ROS can react again with the photosensitizer to oxidize it, a phenomenon that is called photobleaching, decreasing its capacity to produce singlet oxygen. Photobleaching manifests itself as a reduction of the photosensitizer fluorescence and is believed to be a potential method of dosimetry since a relationship exists between the photobleaching and the singlet oxygen concentration.[21]

Therefore, the key factors affecting photodynamic therapy are oxygen concentration, light and photosensitizer doses; the treatment modality and outcome is set by the lowest among

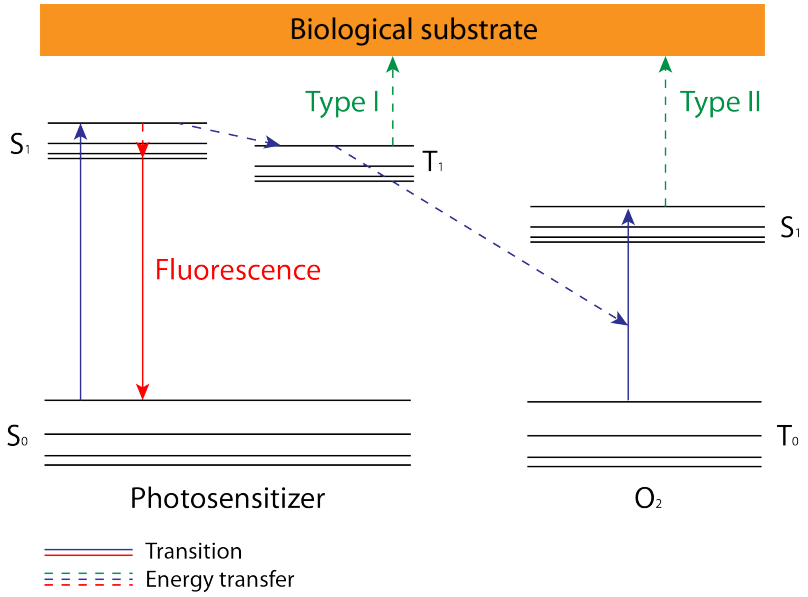

Figure 2.1: *Energy-level diagram of the type I and type II reactions for a general photosensitizer.*

these. If the oxygenation level is <2% the site is resistant to PDT[43] since no cytotoxic radicals can be formed.

The complete picture is more complex than that. In fact, parameters like tissue sensitivity to PDT[44] and wavelength penetration have an important role in the dosimetry calculations. The main issue when dealing with these parameters is their dynamic nature, photosensitizer photobleaching is one example.

Oxygen concentration, light and photosensitizer doses affect each other during the therapy therefore their change is not independent. For instance, the light and photosensitizer distribution affect the oxygen concentration, modifications to the oxygenation, in turn, can change the absorption properties of the tissue, hence the light distribution. Because of this, the outcome of the treatment can be affected not only by the total light fluence delivered to the tissue, but even its rate.[44] As a matter of fact, a wrong choice of the light fluence rate can result in an ineffectiveness of the therapy. This because high fluence rates can cause the oxygen depletion from specific sites; these sites happen to be in a state of hypoxicity, so immune to the PDT action. On the contrary, if the same total light energy is delivered to the tissue at a low fluence rate, or in fractionated irradiation times, oxygen consumption in the tissue is reduced or compensated by reperfusion. The treatment times are longer but the effect is an increased treatment response of the site.[11]

As mentioned before, PDT is a local treatment. This is due to the local irradiation of the tumor site and to the selective uptake of the photosensitizer into the tumor tissues. The main cause for this effect is the higher metabolism of malignant cells and, in the case of hydrophobic

photosensitizers, a poorly developed vasculature that is not able to avoid the leakage of fluids into the tissue structure.[11]

The effectiveness of PDT is in the ability to cause local irreversible tissue damage and rely on the body to clear itself from the death cells. This damage can be caused directly, by induction of cell necrosis or apoptosis, or indirectly, by destruction of vasculature structures and stimulus of the immune system. The long-term efficacy depends on all these processes.[47]

The main mode of cell death varies with the treatment parameters. The fluence rate is the most significant of these parameters. In fact, as the fluence rate diminishes, the prevalent cell death modality shifts from necrosis to apoptosis, since the biological response is different depending on the energy irradiated and so absorbed by the tissue.[6] This shift is caused by the progressive reduction with the fluence rate of the photodamage to cell membranes that causes necrosis.[48] Apoptosis induction rather than necrosis is, in some cases, preferred since it is not as a traumatic event for the tissue because it occurs in the tissues even if not under treatment. The consequence is that the inflammatory reactions associated with necrosis are sensibly attenuated if an apoptotic cell death modality is chosen.[48]

Indirect modalities are as important as the direct ones since they can participate to the cell death and impede the tumor regrowth. In fact, it is believed that the effectiveness of the PDT treatment in solid tumors is, in many cases, due to the destruction of the blood vessels and the consequent induction of ischemia.[49] In addition, photodynamic therapy can stimulate anti-tumor immunity since it forces the immune system to produce lymphocytes, i.e. T-cells, cytokine and vasoactive peptides as a stress response to induce the cell death and inflammation.[46]

2.3 Monitoring for real-time assessment and dosimetry

Real-time monitoring of the optical parameters during photodynamic therapy is a fundamental aspect for the treatment of tissues with light, both because the optical parameters are different from patient to patient and because they change during the treatment. The detection of the optical properties can, in fact, be vital to obtain correct calculations for the light dosimetry during both PDT and laser surgery.[50] The improving of on-line assessment and dosimetry is still a challenge and one of the main research topics in this field.

One of the alternatives to perform these measurements is to use a set-up similar to those presented in section 1.4. For interstitial PDT, different groups have been working on different designs. The two most diffused approaches are presented in Figure 2.2. One alternative is to use the same treatment sources and optical fibers for the measurements, in an interactive system that alternates the treatment times with the measurements ones. Another alternative is to insert a different optical probe into the tissue; the same measurement probe shines and

detects light at two different distances using only one needle. Both these designs cause minor distortions of the light distribution during the treatment.[29,51]

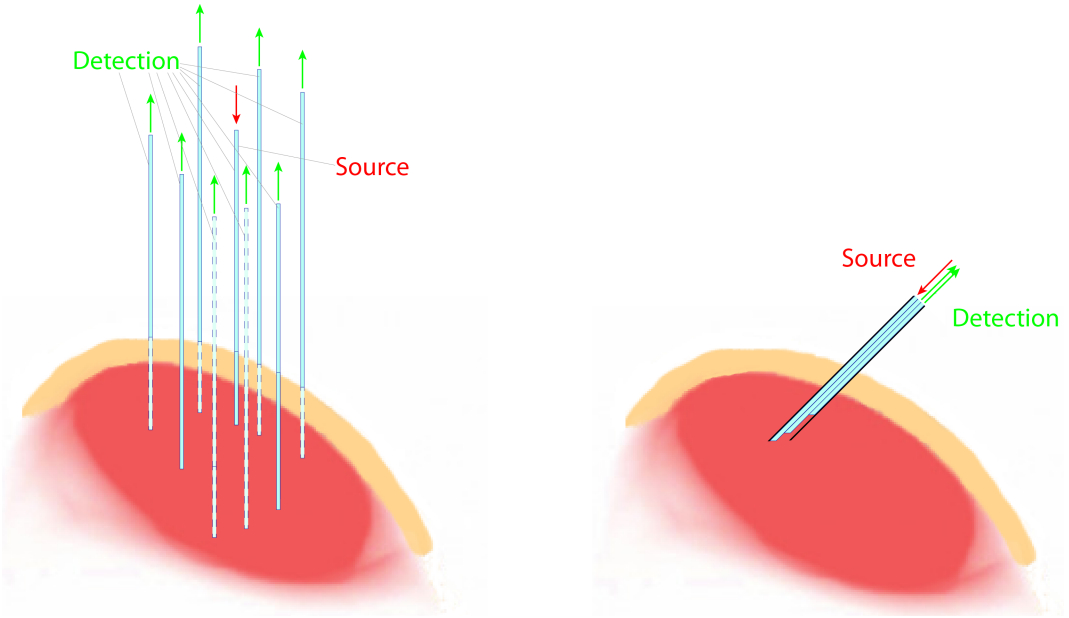

Figure 2.2: *Two possible measurement set-ups for real-time monitoring of IPDT.*
Svanberg et al.[51] (left) and G. Yodh et al.[29] (right).

The main aim of the on-line monitoring is to assess the treatment progression and eventual changes in the optical properties of the treated volume during the treatment itself. This procedure is necessary since the tissue response is very rapid and not entirely predictable because of the heterogeneity of possible reactions.[6] So its importance in photodynamic therapy lies in the possibility to adjust the treatment condition during the therapy, in order to compensate for the changes in the treated volume that can affect the light dosimetry. Along with that, it is possible to compensate for source power fluctuations and changes in the photosensitizer concentration and oxygenation, that are, as said before, dynamic parameters. These kind of adjustments can be crucial for the treatment outcome since an improper dosimetry is believed to be among the possible causes for a treatment failure.[52] In fact, if the tissue is sufficiently oxygenated and a sufficient amount of photosensitizer is provided to the tissue, the light distribution and dosimetry is the only parameter that can affect the treatment outcome. In addition, the light delivery can be considered the only variable that is almost entirely controllable by the operator at the time of the treatment.

Photodynamic therapy has a threshold behavior.[53] This threshold behavior is extremely useful when the treatment site is within a sensitive surrounding, but the fluence dosimetry needs to be extremely accurate because a too high dose can cause damages to untreated volumes;

on the other hand, a too low light dose can prevent peripheral areas of the tumor volume to be treated.[51] The treatment failure in those areas that are not provided a sufficient light fluence is thought to be due to the possibility for the cells to remove the relatively few ROS formed in the tissue and repair sublethal damages.

The real-time compensation can be considered necessary because the therapy itself can induce floatings in the treatment efficacy, because of the oxygen consumption.[29] It has been assessed that the tissue transmission can decrease over 20% during PDT treatments.[51] In some soft tissues, such as the prostate, the main cause is a change in the hemoglobin concentration, which can heavily affect the value of μ_{eff}. These decreases can be as severe as 15% of the original value. Some of the causes for this significant change in the optical properties are damages to the tissue and cells structures, such as the microvasculature, and blood pools at the fiber tip.[51] In fact, these structural changes can result in a significant increase of the reduced scattering coefficient μ_s' caused by the leakage of blood cells in the tissue.[40] As a matter of fact, the refractive index mismatch between the erythrocytes and the rest of the blood content is among the main causes for the scattering properties of soft tissues.[54]

Thermal effects can affect optical properties even at the relatively low power level used in PDT. In fact, PDT does not provoke irreversible thermal effects since no protein denaturation is induced, but the increase in temperature that PDT causes is sufficient to change the shape of the erythrocytes from disc-shaped to a more spherical shape. This affects the anisotropy of the tissue, so its scattering behavior. It has to be pointed out that changes in the reduced scattering coefficient are less severe than changes in absorption.[55]

2.4 PDT for prostate cancer

Prostate cancer is the most common tumor among the western male population.[56] It almost always develops directly in the gland, therefore it is classified as adenocarcinoma. In most cases it develops as a slow growing tumor and it is generally confined to the gland. If that is the case, the disease results symptoms free. The patient, in fact, does not experience any pain or misfunctioning due to the presence of the cancer. For this reason, in most of these cases, the tumor remains untreated and it is not life-threatening: since usually it occurs in men that are over 50 years of age, they tend to die for other causes before the tumor develops enough to be lethal.[57]

There are some cases when prostate carcinoma progresses at a rate that can be considered fast growing tumor; those carriers are the patient that are in general treated by therapy because they suffer from pain and difficulties in urinating and, most important, their condition is actually life-threatening. This because the fast growing tumor can spread its metastasis to other parts of

the body and attack vital organs such as bones and the lymphatic system. Even in these cases, the chance of survival are really high. In fact, prostate cancer can be treated quite effectively if it is not in the distant stage yet, i.e. the metastasis have already spread to the nearby region but not to distant lymph nodes, bones, or other organs yet. This condition has a 5-years relative survival rate of nearly 100%.[57]

Prostate cancer can be detected and tracked by monitoring the prostate-specific antigen (PSA) through simple blood tests; the PSA is an antigen produced by the prostate gland that is in general contained in the sperma but it can be found in little quantities in blood. Prostate cancer causes, in general, an increase of the PSA level in blood. Other more invasive techniques can be used, such as digital rectal examination (DRE), transrectal ultrasound (TRUS) or biopsy. In many cases, these tests are needed along the PSA level blood test because the latter is sensitive to a number of other factors, including, for instance the intake of aspirin and other common drugs.[57]

Prostate cancer treatment is considered successful if the tumor is eradicated from the gland and the surrounding organs do not result damaged. So the aim of the IPDT for the local treatment of this gland is to treat the whole prostate without affecting the nearby organs, in particular bladder, rectum and urethra.[6] The main issues in this application are the sparing of the sensitive surrounding organs and the fiber positioning. This latter one is solved by positioning the fibers under TRUS imaging guidance.
IPDT for prostate cancer cannot be considered a highly selective modality. In fact, there is a tendency to overdose the light or the photosensitizer dose to ensure the treatment of the whole gland, as long as the surrounding organs are safe. A high light dose can be delivered to the gland if the photosensitizer uptake is selective in the prostate.[11]

Conclusions

An overview of PDT have been presented throughout the chapter. PDT is a local selective technique that can be applied to the treatment of cancer states. The main factors affecting the treatment outcome are the oxygenation of the tissue, the light and photosensitizer dosimetry. Because of the fact that these three are dynamic and interdependent parameters, a proper online monitoring of the process, that enables adjustments in the light dosimetry, is fundamental for a positive treatment outcome and the recovery of the patient. Cells die by different pathways: necrosis, apoptosis, destruction of the vasculature system and activation of the immune response. The predominant cell-death modality is mainly determined my the light fluence rate: high fluence rates bias the cell-death towards necrosis while low fluence rates towards apoptosis. Different modalities are preferred for different applications.

In IPDT for the treatment of prostate cancer, the light is delivered to the prostate using optical fibers. These are positioned in the gland under TRUS guidance and the light dosimetry is calculated in respect of the measured optical properties and the fiber positioning. During the therapy, the whole gland is treated as tumoral tissue so, for this particular case, PDT cannot be considered a selective technique anymore.

Chapter 3

PDT system development and characterization

The core part of this work, the development of an all optical circuit for the light delivery, is illustrated in this chapter. Section 3.1 gives an overview of the current SpecraCure AB IPDT system and of the all optical alternative that has been proposed in this project. Each part of the system, from the light sources to the detection, is described in reasonable detail. The reasons behind the choice of this particular design and the advantages that this approach have in respect of the previous system are also explained throughout the chapter.

The dose plannig of interstitial photodynamic therapy requires a system that allows to estimate the optical properties of the volume under treatment during the therapy session. The measurement technique must be able to evaluate the optical parameters in real-time, without perturbing the treatment. The way SpectraCure AB achieves this goal is to use interstitial fiber optic techniques to take steady-state multi-distance measurements of the fluence rate.

SpectraCure AB developed a system which is capable of taking these kind of measurements during the therapy session. This is achieved by means of a computer controlled mechanical switch that sets the system in treatment or monitoring mode.

The aim of this project is to propose an upgrade to this system, designing an optical circuit to replace the mechanical switch. The possibility to use fiber optics and the introduction of a module based approach, gives this system a great design flexibility; its strength lies in simplicity and relatively reduced costs.

The new proposed system has been developed with the idea to allow simultaneous therapy and monitoring and, at the same time, provide as much information as possible. It has been

designed to take only fluence measurements, using all the fibers as sources all at once, but the possibility of assessing additional important parameters, such as the oxygen saturation, has been kept open. This upgrade, in fact, can be achieved by making just some adjustments to the design.

These modifications will be discussed, along with the system, throughout this chapter.

3.1 Global description of the systems

The main aim of this project is to design an all-optical passive circuit to eliminate the mechanical part of the current SpectraCure AB PDT system and to allow simultaneous treatment and monitoring. In particular, a module approach has been adopted for the design of the new circuit, meaning that the complete system is built repeating the module designed for the single channel. The global scope of the measurements is the same in the two systems: perform multi-distance steady-state measurements of the fluence rate to assess the value of the effective attenuation coefficient μ_{eff} using the treatment fibers inserted in the tissue. On the other hand, the new system would enable to broaden the measurement possibilities because the design of each channel is expandable to have multiple measurement sources. This allows the operator to obtain information on the tissue status, virtually, for every measurable property. The original idea behind the extensibility of the module on the source side is to leave the possibility to perform measurements to monitor the blood oxygenation open. Few other examples are estimation of water, lipids and blood content.

SpectraCure AB intersitial photodynamic therapy system

SpectraCure AB developed a commercial system for IPDT for prostate cancer. The system developed and tested for this work is meant to be the proposed follower of the system object of this section, of which it keeps the working principle and the dosimetry and therapeutic aspects.

A flow chart of the treatment procedure is presented in the right part of Figure 3.1.
The fiber positioning is performed under ultrasound guidance. A first positioning is proposed after an initial dosimetry plan based on a TRUS 3D image of the gland. After the insertion of the 18 fibers, the TRUS imaging is repeated to correct the information about the real fiber positioning and adjust the dosimetry plan to the measured optical properties. The measurements are performed using a multi-distance configuration. This stage is followed by an alternation of treatment times and measurement times. The measurement times are eventually followed by the calculation of the new dose plan, if the optical properties of the tissues have been changing so much that an adjustment is necessary for the positive outcome of the therapy. The dose plan

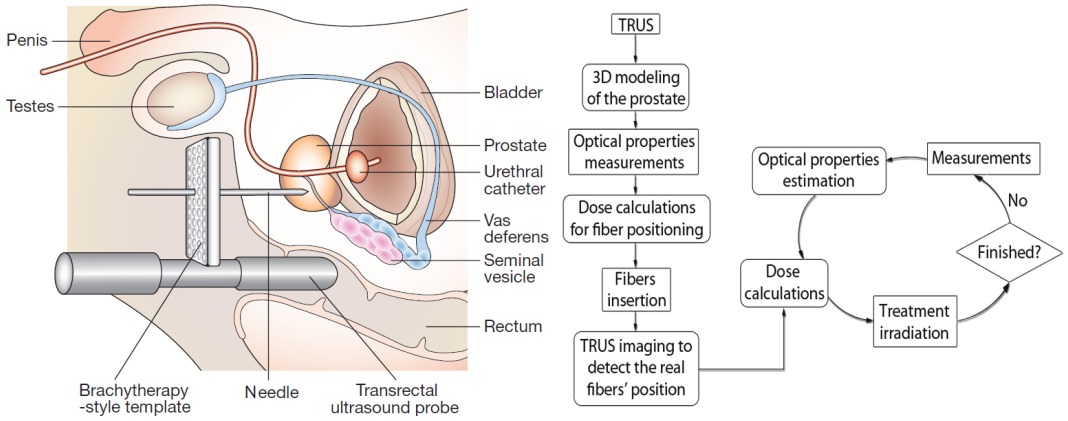

Figure 3.1: *Sketch of the section of the body during treatment, with fiber positioning and TRUS[11] (left) and a flow chart of the treatment procedure of the SpectraCure AB IPDT system[58] (right).*

and all its changes are graphically displayed on the monitor and must be approved by the doctor before the treatment can proceed.
The results of the therapy are assessed, in general, by MRI or biopsy.

The current circuit

A block scheme of the functionality of the current SpectraCure AB IPDT system is shown in Figure 3.2. As assessed before, the system can work in treatment or monitoring mode. During the treatment mode, the laser modules shine light at a wavelength of 690 nm in up to eighteen fibers. The sources are coupled to the patient fibers through a mechanical switch that enables to change the mode from one to the other. In monitoring mode, the measurements are performed in steady state by delivering the light in one single fiber at the time and collecting the diffused light at six neighboring fibers. These are coupled to the detectors, spectrometers, by the same mechanical switch. The measurement is repeated using each of the eighteen fibers as source.

The core of the system is the mechanical switch that allows the machine to work in one mode or the other. The downside with this set-up is that it is fairly expensive, big and complex, both in its mechanical parts and from the drivers point of view. For the same reasons, it is not flexible to changes in terms of sources and number of channels.

Another relatively weak point of the whole system is that it can work either on therapeutic mode or on monitoring mode. This means that the treatment is halted when the measurements are performed. As assessed, this is only a minor problem because a fractionated treatment time

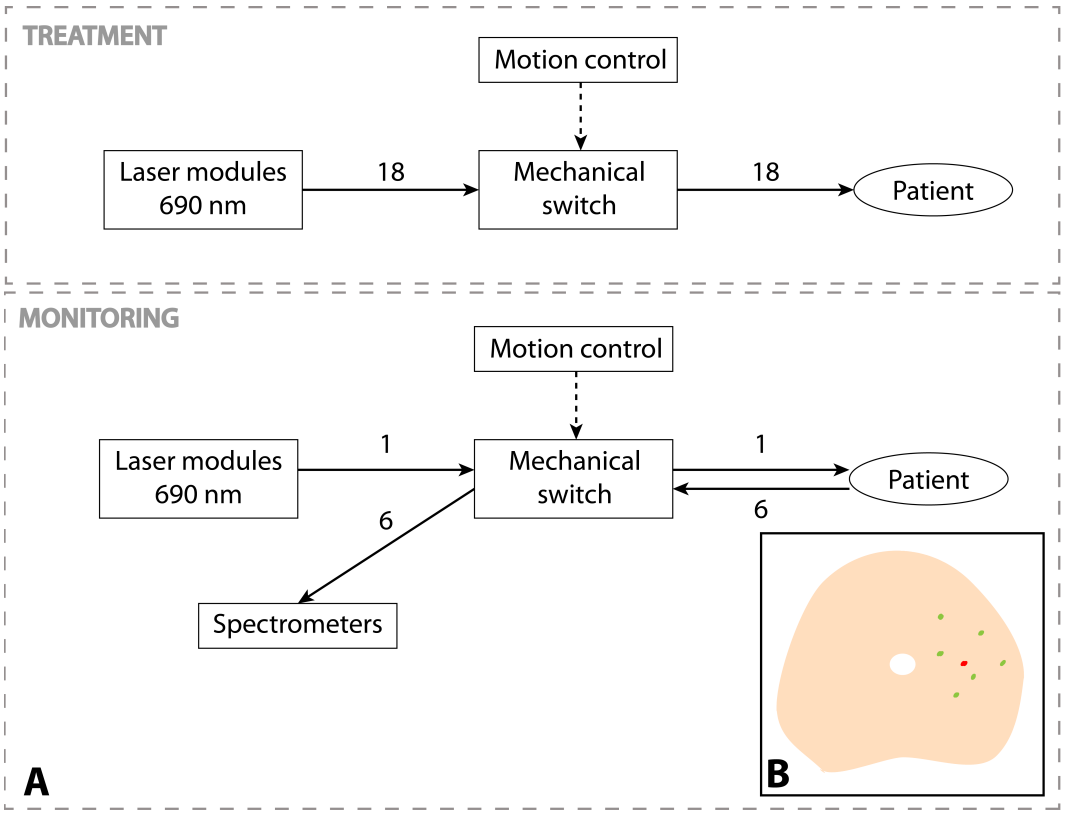

Figure 3.2: *Block scheme of the current SpectraCure AB PDT set-up (A) and a sketch of the fibers during the monitoring mode(B).*

Source fiber (red) and detection fibers (green).

is useful for the gland reperfusion and reoxygenation, that is essential for PDT. On the other hand, the total time during which the patient can be under treatment is limited, about four hours. This restrains the monitoring times and so the accuracy of the measurements. The treatment times, in fact, cannot be reduced. According to this argument, a system that allows to perform measurements also during the treatment times has the potential to give better optical properties estimation and, potentially, better treatment outcome.

The proposed new circuit

A schematics of the proposed system is presented in Figure 3.3. The single module functioning is fairly easy. The light is delivered to the patient through the common end of a bifurcated fiber. One of the legs is connected to the detection module, while the other is connected to another bifurcated fiber to allow the simultaneous delivery of the light from the treatment lasers and the one from the monitoring lasers, on each channel.

Each measurement channel is tagged by a modulation frequency. This allows to estimate the effective attenuation coefficient μ_{eff} using, ideally, all the fibers as sources at the same time. In

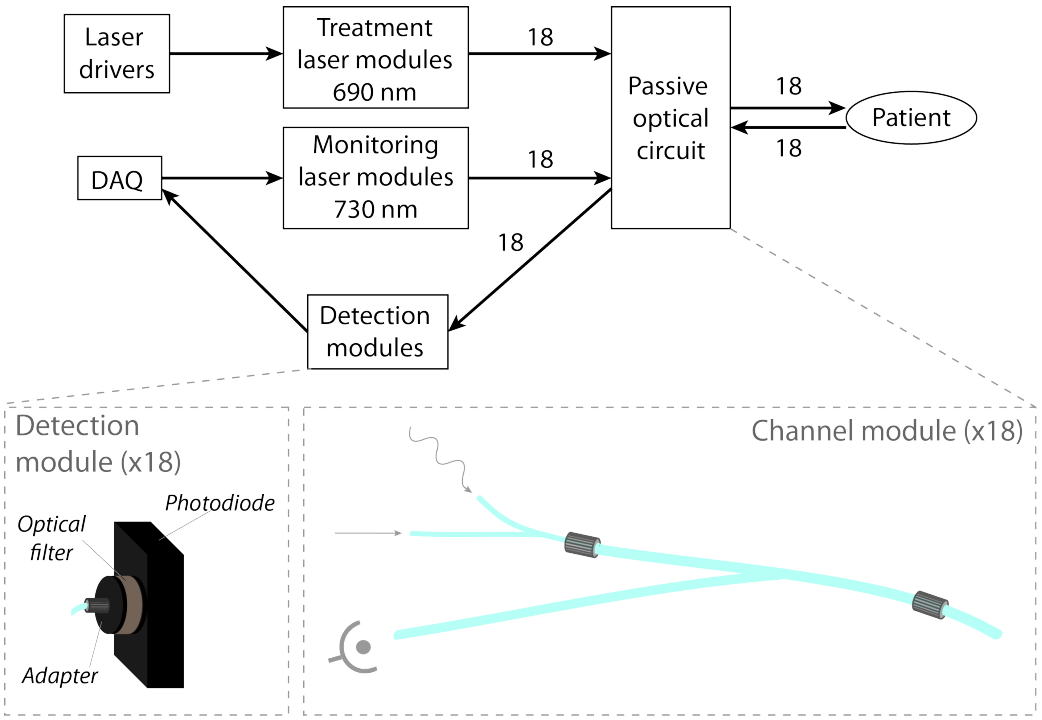

Figure 3.3: *Overview of the proposed set-up. A block scheme of the interaction between the module and sketches of the single channel and detection modules.*

fact, the modulation frequency tag enables to discriminate which part of the signal comes from each fiber. As it is easy to understand, this approach increases the robustness of the optical parameters assessment because of the larger amount of data that can be collected in the same measurement duration, if compared to the system presented previously.

The detection module is basically an optical filtering system followed by a photodiode. The filtering system is necessary to prevent the photodiode saturation and to lower the noise level; it filters out the signal coming from the treatment lasers, both the backreflected and the one collected from the other sources.

A DAQ is used to control the monitoring process. The analog output channels are used to drive the lasers, while the analog inputs are used to register the signal coming from the photodiode. This signal is further processed by the software to calculate its spectral components and thus the optical parameters of interest.

As addressed before, this circuit is module based. The connections to the sources for each channel are, in turn, modules that can be expanded or changed to have, virtually, a customary number of sources. This particular design aspect makes this system extremely simple and versatile to changes in terms of number of channels and sources. On the other hand, it must be pointed out that an increase in the number of monitoring sources implies, by itself, an increase

in the complexity of the system, both from the software and from the hardware point of view. In fact, if sources at different wavelengths are used, it is necessary to either replace the photodiode with a spectrometer, or introduce a higher number of modulation frequencies to be able to discriminate the additional sources.

Other advantages of this system are space and costs wise. In fact, it avoids the use of the spectrometers, replaced by the cheaper and smaller photodiodes, and the complex and big mechanical switch with the motion control module. In addition, the detection is connected with the software by means of ordinary DAQs, which are relatively cheap and can interface different channels simultaneously.

Each part of the system is described in further detail throughout this chapter.

3.2 Light sources

The light sources are pigtailed laser diodes (LD) at 730 nm for the monitoring and at 690 nm for the treatment. The treatment lasers are left unaltered from the previous set-up since no aspect of the treatment has been changed. This parameter is, in fact, set by the specific photosensitizer used.
The criteria behind the choice of the monitoring wavelength are due to the emission properties of the photosensitizer, the optical properties of blood perfused tissue and what is available on the market. In fact, the original idea was to have a laser at 710 nm, which corresponds to the emission peak of the photosensitizer used in this application, so that the monitoring laser light and the fluorescence would have been experiencing the same optical properties. A wavelength close to that value is convenient even because the absorption due to the presence of blood has a minimum in that region, one can refer to Figure 1.6. The shift to 730 nm has been forced by the technical choice of having a LD source. In fact, there are only few materials available that have a gap in the range between approximately 690 nm and 800 nm. It is possible to find LDs that have a nominal wavelength of 710 nm or 715 nm but the uncertainty over the wavelength is up to $\pm$10 nm from the central one, which, in the worst case, would not have left enough margin for the optical filtering to be effective only on the treatment signal.

The choice of using a LD source is a general tendency in photodynamic therapy. This is because they are relatively cheap, have a stable output and are reliable in the clinical environment. In this case, the main argument for picking a LD source is that they are easy to modulate. In fact, the modulation is achieved by feeding the diode with a modulated input voltage or current. In this proposed set-up, this feature is obtained using the analog output of a simple DAQ. The modulation of the laser input is covered in subsection 3.4.3.

The 730 nm source can be replaced or come abreast by a white light source if chromophore concentrations or oxygenation are to be monitored, for example.

3.2.1 Modulation frequency encoding

As discussed before, the frequency modulation of the monitoring sources has been introduced to label each channel to allow the measurements on all channels simultaneously. The general idea is, therefore, to have eighteen different modulation frequencies that characterize each channel; the signal at the detector results as a composition of these signals. Photodiodes are sensitive to the light modulation, hence this information is translated into a voltage signal, which is then processed to discriminate the signal coming from each source.
The same modulation can be used to separate the emission from the monitoring light so that the two can be measured at the same time, avoiding the need for a spectrometer, as the non-modulated light from the treatment lasers is filtered in any case to prevent the photodiode from saturation. This feature is not covered in this project since there are some issues due to the modulation offset and the duty cycle of the LD that would have required more time to be solved. However, it is important to mention such a potentiality for further developments.

The system is based on a property that is common to the frequency domain measurements: when the modulated light propagates through highly scattering tissues, it moves with a coherent front forming a photon density wave (PDW).[4] In this way, the light is able to keep the modulation tag at each point in the media.

The modulation frequency encoding presents some issues. The main one, which is the same that affects the possibility to monitor the emission of the photosensitizer, is the duty cycle that characterizes the modulated light from a LD. The duty cycle of the laser used in the system is about 60%, this means that the modulated part of the light is only 60% of the DC component; an example is shown in Figure 3.4 for a modulation frequency of 30 Hz. This limitation affects the maximum distance at which the modulated part of the signal can be detected because most of the power is "wasted" in the "untagged" DC component. Hence, the signal detected at relatively long distances is distorted by the noise since their levels are comparable, therefore unusable.

The second main issue is exactly the noise. This problem can be partly bypassed by a proper choice of the spectral range in which the modulation frequency should be chosen. In this case, a suitable part of the spectrum would have been the one between 250 Hz and 300 Hz. A modulation in this frequency range gives a large enough separation between the harmonics of the signal to allow to fit all the channels with a proper spectral separation. However, a far lower

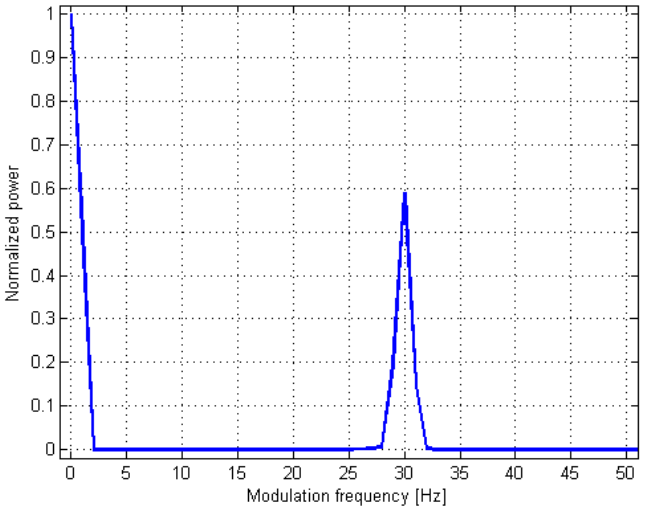

Figure 3.4: *Spectrum of the 730 nm LD output, being modulated at 30 Hz. The values are normalized over the DC component amplitude. The duty cycle of the LD is 60.19%*

modulation frequency have been used in the experiments because of limitations imposed by the specifications of the DAQ that was available at the moment.

3.3 Delivery fibers

For the design of the connection between the sources, the patient and the detection module, the focus has been kept on developing a system that is simple, cost-effective and efficient. The best solution has been found searching the market for the fiber designs which best suited the system and adapting the technical specifications to what is available off-the-shelf or with a minimum level of customization, in order to achieve the best compromise between these aspects.

The first goal, simplicity, has been accomplished by adopting a model based approach, while finding a compromise between the other two aspects, affected mainly the choice of the kind of optical device used, a basic optical splitter, and the design specifications in terms of fiber core diameter and numerical aperture.

3.3.1 Channel module

The channel module design, first presented in Figure 3.3, is shown in more detail in Figure 3.5. This design has been preferred before the other option, a circulator, mainly because of its price and availability in the wavelength range 600-800 nm. A circulator is, as a matter of fact, a good solution to this problem since it drives the light from one of the legs to the common end and back

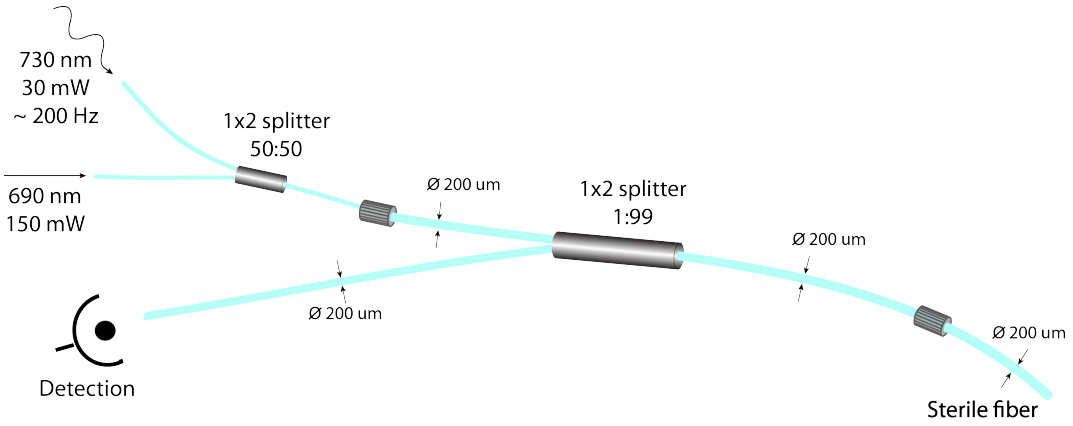

Figure 3.5: *Design of the channel module.*

to the other leg avoiding leakages between the two legs since it is an highly directional device.

A large core bifurcated fiber is used to deliver the light to the sample and then direct it back to the detector. In the optimal case, the optical splitter has unbalanced splitting ratio of 1:99 to achieve that most of the collected light is directed towards the photodiode. This aspect becomes more and more important the further away the collection fiber is from the source fiber since the signal is strongly attenuated by the propagation in the tissue. The detected monitoring signals have a power in the order of few nW, so the less the signal is lost, the better the parameters estimation is because it is possible to measure the signal at longer distances.
The silica fiber have a numerical aperture of 0.22, one of the standard commercial value for relatively thick optical fibers, and a suggested core diameter of 200 μm, with a ratio between the core and the cladding diameter of about 0.91; the reasons and the open problem behind the proposal of reducing the fiber core diameter are discussed in the next chapter.
There are no special requirements on the length of the three ends because the splitter serves only as a a guide for the light and not as a connection between three fixed points. The standard value usually is 1 m per end. In addition, the eventual instability of the modes in the coupling stretch is not an issue once the losses have been measured since the splitters are included in a black box that is isolated by the structure from the surrounding.

The sources deliver the light into the legs of a second splitter that is coupled to the source leg of the primary one. This second bifurcated fiber has no requirement in efficiency or core diameter since high losses are tolerable at the source side. Therefore, a standard, relatively cheap, bifurcated fiber with a splitting ratio of 50:50 can be used for this purpose. The slitter must have the same numerical aperture of 0.22, as the primary one, and can have a core diameter of 100 μm or 65 μm, depending on the core size of the fiber coupled to the laser output. As mentioned before, this splitter can be expanded or changed to a 1xM splitter to allocate more than two laser

sources. The other leg of the main splitter is connected to the detector unit, and the common end to a bare end fiber, to the sample.
All the fibers are multi-mode because there are no requirements on the beam profile and are generally cheaper than the single mode fibers.
All the different parts are put together by means of SMA905 connectors. Another type of connector can be used, keeping into account the difference in losses that another kind of connector would imply.

3.4 Detection and signal processing

The detection module is composed of three parts: filtering, detection and acquisition. The acquisition of the signals is followed by the processing: the signal undergoes Fourier spectral analysis that is performed and displayed by a Labview program.

The characteristics of these three parts and the Labview code are presented in this section. In particular, the subsection on the DAQs explains both their use as a signal recorder and as a signal generator, as mentioned in section 3.2.

3.4.1 Optical filtering

Monitoring the optical parameters during the treatments implies a high level of light power coupled into all the fibers because of the treatment lasers. The magnitude of this component of the signal can cause the saturation of the photodiode, since this latter one have been chosen to be sensitive to the smaller monitoring signals. Therefore, optical filtering before the detection is necessary.

The original idea was to use two fiber coupled collimators and a filter between them. The collimator is a dual device, hence, one collimator is used to collimate the light from the bifurcated fiber and another collimator of exactly the same kind collects the light to couple it back into an optical fiber towards the photodiode. However, this configuration is neither optimal nor needed in this system because the detector is a large area photodiode. This device allow to position the filter directly between the fiber and the photosensitive surface of the junction since all the light coming from the fiber can be collected after the filtering despite the divergence of the light beam that exits the fiber. Such a solution has many advantages: it is compact, more efficient since no additional losses are introduced, cheaper and does not require alignment. A possible configuration is shown in Figure 3.6.
The suggested filter is a long-pass interference filter with a cut-off wavelength of 700 nm and a steep transition to band, such as the Thorlabs FEL0700 which has a transmission at 710

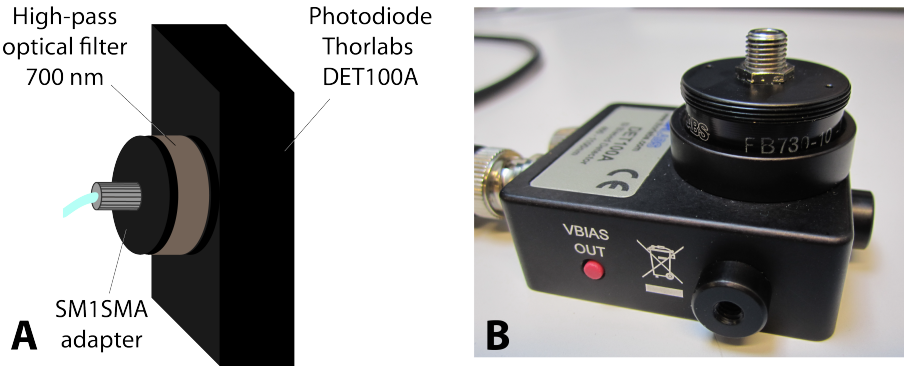

Figure 3.6: *(A) Schematics of the detection part.*
(B) Picture of the arrangement for the detection with the filter used in the experiments.

nm and 730 nm of >80% and a transmission at 690 nm, in the stop-band, of approximately 0%. The transmission characteristic of this filter is shown in Figure 3.7. One possible issue that could arise with a filter of this kind is the non-perpendicularity of the beam in every point and a resulting lower rejection of the light in the stop-band. This problem has to be further investigated with the manufacturer company. In fact, this effect could be deniable since the numerical aperture is not that big. In case this effect is not minor, a collimator can be coupled to the fiber before the filtering. The same problem does not arise if a dichroic color filter, such as the one used in the experiments, is used.

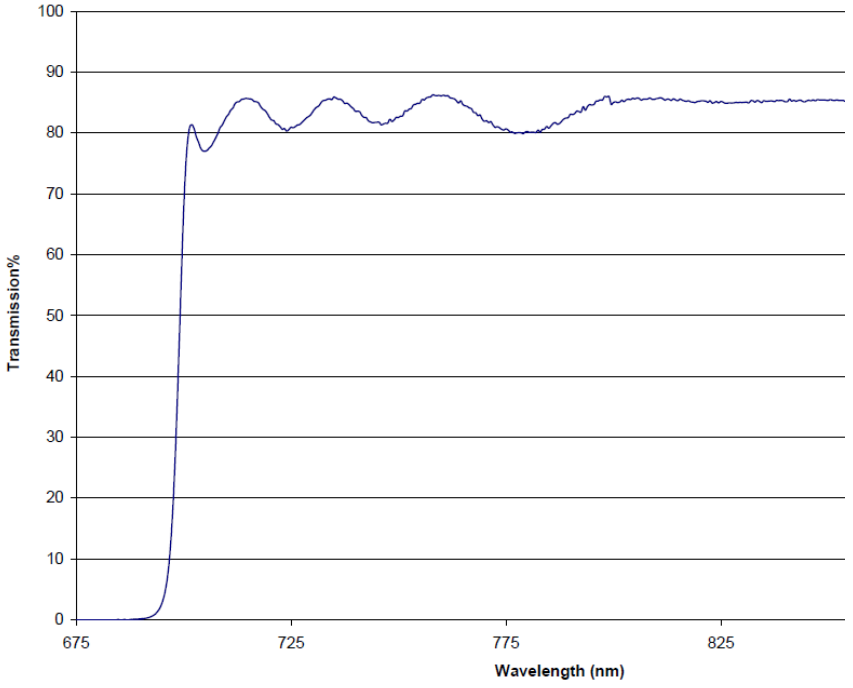

Figure 3.7: *Transmission curve of the filter Thorlabs FEL0700.*[59]

3.4.2 Detection

The light is detected by a large area photodiode, for the measurements in chapter 4.2 a Thorlabs DET100A photodiode have been used.

This photodiode is a Silicon PIN junction that is sensitive within a range of 700 nm, from 400 nm to 1100 nm. The peak response is 65 A/W at 970 nm. The response time is in the order of 40 ns and the dark current is 600nA at the most, which makes it suitable for this application. The output linear range is from 0 to 10 V, which corresponds to a maximum detectable power of 0.245 mW at 730 nm. A similar detector with a larger dynamics is suggested for the final system. An alternative is to filter all the non-modulated components of the light before the detection so the photodiode does not suffer saturation.

The photodiode has been characterized at the wavelengths used in the measurements, since the spectral responsivity curve provided by the manufacturer, in Figure 3.8, is not detailed enough. Figure 3.9 shows the photodiode response at the two wavelengths involved in

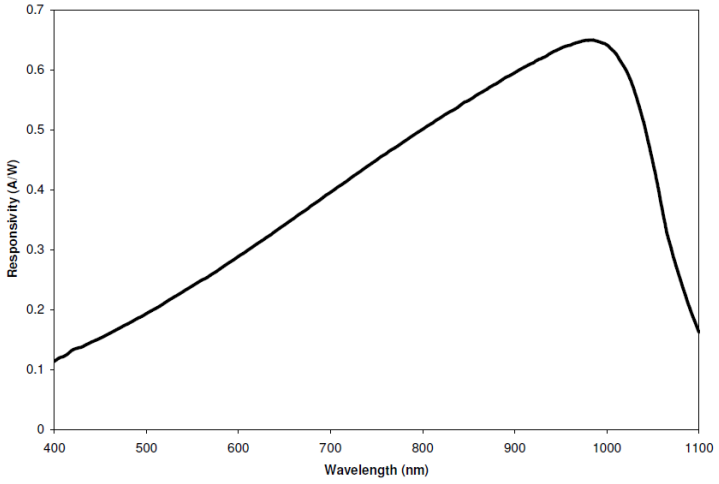

Figure 3.8: *Typical DET100A spectral responsivity curve.*[60]

the measurements. The responsivity of the photodiode resulted increased with the wavelength, as predicted by the spectral responsivity curve provided by the manufacturer. The conversion factors to translate the output voltage value into power values are resumed in Table 3.1.

In case multiple wavelength measurements are required, for example to monitor the oxygen saturation or other chromophores concentrations, the photodiode must be replaced by a spectrometer or a further modulation frequency encoding must be applied to distinguish all the different monitoring sources coming from the different channels. This approach is, of course, more complex because of all the implications that such a modulation encoding demands.

Wavelength [nm]	Conversion factor [W/V]
690	$2.135 \cdot 10^{-8}$
730	$2.435 \cdot 10^{-8}$

Table 3.1: *Conversion factor from output voltage to light power of the photodiode Thorlabs DET100A.*

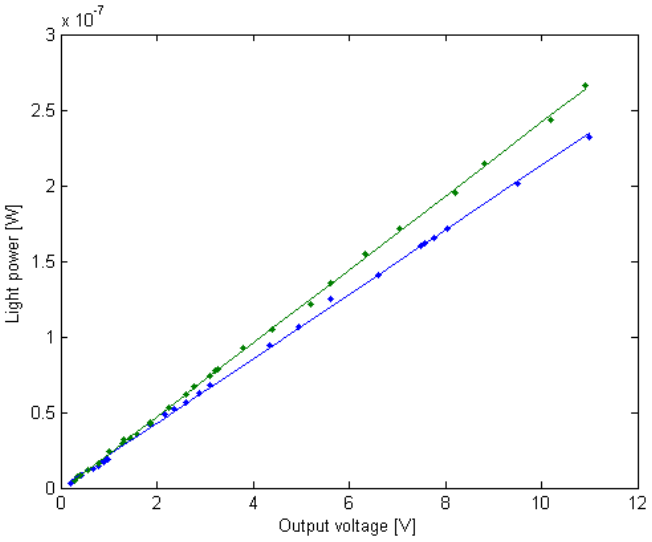

Figure 3.9: *Photodiode response at different wavelengths. 690 nm, P(V)[W]= 2.135e-8 V (blue) and 730 nm , P(V)[W]= 2.435e-8 V (green).*

3.4.3 Acquisition and processing

Data acquisition boards are used to generate the input signal for the monitoring lasers and to acquire the signal from the detector. It is, in general, possible to use the same DAQ for a number of channels both for the acquisition and the signal generation. In fact, some of the USB-DAQs are able to host up to 4 channels in analog output, which is the critical mode of use. This is because the ports of the DAQ are used sequentially, so the speed of the board in terms of output rate must be divided among the ports of the same kind. For instance, the DAQ that has been used in the experiments, NI USB-6009, has a sample rate relative to the output ports of 150 Hz, so it has been possible to use it to drive only one of the lasers at a frequency of 30 Hz or 40 Hz. The same limitation applies on the samples to read but, in this case, the limit in the sampling rate is generally a lot higher so even a DAQ like NI USB-6009, is able to handle few channels at the same time without significantly affecting the measurements.

The DAQ is also equipped with digital inputs and outputs, but these are not of interest in this

application.

The choice of using a DAQ as modulator is significant from the costs point of view because they are in general cheap, and, even if a more expensive one is needed to have the possibility to drive more than one channel, the costs are divided among the channels, so the cost per channel is still low. Moreover, they can be easily interfaced with software.

At this stage of the system development, it has been convenient to work with an USB-DAQ because of its flexibility and ease of use. On the other hand, since the whole system consists of 18 channels, another cheaper approach can be adopted if PCI DAQs are used. The main idea of the final system is to have one DAQ that handles the modulation of all the eighteen channels, at a modulation frequency in the range of hundreds of Hz, and other PCI-DAQs that acquire the signals coming from the photodiodes. A possible solution will be presented in the Conclusions.

Labview program for signal generation, detection and spectral analysis

The developed Labview program consists of two parts, the detection part and the signal generation part.

The signal generation is achieved by driving the two DAQ Assistants with a sinusoid waveform. All the parameters of this waveform are customizable and can be changed by the user at his/her will by means of three controls: modulation frequency, amplitude and offset. Each signal has a different set of controls.

The detection part of the code acquires the signal from the photodiode at the analog input of one DAQ, and the signal that is fed to the lasers at two inputs of the other DAQ. Therefore a total of 3 different signals are acquired. These are sent to the signal analysis part of the code that calculates their fast Fourier transform using Hann windowing. The FFTs, along with the original signals, are displayed on graphs and eventually saved on a file, whenever the user requires it. In fact, it is possible to determine which acquisition to save and with which file name, directly from the graphic interface, shown in Figure 3.10.

The acquisition parameters have been adjusted to have a measurement time of 5s per acquisition, refer to Table 4.3. The graphic code and some facts are given in appendix D.

Conclusions

The all optical system designed during this project in order to replace the complex mechanical switch used in the current SpectraCure AB IPDT system has been described in some detail. The circuit is module based and have been presented dividing the fundamental module in three main

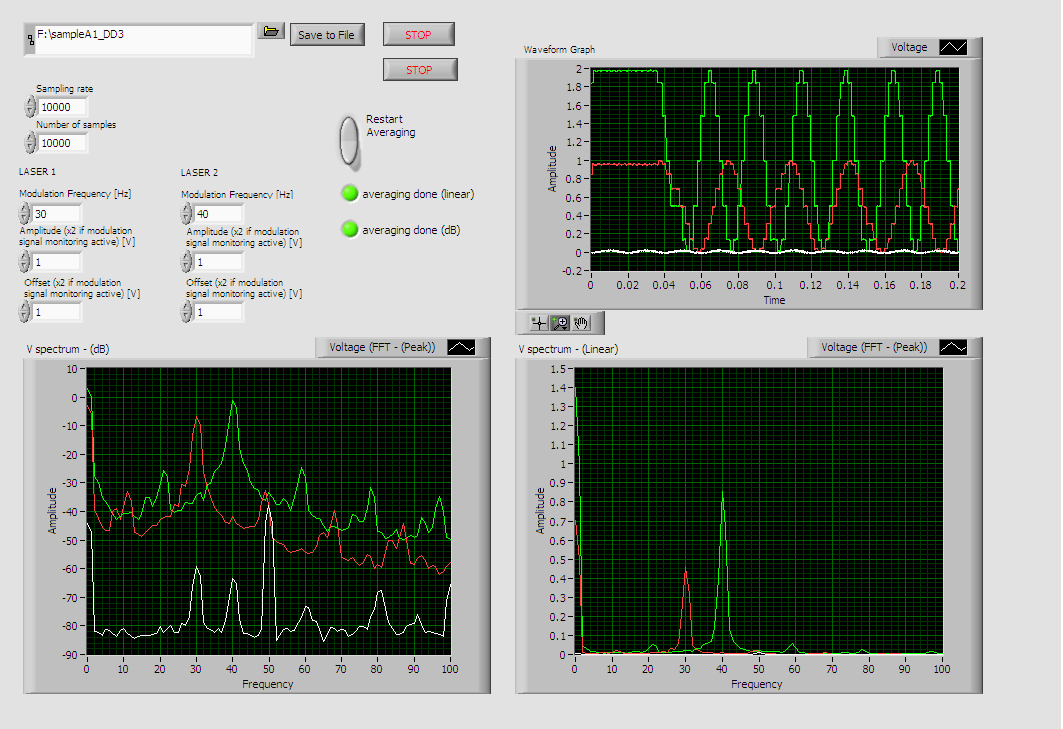

Figure 3.10: *Labview program interface.*

Inputs controllable by the user (top left), waveform graph of the acquired signal (top right) and spectrum in dB (bottom left) and linear scales (bottom right).

parts: the light sources, the channel and the detection. The characteristics that are required by each single component have been emphasized in respect of their function in the whole system and some costs issues have been taken into account. In particular, the choice between different alternatives for each part of the module have been done finding a trade-off between functionality and costs. The sources have been chosen to be laser diodes due to their suitability to the clinical environment, their volume and their price. In fact, one of the main goals of the new design has been to reduce both the complexity and the space occupied by the system. The channel is a graft of two different 1x2 splitters to be able to have sources and detection simultaneously on the same passive channel. The detection is obtained using a photodiode connected to a DAQ to record the light signals coupled into each channel. A DAQ is used also to modulate the monitoring lasers at 730 nm. In fact, the main innovation of this all optical system is the possibility to detect, at each point, the monitoring signals coming from all the eighteen channels during the treatment. This feature has been obtained introducing a modulation frequency encoding that tags each channel and a filtering the treatment light with an optical filter to avoid the photodiode saturation. Throughout the chapter, it has been pointed out how this designed is flexible to changes and how most of the component can be replaced to enhance the measurement possibilities of the system; one example for all is to monitor the oxygen saturation during the treatment.

Chapter 4

System validation

The measurement set-ups and the results of the system evaluation are discussed in this chapter. Section 4.1 presents an overview of the measurement configurations and the characteristics of the hardware used for the experiments. Section 4.2 is divided in two parts: the results of the core diameter experiments are discussed in the first part, while the ones about the estimation of the value of the effective attenuation coefficient, are given in the second part.

The system presented in chapter 3 had to be tested to evaluate its performances and to properly set the hardware parameters. The focus has been kept on different aspects: the collected light by the fiber, the ability of the set-up to estimate the effective attenuation coefficient correctly and how well this parameter can be measured.

The discussion about the possibility to use fibers of smaller diameter to collect light has been based on the idea that it cannot be taken for granted that it is more convenient to use fibers with a larger core in respect of fiber with smaller core, especially for interstitial measurements. As it will be presented throughout the chapter, there are some pros and cons in using smaller core fibers. Some experimental results brought up that the collecting efficiency of a fiber might not depend only on collection area but even on the medium in which the light propagates. This aspect needs to be further investigated because the experimental results are in contrast with the results from the simulations. A more complete discussion follows in the chapter.

Regarding the other aspect of the system validation, statistical approach has been adopted for the evaluation of the goodness of the estimation of the μ_{eff} so the results have been expressed in terms of deviation from the predicted value as well as in terms of standard deviation and relative error, to asses the repeatability of the measurement results.

Some modifications have been made to the system configuration to be able to perform this evaluation with the available hardware. These are presented and explained, along with the results,

in this chapter.

The proposed set-up has been evaluated to be simple and efficient.

4.1 Evaluation methods and measurement set-ups

The different characteristics introduced by the proposed system have been tested and evaluated by means of different experimental measurements and simulations.
The effect of the reduced core diameter has been assessed both experimentally and using Monte Carlo simulations. The Monte Carlo for Multi-Layered media by Jacques et al.[61] have been slightly modified to introduce the effect of the numerical aperture of the fiber.
The measurements for the evaluation of the possibility to assess the effective attenuation coefficient using the modulation frequency encoding have been performed using two simplified set-ups for two different parts of the design. One has been used to test the optical filtering of the treatment light and the other one to evaluate the possibility to use more than one channel as source at the same time. These simplifications have been necessary because of costs and, more important, time issues. As a matter of fact, this project is a proof-of-principle study so these methods have been regarded to be appropriate to simulate the functionality of the final system and evaluate the goodness of the design. In fact, the simplifications that have been made do not affect the object of the single experiment itself, so the results are not fundamentally influenced by them. This aspect will be further clarified for each single experiment.

An overview of the different set-ups and methods will be presented in this section.

4.1.1 Evaluation of the effect of the fiber core diameter on the detected light

I have been suggesting the possibility to change the fiber core diameter from 400 μm to 200 μm, based both on costs and efficiency criteria. From the economical aspects, smaller core fibers are cheaper and more available on the market as non-customary products.

The technical aspect is a bit more complex. It has been proved that the collection efficiency of an optical fiber depends mainly on the optical parameters of the medium and on the numerical aperture (NA) of the fiber.[62] In fact, if isotropically diffused light is to be collected, the collection efficiency of the fiber is proportional to the squared sine of the acceptance angle, i.e. the numerical aperture. The same behavior applies for a bony structure. The situation is a bit different in the case of soft tissues because of their lower effective scattering coefficient. Photons that are collected by the fiber come from deeper points in the tissue, because the main pathlength is longer.[62] In addition, the reflected photons at the boundary are an important part of the collected signal if single fiber measurements are performed, i.e. when no fiber bundles are used for the collection. In this case, due to the strong anisotropy, the reflected photons that happen to be

scattered with a direction included in the half-plane towards the fiber tip have a higher probability to be scattered with a small angle in respect of the normal to the boundary, therefore within the cone of acceptance of the fiber. As a consequence of this effect, the collection efficiency of a fiber in these tissues can be two- or three-folds higher and cannot be entirely predicted by the NA anymore. In fact, if smaller core diameter fibers are used to take measurements over soft tissues, the collected light diminishes, but not directly proportionally to the area. For the fiber cores considered in this work, the collected light can diminish of more than 30%. Some measurement and simulation results are given in section 4.2.1.

The smaller number of photons detected by a 200μm fiber is compensated by another effect in interstitial measurements. In fact, if smaller optical fibers are used, it is possible to use smaller needles that cause smaller blood pools. For instance, assuming that a 24G needle is used to insert a 200μm fiber and a 20G to insert a 400μm one, and that the effect of the blood pools can be estimated by the ratio of the needles radius, i.e. the blood pools are half spheres with a diameter corresponding to the needle diameter, the ratio of the light attenuation due to the blood pooling in these two cases is estimated to be 0.62. The same argument applies when calculating the light lost at the source for this effect. This value will be used in section 4.2.1 to consider the effect of the blood pooling in order to evaluate this same fact with Monte Carlo simulations.

Following this reasoning, it is plausible to assert that for interstitial measurements, a fiber with a reduced core diameter could be as efficient as a fiber with a larger core diameter, given that the two diameter size are comparable as in this case. The price to pay for the reduced costs is the more demanding precision that is required for the alignment and coupling of these fibers.

The effect of the fiber core diameter has been evaluated looking at the light collected by the fibers. The Monte Carlo simulations have been modified to calculate this parameter as the total number of photons that get into the fiber like medium within the fiber core and at an angle smaller than the acceptance angle. In the experimental measurements, the collected light has been measured both by using an integrating sphere, to have a diffused source, and in reflectance configuration over an arm, refer to Figure 1.4, to evaluate the effect of the propagation in biological tissues.

Modified MCML

The Monte Carlo for Multi-Layered media have been modified according to the flow chart presented in Figure 4.1. The numerical aperture is taken into account as a criteria at the boundary: if the photon is not reflected back to the bulk, its angle of incidence is evaluated. If this angle is within the acceptance cone, the photon is transmitted to the fiber, and therefore recorded,

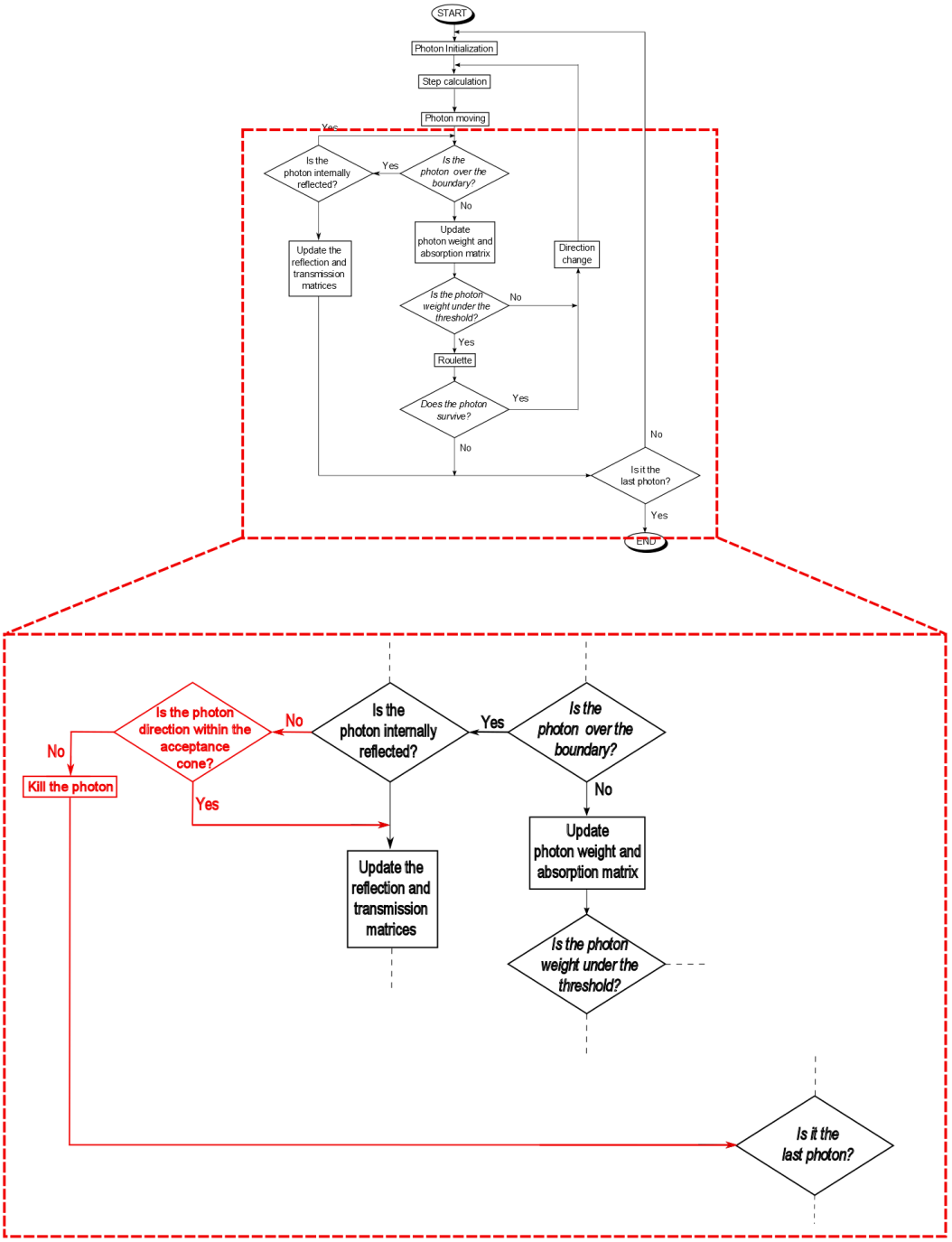

Figure 4.1: *Flow chart of the modifications introduced in the MCML code presented in Figure 1.3 (upper part of this figure), by Jacques et al.,*[61] *to introduce the effect of the numerical aperture. The changes in the MCML C-code are given in appendix B.*

otherwise killed, i.e. lost from the detection. This approach does not bias the results since these photons would have been exiting the medium anyways.

The fiber core diameter has been taken into account by squaring the sum of the number of photons that has been transmitted to the fiber material in a given range of distances from the source. Since the ratio has been calculated, the scaling factors to calculate the area of a circle rather than a square have been discarded. These calculations have been done after convolving the result of the MCML simulations to consider the difference in the source beam radius due to the different core diameters. The source profile (Gaussian) and energy (1 J) has been kept constant in the two cases. The ratio of the number of photons obtained considering a 200 μm and a 400 μm fiber, has been divided by the ratio of the light attenuation due to the blood pooling, obtained in subsection 3.3.1, in order to evaluate the relative efficiency in light collection of the two fiber cores. These calculations, along with the modified MCML code are given in appendix B.
The fact that the simulations are on a semi-infinite media and not on an infinite media have not been taken into account since it has not been regarded to have a major influence on the conclusions.

The input parameters are presented in Table 4.1, these parameters are intended at 730 nm. The adopted value for NA is 0.22, as the fibers used in the measurements. The external refractive index has been chosen to be the same as fused silica for the material above, and the same as biological tissues for the medium beneath.

Layer	n	μ_a [cm^{-1}]	μ_s [cm^{-1}]	g	Thickness[cm]
Above: fibre (fused silica)	1.4545[63]				
Prostate	1.4	0.4	120	0.9	10
Beneath: prostate	1.4				

Table 4.1: *Parameters for the MCML simulations.*

Measurements with the integrating sphere and reflectance measurements

For the experimental measurements, the two set-ups presented in Figure 4.2 have been used: an integrating sphere to render uniform intensity distribution of the light from the laser source and measurements in reflectance configuration on the forearm to have a high diffusive medium.
In both cases, the light has been recorded using a spectrometer, OceanOptics USB4000; the average has been taken over 10 scans and different integration times, ranging from 100 ms to 500 ms, have been used.

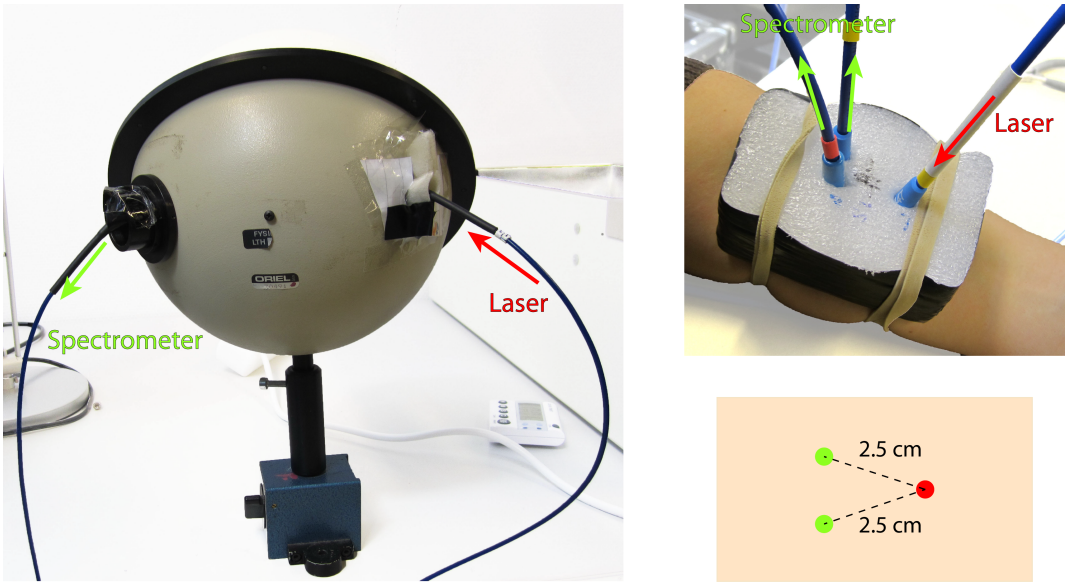

Figure 4.2: *Schematics of the two measurement set-ups used for the evaluation of the effect of the fiber core diameter on the collected light.*
Measurements with the integrating sphere (left) and reflectance measurements on the forearm (right).

A 665 nm and a 730 nm LDs have been used as light sources, for the measurements with the integrating sphere and the reflectance ones, respectively. The power have been kept constant during the measurements for the two different fibers; in particular, a power of 20 mW have been used for the measurements on the arm with an inter-fiber distance of 2.5 cm.

Four OceanOptics bifurcated fibers have been tested, two with 200 μm and two with 400 μm core diameter, BIF200-UV-VIS and BIF400-UV-VIS respectively. The light has been launched from one leg of one of the fibers, and then collected by one legs of the other fiber of the same kind. These bifurcated fibers have been used because they were the only available with both diameters, in order to have all the parameters other than the fiber core diameter invariant.

The photon counts recorded at the peak wavelength by collecting the light at the two legs of each fiber, have been averaged (average over two repetitions). The result has been evaluated confronting the values obtained using the two different fibers.

4.1.2 Measurements for μ_{eff} evaluation with modulation frequency encoding

The aim of these measurements is to assess if it is possible to calculate the value of the effective attenuation coefficient using more that one channel and how stable the result on one channel is in respect of the others.

The ideal measurement set-up for this purpose would have been the one in Figure 4.3A.

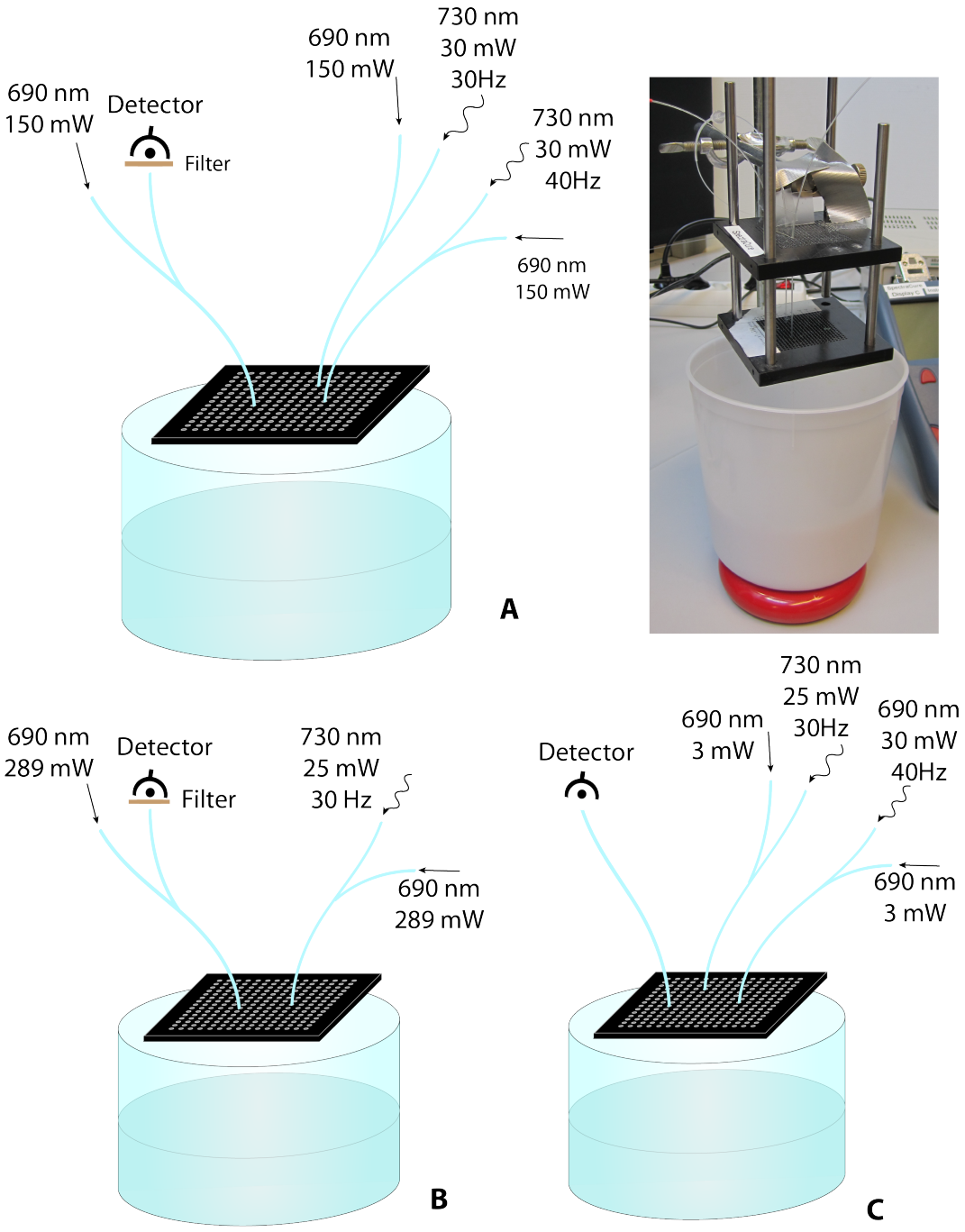

Figure 4.3: *Schematics of the measurement set-up for the evaluation of the effective attenuation coefficient.*

(A) Ideal set-up, (B) set-up for the filtering testing and (C) set-up for the modulation frequency encoding testing.

Three bifurcated fibers are submerged in the Intralipid sample: two of them are used as sources and a third one for detection. No additional bifurcated fiber have been introduced at the source side because it does not affect any other parameter than the power at the source, since it only introduces a loss factor and the power can be adjusted at will. The source fibers are fed with

the treatment light at 690 nm and 150 mW of power and with the modulated monitoring light at 730 nm with a peak power of 30 mW, since this value do not cause any alteration, neither to the tissue nor to the treatment.

The fibers that have been used are balanced optical splitters with coupling ratio of 50:50, OceanOptics XFIBER-PHI-CB18717, with 40% transmission from the common end to the legs and with core diameters: 200 μm for the common end and 100μm for the two legs. The choice of this splitter has been driven only by the necessity to find a good enough splitter within a limited time and limited financial resources. As a matter of fact, no scientific nor technological reason is behind this pick. The modulation frequencies have been taken to be 30 Hz and 40 Hz. The detection fiber is fed with a treatment laser, as the ones before to consider the back-reflections, but a filtering device is attached on the other leg, followed by the detector and the NI DAQ-6009. All the characteristics of this DAQ can be found in Table 4.2. The data acquisition is performed in differential mode, since this is usually preferred to reduce the noise level during the detection of small signals. The filtering is performed placing a band-pass optical filter before the detection,

NI USB-6009	
Analog Inputs	8 single-ended / 4 differential
Input resolution	14 bit
Max sampling rate	48 kS/s
Analog Output	2 single-ended
Output rate	150 Hz

Table 4.2: *Main characteristics of the analog ports of the NI DAQ-6009.*[64]

Figure 4.4: *NI USB-6009.*

between the SM1SMA adapter and the photodiode, to cut out the signal coming from the treatment lasers. This band-pass filter, Thorlabs FB730-10, has been used instead of the FEL0700 because available by the company's lab. This filter is less suitable to this application because it prevents the possibility to detect the fluorescence signal and, most important, its peak transmission is lower, around 64%. The transmission curve is shown in figure 4.5.

The problem that arose with this set-up is the necessity to have two lasers at 730 nm, modulated at different frequencies. Since only one of these lasers was available at the time of the experiments, a 690 nm LD was used to replace the 730 nm LD on one of the channels, so it would not have been possible to filter the treatment light without also filtering the monitoring signal from this channel. Therefore, because of costs and time issues, it has been decided to split the system in two parts: the multi-channel testing part and the filtering testing part.

The filtering testing part has been done by just removing one channel and keeping the rest of

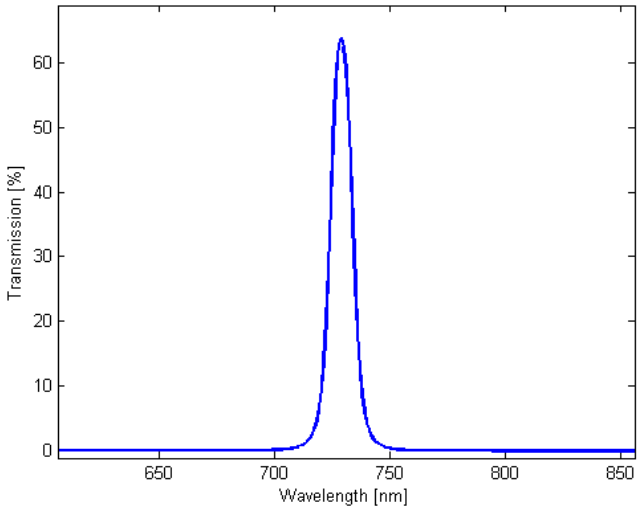

Figure 4.5: *Transmission curve of the filter Thorlabs FB730-10.*[65]

the parameters unchanged, exception made for the treatment lasers power that has been raised to almost 300 mW to increase the quantity of light in the sample in order to be reproduce more closely the clinical case. A scheme of the set-up shown in 4.3B. The measurements have been taken only on Phantom A' and Phantom B (see Table 4.4).

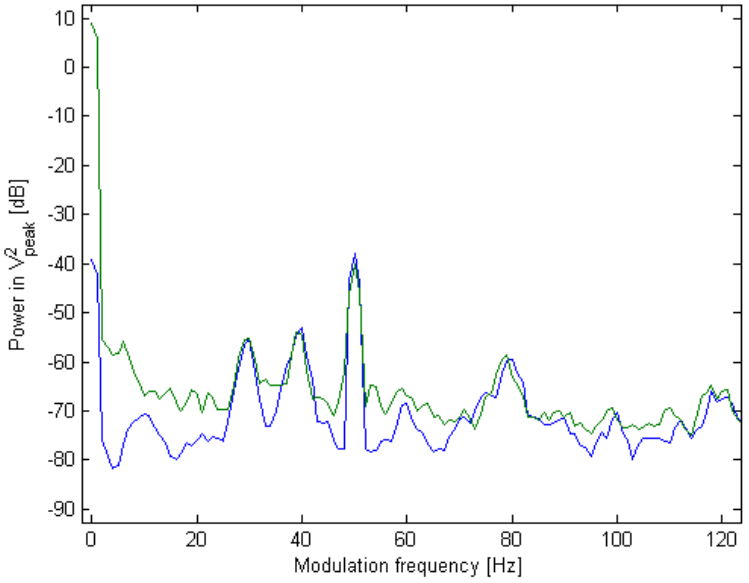

Figure 4.6: *Spectra of the signal at the detector with and without the effect of the back-reflection.*
With (blue) and without (green)

The set-up for the modulation frequency encoding is similar to the ideal one, as presented in 4.3C. One of the lasers at 730 nm have been replaced by a LD at 690 nm. The treatment lasers power has been brought down to 3 mW to prevent the diode saturation, and the peak power of the monitoring laser at 730 nm to 25 mW, due to its limited output power. The diode saturation is controlled by the optical filter in the final system, that enables the instrument to take measurements along with the treatment with a reduced level of noise and without risk of saturation of the photodiodes. The other monitoring laser has been kept at 30 mW since it has been expected to suffer a higher attenuation. The filtering part has been removed, as well as the treatment laser at the detection fiber. In fact, this one has been increasing the noise level too much because of the high backreflections. An example of the distortion that it caused is presented in Figure 4.6. A 400 μm fiber has been used for the detection to have a stronger signal. This choice is discussed in section 4.2. Shortly, the use of a 200 μm fibers for this experiment suffers from two problems that made it preferable to use the thicker fibers. In addition to the fact that no blood pooling effect can be considered using liquid phantoms, the alignment is also more demanding for fibers of this size. This last one would have had to be solved together with the manufacturers and had been regarded to be a secondary problem to this proof-of-principle study.

A resume of all the hardware settings is given in Table 4.3.

Device	Parameter	Value
Treatment lasers	Wavelength	690 nm
	Power at the detection channel, scheme B	150 mW
	Power at the source channel, scheme B	289 mW
	Power at the source channels, scheme C	3 mW
Monitoring laser 1	Wavelength	730 nm
	Power (peak value)	25 mW
Monitoring laser 1	Wavelength	690 nm
	Power (peak value)	30 mW
DAQ	Number of samples per acquisition	10 kS
	Sampling rate	10 kS/s
	Acquisitions to average	5

Table 4.3: *Hardware settings used in the measurements.*

Two measurement configurations have been used on each phantom, each set of acquisition has been repeated four times. The fist set have been taken placing the two source channels at the same distance from the detection fiber, while for the second set of measurements they

have been placed at different distances to see if this could cause any problem for the detection of the signal coming from the furthest channel. The fiber positioning on the matrix in these two configurations is shown in Figure 4.7. The distances fall in the range 0.5-3 cm. The tips of the fibers are at a distance larger than 1 cm from all of the boundaries of the sample to avoid border effects as much as possible.

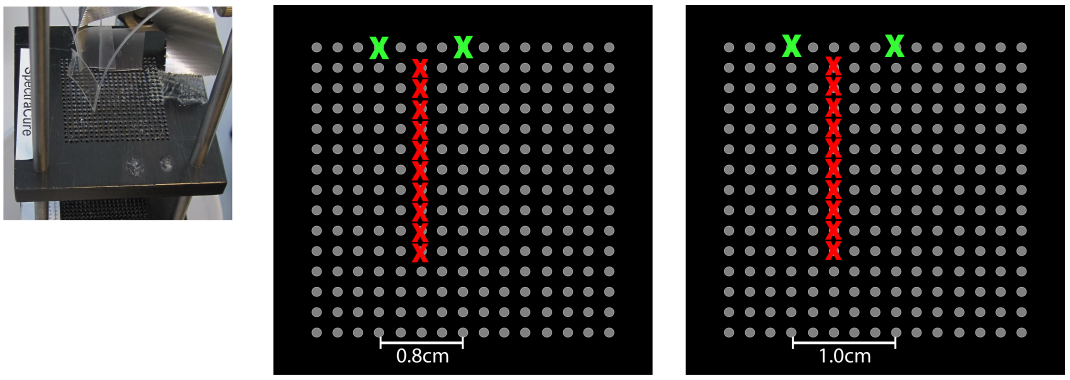

Figure 4.7: *Configurations for the fiber positioning.*

The measurements have been performed in Intralipid and ink phantoms. The optical values at the given concentration have been calculated from[66]

$$\begin{aligned} \mu_s' &= C_{Intralipid}[ml/l]\,(0.58 \cdot \lambda[\mu m] - 0.1) \cdot 0.32 \cdot \lambda[\mu m]^{-2.4} \\ \mu_a &= 914.02 \cdot C_ink[ml/l] \cdot \lambda[nm]^{-0.4366} + 0.001 \end{aligned} \tag{4.1}$$

where C_{ink} and $C_{Intralipid}$ are the ink and Intralipid concentrations. The equation for the absorption coefficient has been retrieved from data collected previously on the ink used to mix the phantoms.

The phantoms optical properties are presented in Table 4.4. The absorption coefficient have been increased progressively because it is the parameter that induces the highest changes in the value of μ_{eff}, and since the scattering does not have as a significant variation during the treatment.

The value of the effective attenuation coefficient has been calculated from the value of the fluence rate at each distance for the two channels. The data have been interpolated using Eq. (1.14) to calculate the value of the measured μ_{eff}. The expected value from Eq. (1.8) has been compared to the mean of the μ_{eff} obtained from each repetition. Because of the uncertainties in the phantom preparation and in the formulas used to derive the optical parameters given the ink and the Intralipid concentrations, three errors have been considered for each group of measurements: the precision, estimated by the standard deviation of the measurements, the relative error, calculated in respect of the theoretical μ_{eff}, and relative standard deviation (RSD), calculated in respect of the mean value $E[\mu_{eff}]$, as it follows:

$$Precision = \sigma[\mu_{eff}] \tag{4.2}$$

Phantom	C_{ink} [ml/l]	C_{IL} [ml/l]		μ_a [cm^{-1}]		μ'_s [cm^{-1}]		μ_{eff} [cm^{-1}]	
			λ [nm]	730	690	730	690	730	690
A*,**	1	29		0.10	0.10	12.1	12.8	1.89	1.97
A'***	1.2	29		0.11	-	12.0	-	2.07	-
B*,***	2	29		0.19	0.20	12.0	12.8	2.67	2.79
C*	3	29		0.29	0.30	12.0	12.8	3.28	3.42
D*	4	29		0.39	0.40	12.0	12.7	3.79	3.95
E*	5	29		0.48	0.49	12.0	12.7	4.24	4.42

Table 4.4: *Composition and optical properties of the phantoms used for the measurements.*

The optical parameters are calculated from Eqq. (4.1) *and Eq.* (1.8).

* *used for the modulation frequency encoding testing with 400μm fiber for detection.*

** *used for the modulation frequency encoding testing with 200μm fiber for detection.*

*** *used for the filtering testing, only the source at 730 nm.*

$$Err_{rel} = \frac{|E[\mu_{eff}] - \mu_{eff}|}{\mu_{eff}} \tag{4.3}$$

$$Err_{RSD} = \frac{\sigma[\mu_{eff}]}{E[\mu_{eff}]} \tag{4.4}$$

Further details about these calculations can be found in the Matlab code in appendix C.

4.2 Results and discussion

4.2.1 Effect of the fiber core diameter on the detected light

The effect of the collecting fiber core diameter has been evaluated with some measurements and Monte Carlo simulations, to asses the effect of a diffused source and of the propagation in a biological medium on the collection efficiency, since this parameter is believed to be predictable, in some cases, by the numerical aperture.

Biological tissues result a special case because of their highly scattering properties. In fact, a change in the sole core diameter has a considerable effect on the collection efficiency. A possible reason behind this, as it will be explained, is the limited penetration depth of the light in the tissue, therefore the shorter height of the acceptance cone of the fiber.

For interstitial measurements it can be still convenient to have a smaller core diameter fiber because of side effects, such as the blood absorption, due to the introduction of a foreign body, the needle, in the tissue.

Since experimental results are in some contrast with the results of the simulations, an attempt to fill this gap is presented. Nonetheless, it has to be pointed out again that the problem requires

further investigation.

Measurements with the integrating sphere and on an arm

The spectra recorded during the measurements using the integrating sphere are shown in Figure 4.8 for the relevant wavelength range around 665 nm. The intensity of the two peaks is visibly approximately the same. The light intensity of the 665 nm component has been calculated as the

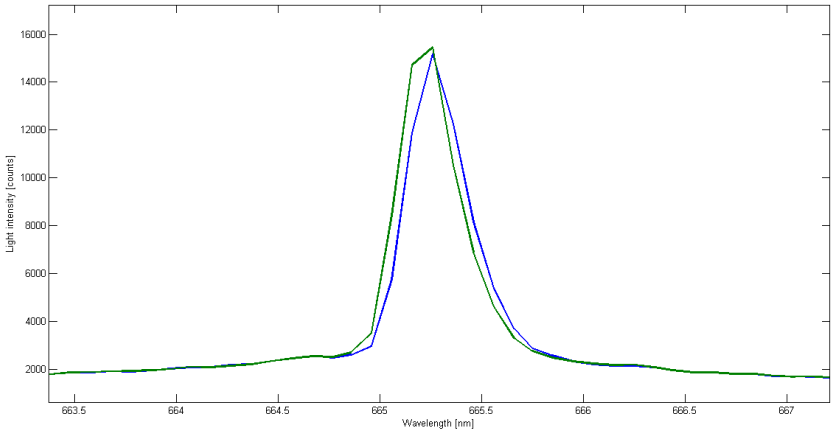

Figure 4.8: *Spectra of the light collected by the fibers from an integrating sphere. 200 μm fiber (blue) and 400μm fiber (green)*

integral of the peak. The ratio of the intensities obtained collecting the light with a 200 μm and a 400 μm fiber results to be 0.97, which means that, basically, the two fibers have the capability to collect the same amount of light from the integrating sphere. This result can be intuitively explained considering the image in Figure 4.9. The photons that can be collected from a fiber are the ones that have a direction that falls within its cone of acceptance. Therefore the amount of collected light can be estimated by the volume of this truncated cone. For light propagating through air, or similar medium, this cone has a height that is considerably larger than the fiber core, virtually infinite. If the radius of the bases radii of the truncated cone are increased of 100 μm, the total volume is affected only in a minor way since just a 100 μm thick layer is added to the total volume. Hence, the collected light is only a few percentage points larger than the light collected by a fiber with a smaller core, as resulted from the measurements.

The situation is different if a biological medium is considered. The results of the reflectance measurements are shown in Figure 4.10. The core diameter can have a considerable effect on the collected light. In fact, the same ratio considered in the previous case resulted to be 0.79 for these measurements.

Using the same geometrical argument, this difference can be explained taking into account that

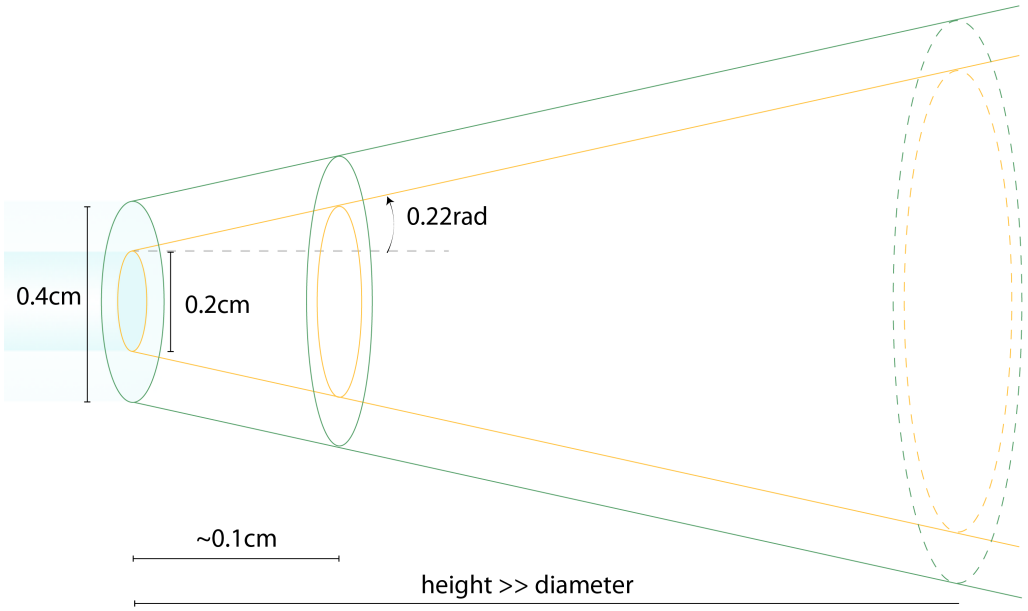

Figure 4.9: *Image of the geometrical argument to explain the differences in the collection efficiency in the case of propagation in air and in a biological tissue.*

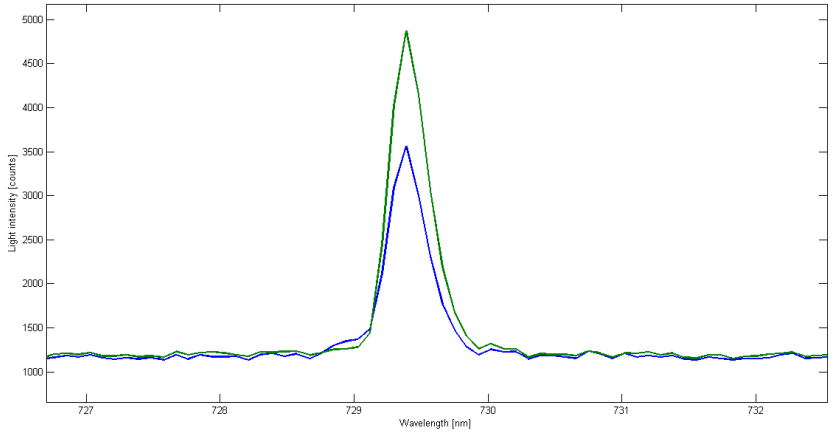

Figure 4.10: *Spectra of the light collected by the fibers during the reflectance measurements.*
200 μm fiber (blue) and 400μm fiber (green)

the deepest point from which the light can be collected is proportional to the inverse of scattering coefficient. Considering that the medium is highly anisotropic, the depth can be roughly approximated using the inverse of the reduced scattering coefficient, which for a soft tissue is around 0.1 cm. If two fibers like the ones that have been used in the experiments are considered, so core diameters of 200 μm and 400 μm and NA of 0.22, the ratio of the volumes can be calculated

to be around 0.5. This ratio has to be modified taking into account the combined effect of the reflections and the highly directed anisotropy, which raises the given ratio of a couple of tenths, bringing its value closer to the one obtained from the measurements. Of course, neither this value nor the one obtained from the measurements are exact. In fact, on one hand, the geometrical argument pretends to be only a first attempt to understand the results of the measurements and not an exhaustive explanation of the problem. On the other hand, the measurements have been repeated only once so the error could not be calculated. This kind of measurements can, in fact, suffer from a number of inaccuracies, which can bias the measurements towards one result or the other. For instance, the distance of the two fibres from the source can be slightly different or dishomogeneities can be present on one path rather than the other. It is possible to change the configuration to take one measurement at the time having each of the detection fibers on exactly the same position in order to avoid these sources of error but, on the other hand, these can suffer from fluctuation in the laser source.

As assessed in chapter 3, there is another factor that has to be taken into account for interstitial measurements: the bleeding. It has been estimated that the absorption effect of the blood pools is reduced of more than 30% if 200 μm fibers are used instead of 400 μm (see subsection 3.3.1). This means that the reduction in the collection efficiency is highly compensated by the reduced absorption due to the smaller blood pools that smaller needles provoke. Therefore, it is possible to conclude that a smaller fiber with a diameter that is still in the order of few hundreds of micron could be as efficient, and in extreme cases even more efficient, than a slightly larger core fiber. Of course, this is only a gross estimation, which has the only scope to evaluate the feasibility of using smaller fibers, and needs further investigation. In fact, it does not consider factors such as difficulties in the alignment and other technical details that can play an extremely important role in order to have a high light intensity at the detector.

Monte Carlo simulations

The results obtained from the modified Monte Carlo simulations gave a slightly worse picture of using a smaller fiber. In fact, the ratio in the number of collected photons has been estimated to be 0.45, in the best case, when a distance of approximately 1 cm of the detection fiber from the source is considered. This value is highly dependent on where the two fibers are positioned. Such a big difference is attenuated in case of interstitial measurements are assumed. In fact, the estimated ratio of the collected light grows to around 0.73 due to the fact that the smaller number of photons collected by a smaller fiber is compensated for when comparing this value with the one due to the blood pooling, 0.62.

Even if the actual values of the ratio obtained by the experiments and by the simulations are different, they both show the same trend, in the sense that both of them conclude that the

collection efficiency of the 200μm core fiber is smaller than the one of the 400μm core fiber, but that it does not scale with the area. Such a discrepancy in the actual numbers that resulted from the calculations can be explained by the fact that the two methods have a totally different nature, therefore different problems. For example, keeping that the approach adopted to modify the MCML code is correct, there may have been some errors in the translation of the idea into the code; the modeling of the boundaries between the fiber and the biological tissue does not include a compensation for the effect of the non perfect contact between the two materials, that might cause important reflections in the real cases and so an error in the simulations. Or there could have been some errors during the measurements. For instance, the fiber tip could have been not in perfect contact with the skin surface, some of the light could have been coupled directly into the detection fiber without probing the tissue. In fact, if this is the case, there may have been light traveling between the outer skin layer and the fiber holder bottom surface that coupled into the detection fiber. Another source of error in the measurements could have been that the distance between the detection fiber and the two launch ones was not exactly the same. In addition, since the arm is not a perfectly homogeneous medium, it is rather a layered tissue, there may have been some dishomogeneities along one path rather then the other that distort the cone of acceptance. The variables and the differences are many between these two approaches so they are not entirely comparable.

In addition to these differences, it has to be pointed out that there are some aspects regarding the simulations that need to be corrected since they have been hard to take into account properly for this project. The most important one is the geometry of the problem. The MCML code is based on cylindrical symmetry. This symmetry provides good results in case the effect of only one fiber is considered, either the launch or the detection fiber. In the problem presented here, this symmetry is altered by the geometry of the configuration; in fact, in case both the launch and the detection fibers need to be considered, the problem does not have cylindrical symmetry anymore. There are some solutions to this problem but the limited amount of time forced the choice to not investigate the problem any further during this project, leaving the whole problem opened.

Stated this, the partial agreement between these two results is adequate enough for the purpose of this study.

4.2.2 Modulation frequency encoding

The experiments to evaluate the possibility to detect the signal coming from different channels with different modulation frequencies simultaneously have given a positive outcome. In fact, the behavior of the fluence rate and the values of the effective attenuation coefficient follow, in the majority of the cases, the ones predicted by the model.

Two-channels measurements using 400μm core for the detection

The measurements performed having two channels used as monitoring sources at the same time have been taken to evaluate the feasibility of this configuration and eventual limitations that it can suffer from. In particular, the possibility of having the two channels at the same distance from the detection fiber or at different distances has been evaluated. The set-up is the one given in Figure 4.3C, in the configurations shown in Figure 4.7. The relevant parameters for the hardware are given in Table 4.3. The diffusion model predicts that the fluence measured at different distances should follow Eq. 1.14, so the first check have been on the linearity of each set of data. In general, this characteristic have been fulfilled extremely good by approximately all the measurements when the modulated part of the signal was not at the noise level. Along with linearity, the model states that the μ_{eff} is exactly the gradient of the line. Therefore, an increase in the absorption in the sample, that causes an increase in μ_{eff}, should result in a set of measurement whose linear fitting has a higher slope. As shown in Figure 4.11, this is the case for the measurements taken with this system. In fact, not even the data are on a straight line but the slope of the curve increases progressively from the bottom line, corresponding to the data collected from Phantom A, to the steepest line, which are detected taking measurements on Phantom E.

For the same reason, the calculated values of μ_{eff} and the slope of the line is supposed to be larger for channel 2, that has a wavelength of 690 nm, so it is subject to a larger absorption. If one refers to Table 4.5, this is generally true for the acquired signals, exception made for some of the measurements performed having the two channels at different distances. An example of this discrepancy is given in Figure 4.12. Here it can be observed that the data obtained from measurements that were taken having the two source fibers at the same distance from the detection follow the behavior predicted by the model, while the ones taken having the sources at different distances do not. Some hypothesis can be made on why this happened. First of all, the channel 2 is positioned further away from the collection fiber. This means that the signal recoded from that channel is, in general, lower than the one coming from channel 1. The sum of these two effects can distort the measurements because cross-talking between the two channels can occur, in particular channel 2, which is the one with the weakest signal at the detection point, is influenced by the stronger signal coming from channel 1. This phenomenon is worsen further by the low quality of the modulation signal coming from the DAQ. In fact, this signal is not a perfect sinusoid because of the limited sampling frequency of the analog output, thus the modulation signal for channel 1 tends to have a spectral tail that overlaps with the peak of the modulation signal for channel 2 and vice versa. The same behavior is followed by the laser signals and so by the diffused light. Therefore, when the signal coming from channel 2 drops down to a certain level, it can be highly affected by the tail at higher modulation frequencies of the light coming from channel 1. Besides that, the photodiode is less sensitive to light at 690 nm so the con-

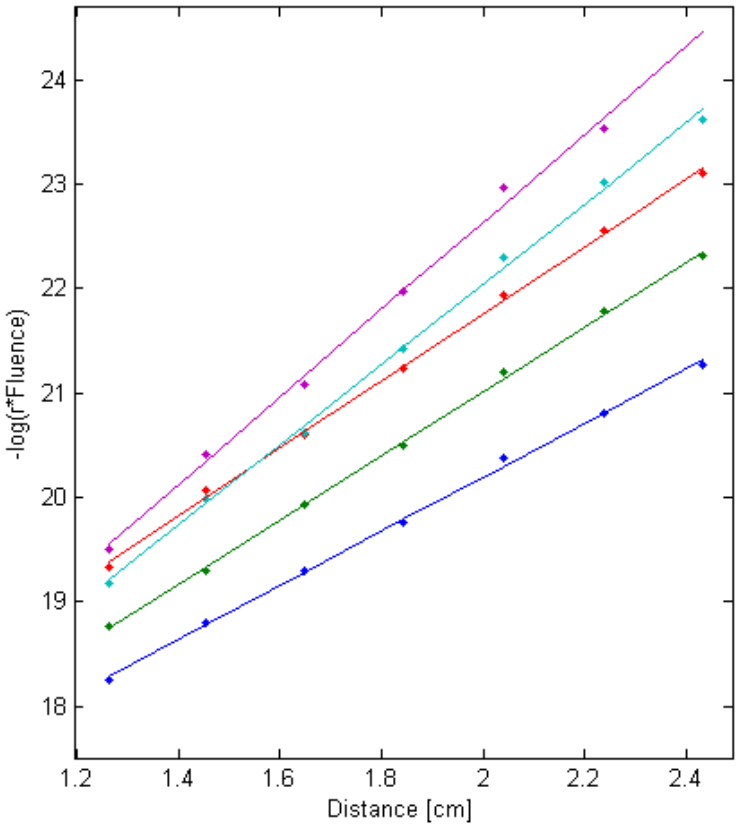

Figure 4.11: *Plot of the measurements from channel 1 on the five different phantoms showing how well the data can be interpolated by lines and how the slope of the line increases with the value of* μ_{eff}.
Phantom A - low μ_{eff} *(blue), Phantom B (green), Phantom C (red), Phantom D (light-blue) and Phantom E - high* μ_{eff} *(purple).*

cealment of this signal is further enhanced. In addition, the light at 690 nm suffers from higher sensitivity to imprecision in the fiber positioning because it experiences a higher absorption. However, this effect does not considerably influence the results if all the data are considered. In fact, these follow the model no matter the fact that the measurements taken having two different distances for the two channels do not. Furthermore, if the whole picture of the eighteen-channels system is considered, these measurement are supposed to be taken from a number of different collecting fibers, meaning that this effect is somewhat evened out. For example, if the signal coming from two general channels X and Y is collected from a fiber at a position where the X component is stronger then the Y component, at the same time there is another fiber that is collecting light at another position where the Y component is stronger than the X component; the μ_{eff} is then calculated taking both of these measurements, so the mutual influence

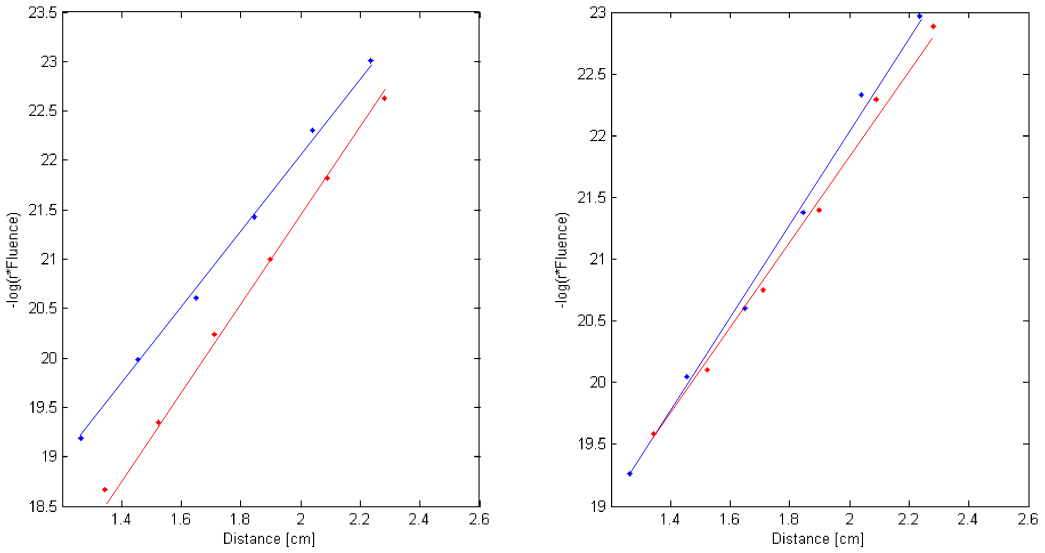

Figure 4.12: *Plots of the measurements from channel 1 and 2 on Phantom D, showing the different behavior in the two different configurations.*

Measurements with channel 1 - 730 nm (blue) and channel 2 - 690 nm (red) at the same distance (left) and at different distances (right).

is evened out. This did not happen during the measurements presented in this work because the fiber corresponding to channel 2 was always further away from the detection fiber than the one corresponding to channel 1, because of the the measurements configuration presented in subsection 4.1.2. In addition, the problem of the cross-talk can be avoided using DAQs with a higher sampling ratio, like the ones included in the proposed set-up, so each monitoring source can be modulated at higher frequency and each channel can be placed further apart along the spectrum.

Two-channels measurements using 200μm core for the detection

As stated in subsection 4.1.2, the measurements have been taken using a 400 μm fiber because the collection efficiency of the configuration having a 200 μm fiber collecting the light was too low for the limited power of the laser and the losses introduced by all the connections. Since the therapy laser on the detection side have been turned off anyways, it has been decided to just remove the whole channel and use only a bare end SMA fiber with a 400 μm core. Nonetheless, there are other factors that make the use of 200 μm fibers feasible for interstitial measurements in soft tissues. In addition, the factors that can concur to low efficiency of such small fibers are many and solvable with more time and accuracy, problems such as the alignment of the fibers in the connections, the polishing, the goodness of the connectors and so on. Therefore, some data have been collected to asses whether it is possible to estimate the effective attenuation

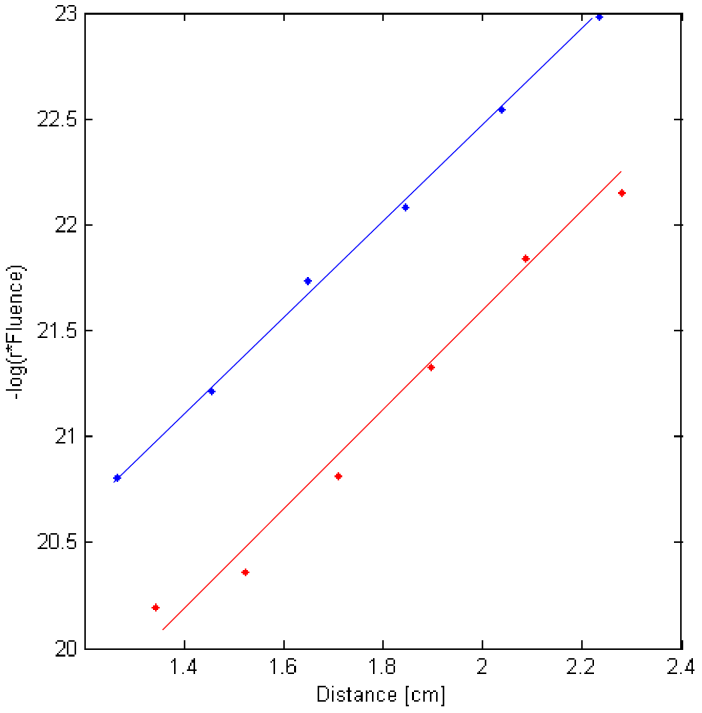

Figure 4.13: *Plots of the measurements from channel 1 and 2 on Phantom A using a 200 μm core fiber for the detection.*
Channel 1 - 730 nm (blue) and channel 2 - 690 nm (red).

coefficient using these small fibers. To do so, measurements have been taken on Phantom A, since the low absorption enables the detection of a higher signal for a longer distance than the other phantoms. The measurement set-up is the same as the experiments in the previous part but only the configuration in which the fibers are at the same distance has been used. The results of the measurements are shown in Figure 4.13. As noticeable, these measurements fulfill all the criteria listed above: the data are on a straight line, with good approximation, the effective attenuation coefficient is larger for channel 2 at 690 nm and the values are estimated within an acceptable error, a global relative error of 10% and a RSD of about 4%.

Hence, this demonstrate, along with all the considerations made in the previous sections, that it is possible to use these fibers for interstitial measurements since they provide data that is good enough to give an accurate estimation of the μ_{eff}, assumed that enough light is delivered from the laser sources.

Filtering measurements

These experiments have been taken to evaluate the possibility to take the monitoring measurements during the treatment. The data have been collected according to the set-up shown in

Figure 4.3B, with the hardware parameters given in Table 4.3. The results of the filtering experiment mimic every aspect of the behavior above so they do not need any further discussion, except stating that the filtering part of the detection have the only effect of removing the therapy component of the light, which is what it is meant for. The 730 nm component is of course attenuated by the filter itself but this does not affect the goodness of the estimation of the optical properties, as clearly deducible from Table 4.5. The plots of two measurements taken on Phantom A' and Phantom B are shown in Figure 4.14.

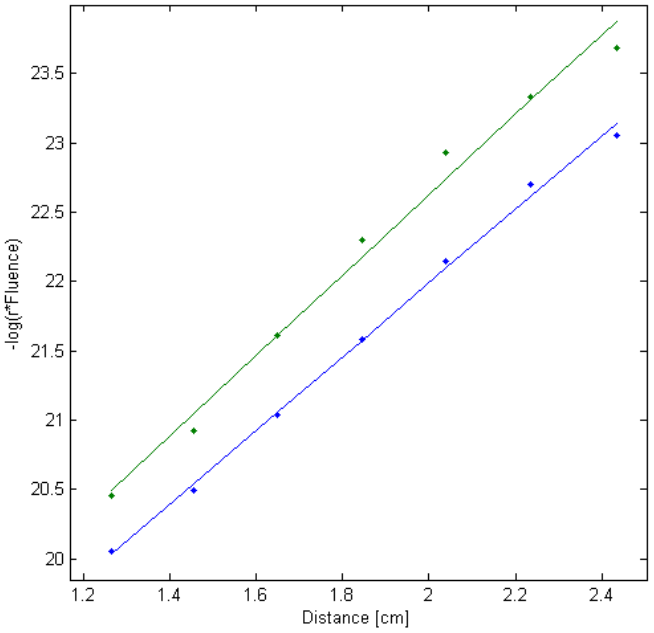

Figure 4.14: *Plots of the measurements on Phantom A and Phantom B during the filtering experiments.*
Phantom A - low μ_{eff} (blue) and Phantom B - high μ_{eff} (green).

Error statistics and discussion of the results

The values of the measured μ_{eff} and the errors obtained are summarized in Table 4.5. The measured value of μ_{eff} has been obtained taking the mean of the ones obtained in each single measurement. The estimation resulted to have an average standard deviation of 0.086, which corresponds to an average relative error of 9% and a RSD of 3%. These numbers are considered to be good results since they are comparable with the ones obtained while testing the current SpectraCure's IPDT system. Furthermore, such a small value of the RSD indicate that the measurements are consistent. The discrepancy between the relative error and the RSD is mainly due to the big relative error committed on the estimation of the effective attenuation coefficient

for Phantom A. In fact, the relative error diminished to 6% if the measurements on Phantom A are excluded from the statistics. These measurements are the only ones that present a systematic error, an overestimation, and not a randomly distributed error as in the other cases. The reason why the results on this phantom differ so much from the predicted values is not totally clear. One possibility is that the light attenuates too little within the measurements distance, so too high signal is collected at the detection fiber. This is suggested by the fact that the relative error is about 10% smaller for channel 2, which suffers from an higher attenuation, and that the measured value is estimated with a relative error of about 10% if a 200 μm fiber is used for detection, so less light is collected. This effect, among other possible causes, can be due to an insufficient dynamic range of the system, even if the diode did not saturate during the measurements. An alternative possibility is that the overestimation is caused by losses at the boundaries. In fact, these introduce a factor of attenuation that is less severe for measurements where the light suffers from a higher effective attenuation coefficient, as it happens for the other samples and for the light at 690 nm. On the same trend, the very presence of the detecting fiber affects the propagation, more the more the light propagates through the medium. In this case, it would be reasonable that the use of smaller fibers for the detection gives a better estimation of the μ_{eff}, as it is true for the measurements presented in this work. On the other hand, such small values of μ_{eff} are difficult to encounter in the real cases. As a matter of fact, the value of this parameter is around 3.3 cm^{-1} at 732 nm in the prostate.

The sources of error that can affect the measured values are many. The main problem with these kind of measurements lies in the phantom and the knowledge of its optical properties. In fact, these are affected by a number of uncertainties due to imprecisions in the characterization of the ink and Intralipid optical properties, and the change in these properties due to temperature and aging of the sample; to avoid this last, the samples have been used for a maximum of 24 hours from the mixing time. Errors in the mixing doses, expressed in volume, can sensitively deviate the real effective attenuation coefficient from the predicted one, reason why it has been decided to present the error also in terms of the relative standard deviation, since this parameter does not take into account the expected value at all.

The fluctuations of the hardware output, in particular of the laser power and the modulation signal from the DAQ, are also significant factors that can affect the measurements. In fact, if either of those two changes during a single set of measurements, so while the detecting signals at different distances for the single repetition, the slope of the curve can change significantly and weird behaviors can be induced. This effect can, in some cases, be clearly visible and the measurement discarded, or more subtle, in which cases it induces errors in the estimation. For instance, in Figure 4.15, the red curve (channel 2) should have had approximately the same behavior as the blue one (channel 1), since these measurements have been taken on a sample

	Mean values on all the measurements							
	$\mathbf{Precision} = \mathbf{0.086}$ $\mathbf{Err_{rel}} = \mathbf{9.0\%}$ $\mathbf{RSD} = \mathbf{3.2\%}$							
	Channel 1				Channel 2			
	λ =730 nm, f$_m$=30Hz				λ =690 nm, f$_m$=40Hz			
	Two-channels measurements: same distance from the detection							
Phantom	μ_{eff} [cm^{-1}]	$\mid \sigma \mid$ [cm^{-1}]	Err_{rel}	RSD	μ_{eff} [cm^{-1}]	$\mid \sigma \mid$ [cm^{-1}]	Err_{rel}	RSD
A	2.42	0.10	0.28	0.04	2.3	0.06	0.17	0.03
A*	2.00	0.08	0.06	0.04	2.25	0.11	0.14	0.05
B	2.92	0.07	0.09	0.02	3.07	0.08	0.01	0.03
C	3.19	0.05	0.03	0.02	3.48	0.17	0.05	0.05
D	3.75	0.08	0.01	0.02	4.07	0.05	0.03	0.01
E	4.12	0.07	0.03	0.02	4.53	0.05	0.02	0.01
	Two-channels measurements: different distances from the detection							
Phantom	μ_{eff} [cm^{-1}]	$\mid \sigma \mid$ [cm^{-1}]	Err_{rel}	RSD	μ_{eff} [cm^{-1}]	$\mid \sigma \mid$ [cm^{-1}]	Err_{rel}	RSD
A	2.36	0.05	0.25	0.02	2.22	0.02	0.13	0.01
B	2.91	0.10	0.09	0.04	2.88	0.07	0.03	0.02
C	3.16	0.03	0.04	0.01	3.24	0.06	0.05	0.02
D	3.79	0.11	0	0.03	3.59	0.06	0.09	0.02
E	4.16	0.04	0.02	0.01	4.03	0.04	0.09	0.09
	Statistics using all the data from the two-channels measurements							
Phantom	μ_{eff} [cm^{-1}]	$\mid \sigma \mid$ [cm^{-1}]	Err_{rel}	RSD	μ_{eff} [cm^{-1}]	$\mid \sigma \mid$ [cm^{-1}]	Err_{rel}	RSD
A	2.39	0.09	0.27	0.04	2.27	0.06	0.15	0.03
B	2.91	0.09	0.09	0.03	2.97	0.12	0.07	0.04
C	3.17	0.05	0.03	0.01	3.36	0.18	0.02	0.05
D	3.77	0.10	0.01	0.03	3.83	0.24	0.03	0.06
E	4.14	0.06	0.02	0.01	4.28	0.25	0.03	0.06
	Filtering							
Phantom	μ_{eff} [cm^{-1}]	$\mid \sigma \mid$ [cm^{-1}]	Err_{rel}	RSD	μ_{eff} [cm^{-1}]	$\mid \sigma \mid$ [cm^{-1}]	Err_{rel}	RSD
A'	2.52	0.05	0.22	0.02	-	-	-	-
B	2.71	0.03	0.02	0.01	-	-	-	-

Table 4.5: *Results for the estimation of the effective attenuation coefficient.*

** These measurements have been taken using a 200 μm fiber for the detection.*

with extremely low absorption so the optical properties were similar for light at 730 nm and at 690 nm, but the power of the laser in channel 1 increased progressively while the detection fiber was moved at shorter distances from the sources, deviating the curve from being a straight line. If such effect is less prominent, it is not visible and can affect the estimation of the line parameters, therefore the calculation of the effective attenuation coefficient. Along with these major sources

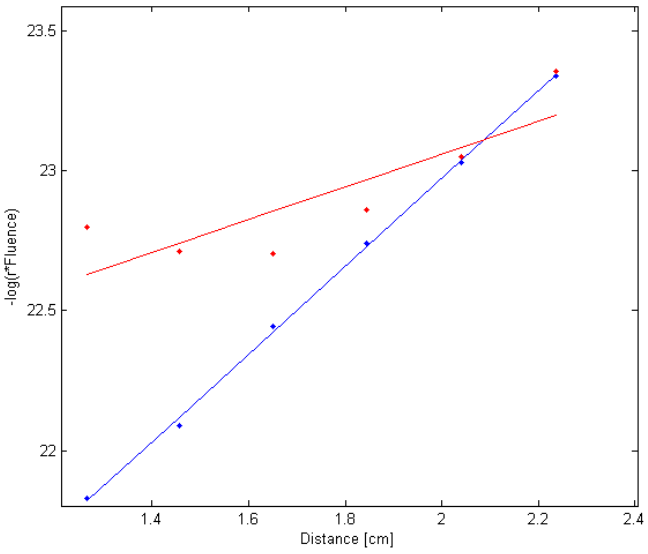

Figure 4.15: *Plot of a measurement on a really low absorbing phantom with a fluctuation in the laser power.*
Signal from channel 1 (blue) and channel 2 (red).

of error, an imperfect fiber positioning is also possible, and this can, of course, introduce errors since the calculations for the μ_{eff} depend explicitly on the distance so if the actual inter-fiber distance differs from the assumed one, the trend of the line is affected, hence the measured effective attenuation coefficient.

Conclusions

The different parts of the optical circuit have been tested: methods, materials and results have been presented in this chapter. The system has been proved to be reliable, efficient, robust for the evaluation of the μ_{eff} and relatively cheap. The measurement to assess whether it would have been better to use 200 μm or 400 μm fibers have been given results that are not so significant. The initial hypothesis that fibers with such core diameters have a comparable collection efficiency has revealed itself as partly true. In fact, this statement has been proved to be true for light propagating in air but not for light propagating through media that have a limited propagation depth, such as biological tissues. As it will presented in the following chapter,

the option to have smaller core fibers have been kept since the blood pooling effect in IPDT compensates for the lower collection efficiency that characterize 200 μm core fibers in respect of the 400μm. Because of time and costs issues, the possibility to have a modulation frequency encoding has been tested on slightly different components than the ones presented in chapter 3, relying on the fact that these changes are not significant this evaluation in the sense that: worse components have been used so, since the evaluation had a positive outcome, more proper components cannot do anything else than giving better results. The testing has been divided in two parts: the filtering and the multi-channel configuration experiments. Both these proved that the system is efficient and reliable since the evaluation of the effective attenuation coefficient suffered from en error as small as few percentage points in most of the cases, and the behavior of the data followed the one predicted by the model. In addition, the results have been shown to be repeatable with values that have a RSD of about 4% for the group of measurements that have been taken during this evaluation. I am confident the even better results can be obtained using the parts suggested in the chapter “Conclusions and future work”.

Conclusions and future work

The system design has revealed itself as reliable, efficient and robust for the evaluation of the μ_{eff}. Even if worse components than the one presented in the following section have been used, the evaluation had a positive outcome. The testing has been divided in two parts: the filtering and the multi-channel configuration experiments. Both these proved that the system is feasible since the evaluation of the effective attenuation coefficient suffered from en error as small as few percentage points in most of the cases. In addition, the behavior of the data followed the one predicted by the model. The results have been shown to be repeatable with values of the RSD of about 4% in mean.

About the possibility to reduce the fiber core diameter, the initial hypothesis that fibers with 200 μm or 400 μm core diameters have approximately the same collection efficiency has been partly proved. In fact, the experiments confirmed this hypothesis only if the light propagates through air but through media such as biological tissues. Indeed, the light in these kind of media have a limited propagation depth that affects heavily the amount of collected light in respect of the core diameter. Nonetheless, smaller core fibers have been chosen for the proposed system because it has been estimated that the blood pooling effect, that affects interstitial measurements, compensates for the lower collection efficiency of the 200 μm core fibers in respect of the 400μm.

Proposed set-up for the new generation of IPDT machines

The suggested set of hardware and relative specifications for the new system are presented in Table 5.1. Some of these specifications are different from the ones presented throughout the report, as being the characteristics of the actual hardware used for the experiments, since it was not possible for various reasons, such as time and costs, to get in hold of all the parts exactly as they are presented in this section. The channel scheme and the system set-up presented in chapter 3 has been kept unchanged. The specifications given in Table 5.1 are taken, for the main components, from specification sheets of existing hardware on the market. The other parts, such as the light sources and the 1x2 optical splitters for the sources side, are not entirely specified. These are components for which the characteristics that have not been fully defined

are not significant for the functioning of the system.

HARDWARE PARTS	
Monitoring laser (18 pc)	
Type	LD
Wavelength	730 nm
Power (peak)	30 mW after losses
Modulation frequency range	200-500 Hz
Treatment laser (18 pc)	
Type	LD
Wavelength	690 nm
Power	150 mW after losses
Sources 1x2 splitter fiber (18 pc)	
Core diameter	65/100/125 μm
Coupling ratio	50:50
Wavelength range	UV/VIS
Channel 1x2 splitter fiber (18 pc)	
Core diameter	200 μm
Coupling ratio	1:99
Wavelength range	UV/VIS or VIS/IR
Filter (18 pc)	
Type	High-pass
Cut-off wavelength	700
Transmission (in-band)	$>$80%
Transmission (stop-band)	$\sim$ 0%
Photodiode* (18 pc)	
Active area	$\permil$ 9.8 mm
Wavelength range	400-1100 nm
Peak wavelength	970 nm
Peak response	0.65 A/W
Output	BNC
Output voltage range	0-10 V
Rise time	43 ns
Junction capacitance	300 pC
NEP	$3.96 \cdot 10^{-14}$

Table 5.1: *Hardware characteristics of the proposed system.*

**used in the measurements in section 4.2.2*

Dark current	100-600 nA
DAQ - Analog Output (1 pc)	
Analog outputs	32 single-ended
Output rate	800 kS/s per channel for one channel
	45 kS/s per channel for 32 channels
Resolution	13 bits
Voltage Range	$\pm$ 10 V
DAQ - Analog Input (3 pc)	
Analog Inputs	16 single-ended / 8 differential
Sample rate	200 kS/s
Resolution	16 bits
Voltage Range	$\pm$ 5 V / 10 V differential

Table 5.1: *Hardware characteristics of the proposed system.*
**used in the measurements in section 4.2.2*

Since the system have been designed paying attention also to the economical aspect of the project, an estimation of the costs can be done (1 € $\approx$ 9 SEK). The suggested configuration has been assessed to be relatively cheap since each module of the circuit has been evaluated to cost less than 1000 € ($\sim$9000 SEK), excluding the laser sources. In fact, the cost of each channel is about 1200€ ($\sim$11000 SEK) if each part is bought separately, but if at least one entire circuit is produced, a scaling factor of 0.7 can be applied to the components prices since this factor seems a good estimation for small order purchase discount on products in the price range lower than 1000 € ($\sim$9000 SEK). This, of course, excludes the DAQs components since they are only four in the whole system. If such scaling factor is applied, each channel is estimated to cost around 900€, excluding the LD sources, for a total cost per system of about 43000€ ($\sim$390000 SEK). For costs estimation it is reasonable to use a scaling factor of 0.5 because this applies, in the same price range, for purchases of 100 pieces, which is the quantity needed to build roughly five IPDT machines. In this case the price per channel, excluding the laser sources, drops to about 700 € ($\sim$6300 SEK), which means that each optical circuit can be built for approximately 31000 € ($\sim$280000 SEK), so around 1800 € ($\sim$16000 SEK) per complete channel.

Alternative components are also possible, for example, the main 1x2 splitter could be replaced by a custom component, with approximately the same characteristics, inspired from the optical splitter from OceanOptics used in the measurements. Other DAQs can also be used.

More tests are required to prove that the suggested system, with the right components, works as it should. In addition, it would be necessary to measure the coupling losses along the channel to calibrate the system and calculate the power of the laser sources that is needed to have the desired power at the patient side. Moreover, it is suggested to perform a test on the overall responsivity of the system to understand if major or minor changes to the hardware should be applied.

Throughout chapter 3 it has been discussed how it is possible to modify this system to enable multi-spectral measurements to obtain information about parameters such hemoglobin, water and other chromophores concentrations, oxygen saturation and blood volume fraction since these allow to separate the contribution of each component to the total absorption and scattering coefficient. In particular these photodiodes could be replaced by spectrometers. Of course, this can be achieved at the expenses of larger costs since a spectrometer can be more than ten times the price of a photodiode, like the one suggested here. For instance, a general OceanOptics spectrometer has a price that ranges around 2500 €/pc ($\sim$ 23000 SEK), that goes down to a bit less than 2000 € ($\sim$18000 SEK) for larger orders. However, the higher costs are compensated by a larger measurement and parameter assessment capability of the machine, that increases its value on the market.

Moreover, the detection can be changed to allow the independent measurement of the phase and amplitude of the collected modulated signal to allow the separation between scattering and absorption, even without performing multi-spectral measurements. As a matter of fact, these two parameters of the PDW depend on the optical characteristics of the material in which it propagates and can be detected through single-wavelength multi-distance measurements.

The system can also be modified to allow fluorescence measurements. Another source, for instance at 660 nm, has to be introduced. The fluorescence signal can be detected as the remaining DC part of the signal, once the contributions from the monitoring lasers are calculated from the modulated component and removed.

As a conclusion, it can be stated that this proposed integrated optics set-up is efficient, flexible, relatively compact and cheap, so it has all the prerequisites to be the basic set-up for the next generation of IPDT machines.

Appendix A

Abbreviations

CT - Computed Tomography

DAQ - Data Acquisition Board

DRE - Digital Rectal Examination

IPDT - Interstitial Photodynamic Therapy

LD - Laser Diode

MCML - Monte Carlo Multi Layer

MRI - Magnetic Resonance Imaging

NA - Numerical Aperture

NADPH - Nicotinamide Adenine Dinucleotide Phosphate

NEP - Noise Equivalent Power

NIR - Near Infra-Red

PDT - Photodynamic Therapy

PSA - Prostate-Specific Antigen

PDW - Photon Density Wave

ROS - Reactive Oxygen Species

RSD - Relative Standard Deviation

RTE - Radiant Transport Equation

SDE - Standard Diffusion Equation

TOF - Time Of Flight

TRUS - Transrectal Ultrasound

Appendix B

Modifications to the MCML code and Matlab script for the evaluation

The code has been modified in the file *mcmlgo.c*.

The basic idea behind these modifications is to introduce a discrimination on which photon directions can enter into the fiber layer and assume all the other ones as lost. This is achieved defining a parameter that corresponds to the cosine of acceptance angle, given the numerical aperture. The cosine has been chosen since the whole program makes use of this parameter to define the directions. The value of 0.22 has been considered as numerical aperture since this is the numerical aperture of the fibers that have been used.

```
24      #define cosNA sqrt(1-0.22*0.22)
```

The check on the incidence angle for the transmission to the fibre is performed introducing the condition in the function that records part of the photon weight in the reflectance matrix.

```
482     void RecordR(double                      Refl,
483                              InputStruct  * In_Ptr,
484                              PhotonStruct * Photon_Ptr,
485                              OutStruct *    Out_Ptr)
486     {
487       double x = Photon_Ptr->x;
488       double y = Photon_Ptr->y;
489       short  ir, ia;        /* index to r & angle. */
490
491       if(fabs(Photon_Ptr->uz) < cosNA){
492         ir = (short)(sqrt(x*x+y*y)/In_Ptr->dr);
493         if(ir>In_Ptr->nr-1) ir=In_Ptr->nr-1;
494
```

```
495          ia = (short)(acos(-Photon_Ptr->uz)/In_Ptr->da);
496          if(ia>In_Ptr->na-1) ia=In_Ptr->na-1;
497
498          /* assign photon to the reflection array element*/
499          Out_Ptr->Rd_ra[ir][ia] += Photon_Ptr->w*(1.0-Refl);
500
501          Photon_Ptr->w *= Refl;
502        } else {
503               Photon_Ptr->w = 0;
504               Photon_Ptr->dead = 1;
505        }
506      }
```

The number of detected photons has been calculated summing all the photons that have been absorbed in an area of the fibre layer at 1 cm from the source and with a length of 200 μm and 400 μm, respectively. The difference in detected light has been estimated taking the ratio of these numbers and dividing it for the ratio of the absorption due to the blood, presented in subsection 3.3.1, as follows:

$$Ratio\ collected\ light\ =\ \frac{1}{blood\ absorption}\left(\frac{photons\ collected(200\mu m)}{photons\ collected(400\mu m)}\right)$$

The Matlab code follows.

```
%------------------------------------------------------------
% IINPUTS MCML.m

filename = 'fibers';
number_of_photons = 10^7;
n = 1.4;
mua = 0.4;
mus = 120;
g = 0.9;
th = 10;
layers = [1.4546 100 0.001 0.001 0.01; n mua mus g th];
n_above = 1.4546;
n_below = 1.4;
dz = 0.001;
dr = 0.002;
number_of_dz = 1000;
number_of_dr = 1000;
number_of_da = 1;

% Run MC simulation
```

```
s=MCML(filename,number_of_photons,layers,n_above,n_below,...
       dz,dr,number_of_dz,number_of_dr,number_of_da);
cs2 = conv();
cs4 = conv();

blood_att = 0.62;

d2 = sum(sum(cs2.data(:,500:600)))^2;
d4 = sum(sum(cs2.data(:,500:700)))^2;
collected_d2_d4 = (d2/d4) / blood_att
```

Appendix C

μ_{eff} estimation in Matlab

```
%-------------------------------------------------------------
% INPUT DATA

    path = 'D:\Dropbox\Thesis\Measurements\Data\2012.03.27\';
    file = 'sampleA3_D';

    num_data = 9;           % number of recorded signals
    num_samples = 10000;    % number of samples per recording

    num_distances = 10;     % number of distances

    Ink = 1;                % ink solution (1:100) volume [ml]
    IL = 29;                % Intralipid volume [ml]
    Water = 500;            % Water volume [ml]

    mod_freq = [30 40];     % [Hz]

%-------------------------------------------------------------
%CONSTANTS AND PARAMETERS CALCULATION

L730 = 0.730;               %[um]
L690 = 0.690;               %[um]

% --- Distances ---
n_r = [1:1:num_distances]';
d1 = 0.4;
d2 = 0.2;
```

```
r = [sqrt(0.4^2+(d2*n_r+1).^2) sqrt(d1^2+(d2*n_r+1).^2)];
                                                        %[cm]
%r = [sqrt(d1^2+(d2*n_r+1).^2) sqrt(0.6^2+(d2*n_r+1).^2)];

% --- Optical parameters ---
muaINK = 0.001;
Ca = 914.02;
Ea = -0.4366;
Cs1 = 0.58;
Cs2 = 0.1;
Cs3 = 0.32;
E2 = -2.4;

mua = [Ca*Ink/(Ink+Water+IL)*(L730*10^3)^E1+muaINK ...
    Ca*Ink/(Ink+Water+IL)*(L690*10^3)^E1+muaINK];
                                                        %[cm^-1]
mus_p = [IL/(Ink+Water+IL)*10^3*(Cs1*L730-Cs2)*Cs3*L730^E2 ...
    IL/(Ink+Water+IL)*10^3*(Cs1*L690-Cs2)*Cs3*L690^E2];
                                                        %[cm^-1]

D = 1./(3*(mua+mus_p));             %[cm]
mueff_calc = sqrt(mua./D)           %[cm^-1]

%-------------------------------------------------------------
% INITIALIZATION

Mfiles = num_distances;
S = zeros(num_samples, num_data*2,Mfiles);
Vmod = zeros(Mfiles,2);
Pmod = zeros(Mfiles,2);
Fluence = zeros(Mfiles,2);
mueff = zeros(Mfiles,2);

%-------------------------------------------------------------
% ESTIMATION

R730 = 2.435e-8;
R690 = 2.135e-8;

for n=1:Mfiles
    S(:,:,n) = importdata([path,file,num2str(n+1),'_1']);
```

```
    pos1 = find(S(:,1,n) == mod_freq(1));
    pos2 = find(S(:,1,n) == mod_freq(2));
    Vmod(n,1) = sum(S(pos1-3:pos1+3,8,n));    %[V]
    Vmod(n,2) = sum(S(pos2-3:pos2+3,8,n));    %[V]
    Pmod(n,1) = R730*Vmod(n,1);               %[W]
    Pmod(n,2) = R690*Vmod(n,2);               %[W]
    Fluence(n,1) = Pmod(n,1)/(4*pi*r(n,1).*D(1));
    Fluence(n,2) = Pmod(n,2)/(4*pi*r(n,2).*D(2));
end

p(:,1) = polyfit(r(:,1),-log(r(:,1).*Fluence(:,1)),1);
p(:,2) = polyfit(r(:,2),-log(r(:,2).*Fluence(:,2)),1);
mueff = p(1,:)

%-------------------------------------------------------------
```

Appendix D

Labview graphic code

The Labview graphic code used to drive the DAQ is illustrated in this appendix. Its functioning is explained in subsection 3.4.3.

The first loop in the upper part of the code is relative to the detection of the signals. The first DAQ records the signal coming from the detector while the second one records the signals used to modulate the lasers.

The second loop contains the command to generate the signals that drive the lasers. Some conversion factors are introduced to translate the modulation frequency into the actual value that the code needs to generate such a signal. These conversion parameters depend totally on the hardware used, including the speed of the computer itself, so it is likely that it must be changed if the hardware changes.

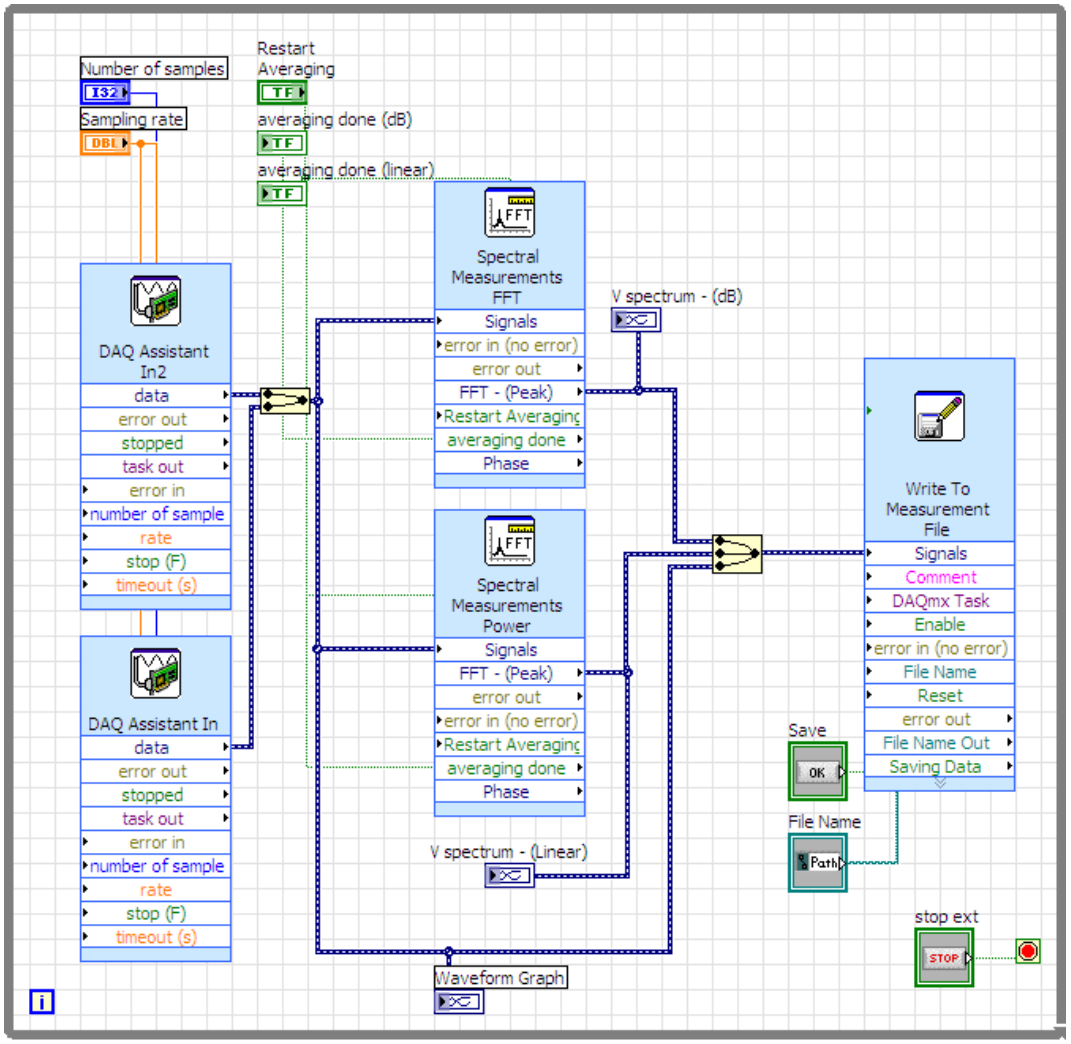
Number of samples
I32
Sampling rate
DBL
Restart Averaging
TF
averaging done (dB)
TF
averaging done (linear)
TF
DAQ Assistant In2
data
error out
stopped
task out
error in
number of sample
rate
stop (F)
timeout (s)
DAQ Assistant In
data
error out
stopped
task out
error in
number of sample
rate
stop (F)
timeout (s)
Spectral Measurements FFT
Signals
error in (no error)
error out
FFT - (Peak)
Restart Averaging
averaging done
Phase
Spectral Measurements Power
Signals
FFT - (Peak)
error out
error in (no error)
Restart Averaging
averaging done
Phase
V spectrum - (dB)
V spectrum - (Linear)
Waveform Graph
Write To Measurement File
Signals
Comment
DAQmx Task
Enable
error in (no error)
File Name
Reset
error out
File Name Out
Saving Data
Save
OK
File Name
Path
stop ext
STOP

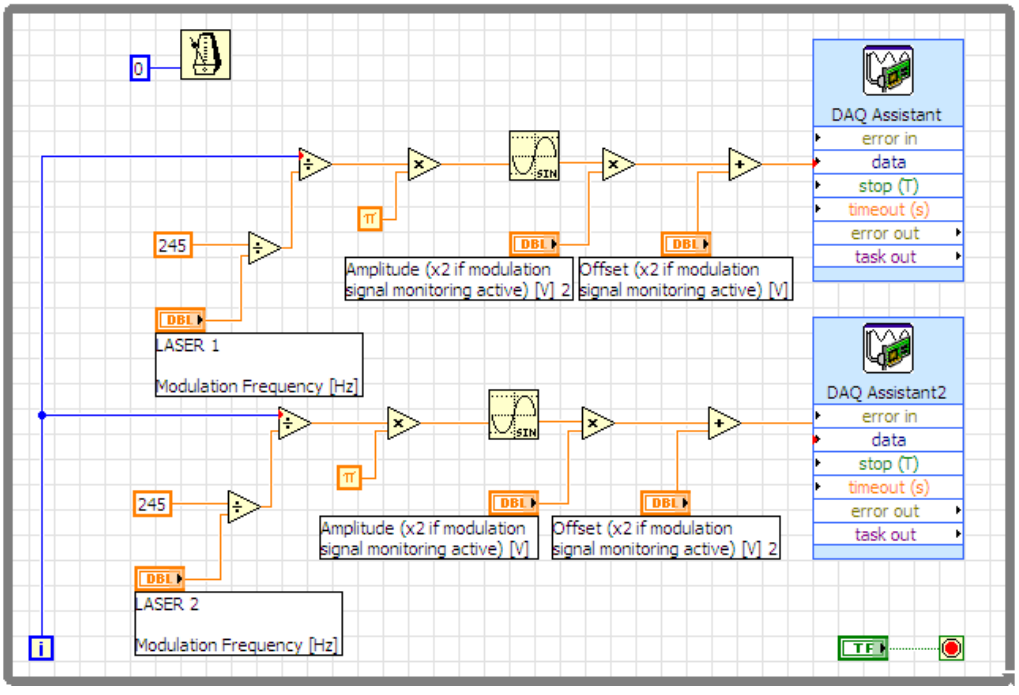
0
245
LASER 1
Modulation Frequency [Hz]
Amplitude (x2 if modulation signal monitoring active) [V] 2
Offset (x2 if modulation signal monitoring active) [V]
DAQ Assistant
error in
data
stop (T)
timeout (s)
error out
task out
245
LASER 2
Modulation Frequency [Hz]
Amplitude (x2 if modulation signal monitoring active) [V]
Offset (x2 if modulation signal monitoring active) [V] 2
DAQ Assistant2
error in
data
stop (T)
timeout (s)
error out
task out
TF

Bibliography

[1] S. Fantini, M. A. Franceschini, J. B. Fishkin, B. Barbieri, and E. Gratton. Quantitative determination of the absorption spectra of chromophores in strongly scattering media: a light-emitting-diode based technique. *Appl. Opt.*, 33(22), 1994.

[2] P. Thueler, I. Charvet, F. Bevilacqua, B. Barbieri, M. St. Ghislain, G. Ory, P. Marquet, P. Meda, B. Vermeulen, and C. Depeursinge. In vivo endoscopic tissue diagnostics based on spectroscopic absorption, scattering, and phase function properties. *J. Biom. Opt.*, 8:495–503, 2003.

[3] F. Bevilacqua, A. J. Berger, A. E. Cerussi, D. Jakubowski, and B. J. Tromberg. Broadband absorption spectroscopy in turbid media by combining frequency-domain and steady-state methods. *Appl. Opt.*, 98:6498–6507, 2000.

[4] J. B. Fishkin, O. Coquoz, E. R. Anderson, M. Brenner, and B. J. Tromberg. Frequency-domain photon migration measurements of normal and malignant tissue optical properties in a human subject. *Appl. Opt.*, 36(21):6498–6507, 1997.

[5] B. J. Tromberg, O. Couoz, J. B. Fishkin, T. Pham, E. R. Anderson, J. Butler, M. Cahn, J. D. Gross, V. Venugopalan, and D. Pham. Non-invasive measurements of breast tissue optical properties using frequency-domain photon migration. *Phil. Trans. R. Soc. Lond. B*, 352:661–668, 1997.

[6] B. C. Wilson and M. S. Patterson. The physics, biophysics and technology of photodynamic therapy. *Phys. Med. Biol.*, 53:R61–R109, 2008.

[7] V. V. Tuchin. *Tissue optics: light scattering methods and instruments for medical diagnosis*. SPIE Press, second edition, 2007.

[8] D. K. Chatterjee, L. S. Fong, and Y. Zhang. Nanoparticles in photodynamic therapy: An emerging paradigm. *Advanced Drug Delivery Reviews*, 60:1627–1637, 2008.

[9] S. J. Matcher and C. E. Cooper. Absolute quantification of deoxyhaemoglobin concentration in tissue near infrared spectroscopy. *Phys. Med. Biol.*, 39:1295–1312, 1994.

[10] R. Nossal, S. Havlin, G. H. Weiss, and R. F. Bonner. Model for photon migration in turbid biological media. *J. Opt. Soc. Am. A*, 4(3), 1987.

[11] C. M. Moore, D. Pendse, and M. Emberton. Photodynamic therapy for prostate cancer - a review of current status and future promise. *Nature clinical practice*, 6(1), 2009.

[12] S. Lin, L. Wang, S. L. Jacques, and F. K. Tittel. Frequency-domain photon migration measurements of normal and malignant tissue optical properties in a human subject. *Appl. Opt.*, 36(1), 1987.

[13] W. F. Cheong, S. A. Prahl, and A. J. Welch. A review of the optical properties of biological tissues. *IEEE J. Quantum Electron.*, 26:2166–218, 1990.

[14] M. Solonenko, R. Cheung, T. M. Busch, A. Kachur, G. M. Griffin, T. Vulcan, T. C. Zhu, H.W. Wang, S. M. Hahn, and A. G. Yodh. In vivo reflectance measurement of optical properties, blood oxygenation and motexafin lutetium uptake in canine large bowels, kidneys and prostates. *Phys. Med. Biol.*, 47:857–873, 2002.

[15] T. C. Zhu, A. Dimofte, J. C. Finlay, D. Stripp, T. Busch, J. Miles, R. Whittington, S. B. Malkowicz, Z. Tochner, E. Glatstein, and S. M. Hahn. Optical properties of human prostate at 732 nm measured during motexafin lutetium-mediated photodynamic therapy. *Photochem. Photobiol.*, 81(1):96–105, 2005.

[16] T. Franiel, L. Lüdemann, B. Rudolph, E. Lutterbeck, B. Hamm, and D. Beyersdorff. Differentiation of prostate cancer from normal prostate tissue: Role of hotspots in pharmacokinetic mri and histologic evaluation. *AJR*, 194(3):675–681, 2010.

[17] J. B. Fishkin, O. Coquoz, E. R. Anderson, M. Brenner, and B. J. Tromberg. Frequency-domain photon migration measurements of normal and malignant tissue optical properties in a human subject. *Appl. Opt.*, 36:10–20, 1997.

[18] R. M. P. Doornbos, R. Lang, M. C. Aalders, F. W. Cross, and H. J. C. M. Sterenborg. The determination of in vivo human tissue optical properties and absolute chromophore concentrations using spatially resolved steady-state diffuse reflectance spectroscopy. *Phys. Med. Biol.*, 44:967–981, 1999.

[19] T. Svensson, S. Andersson-Engels, M. Einarsdóttír, and K. Svanberg. In vivo characterization of human prostate tissue using near-infrared time-resolved spectroscopy. *J. Biom. Opt.*, 12(1), 2007.

[20] M. Monici. Cell and tissue autofluorescence research and diagnostic applications. *Biotechnol. Annu. Rev.*, 11:227–253, 2005.

[21] A. Johansson, F. W. Kreth, W. Stummer, and H. Stepp. Interstitial photodynamic therapy of brain tumors. *IEEE J. Quantum Electron.*, 1(227-253), 2010.

[22] V. V. Sobolev. *A Treatise on Radiative Transfer*. Van Nostrand-Reinhold, Princeton, 1963.

[23] E. D. Cashwell and C. J. Everett. *Monte Carlo Method for Random Walk Problems*. Pergamon, 1959.

[24] K. M. Case and P. F. Zweifel. *Linear Transport Theory*. Addison-Wesley, 1967.

[25] S. A. Prahl, M. Keijzer, S. L. Jacques, and A. J. Welch. A monte carlo model of light propagation in tissue. *SPIE Institute Series*, IS 5, 1989.

[26] S. L. Jacques, C. A. Alter, and S. A. Prahl. Angular dependence of hene laser light scattering by human dermis. *Lasers Life Sci.*, 1:309–333, 197.

[27] M. S. Patterson, B. Chance, and B. C. Wilson. Time resolved reflectance and transmittance for the non-invasive measurement of tissue optical properties. *Appl. Opt.*, 28(12), 1989.

[28] M. A. Franceschini, K. T. Moesta, S. Fantini, G. Gaida, E. Gratton, H. Jess, W. W. Mantulin, M. Seeber, P. M. Schlag, and M. Kaschke. Frequency-domain techniques enhance optical mammography: Initial clinical results. *Proc. Natl. Acad. Sci. USA*, 94:6468–6473, 1997.

[29] G. Yul, T. Durduran, C. Zhou, T. C. Zhu, J. C. Finlay, T. M. Busch, S. B. Malkowicz, S. M. Hahn, and A. G. Yodh. Real-time In situ monitoring of human prostate photodynamic therapy with diffuse light. *Photochem. Photobiol.*, 82:1279–1284, 2006.

[30] H. Heusmann, J. Kölzer, and G. Mitic. Characterization of female breasts in vivo by time-resolved and spectroscopic measurements in near-infrared spectroscopy. *J. Biom. Opt.*, 1(4):425–434, 1996.

[31] A. Dimofte, J. C. Finlay, and T. C. Zhu. A method for determination of the absorption and scattering properties interstitially in turbid media. *Phys. Med. Biol.*, 50:2291–2311, 2005.

[32] URL: http://www.medphys.ucl.ac.uk/research/borl/research/NIR_topics/spectra/spectra.htm.

[33] J. Swartling, G. Ahlgren, K. M. K. S. Nilsson, S. Svanberg, K. Svanberg, and S. Andersson-Engels. System for interstitial photodynamic therapy with online dosimetry: first clinical experiences of prostate cancer. *J. Biom. Opt.*, 15(5), 2010.

[34] J. Swartling. *Biomedical and atmospheric applications of optical spectroscopy in scattering media*. PhD thesis, Lund University, Faculty of Engineering, 2002.

[35] M.D. Daniell and J.S. Hill. A history of photodynamic therapy. *Aust N Z J Surg*, 61:340–348, 1991.

[36] S. G. Bown, A. Z. Rogowska, D. E. Whitelaw, W. R. Lees, L. B. Lovat, P. Ripley, L. Jones, P. Wyld, A. Gillams, and A. W. R. Hatfield. Photodynamic therapy for cancer of the pancreas. *Gut*, 50:549–557, 2002.

[37] S. K. Bisland, L. Lilge, A. Lin, R. Rusnov, and B. C. Wilson. Metronomic photodynamic therapy as a new paradigm for photodynamic therapy: rationale and preclinical evaluation of technical feasibility for treating malignant brain tumors. *Photochem. Photobiol*, 80:22–30, 2004.

[38] U. O. Nseyo, J. DeHaven, T. J. Dougherty, W. R. Potter, D. L. Merrill, S. L. Lundahl, and D. L. Lamm. Photodynamic therapy (PDT) in the treatment of patients with resistant superficial bladder cancer: a long-term experience. *J. Clin. Laser Med. Surg.*, 16:61–68, 1998.

[39] N. L. Oleinick and H. H. Evans. The photobiology of photodynamic therapy: cellular targets and mechanisms. *Radiation Research*, 150:S146–S156, 1998.

[40] N. Honda, K. Ishii, T. Terada, T. Nanjo, and K. Awazu. Determination of the tumor tissue optical properties during and after photodynamic therapy using inverse monte carlo method and double integrating sphere between 350 and 1000 nm. *J. Biom. Opt.*, 16(5), 2011.

[41] A. P. Castano, T. N. Demidova, and M. R. Hamblin. Mechanisms in photodynamic therapy: part three-photosensitizer pharmacokinetics, biodistribution, tumor localization and modes of tumor destruction. *Photodiagnosis Photodyn. Ther.*, 2(2):91–106, 2005.

[42] M. H.Gold. Acne vulgaris: lasers, light sources and photodynamic therapy - an update 2007. *Expert. Rev. Anti Infect. Ther.*, 5:1059–1069, 2007.

[43] H. I. Pass. Photodynamic therapy in oncology: Mechanisms and clinical use. *J. National Cancer Inst.*, 85(6), 1993.

[44] E. Angell-Petersen, S. Spetalen, S. J. Madsen, C. H. Sun, Q. Peng, S. W. Caper, M. Sioud, and H. Hirschberg. Influence of light fluence rate on the effects of photodynamic therapy in an orthotopic rat glioma model. *J. Neurosurg.*, 106:109–117, 2006.

[45] A. Johansson, F. W. Kreth, W. Stummer, and H. Stepp. Interstitial photodynamic therapy of brain tumors. *IEEE J. Quantum Electron.*, 16(4):841–853, 2010.

[46] P.C. Kousis, B. W. Henderson, P. G. Maier, and S.O. Gollnick. Photodynamic therapy enhancement of anti tumor immunity is regulated by neutrophilis. *Cancer Research*, 67, 2007.

[47] E. Buytaert, M. Dewaele, and P. Agostini. Molecular effectors of multiple cell death pathways initiated by photodynamic therapy. *Biochimica et Biophysica Acta*, 1776:86–107, 2007.

[48] Y. Luo and D. Kessel. Initiation of apoptosis versus necrosis by photodynamic therapy with chloroaluminum phthalocyanine. *Photochem. Photobiol.*, 66(4):479–483, 1997.

[49] C. Abels. Targeting of the vascular system of solid tumours by photodynamic therapy (PDT). *Photochem. Photobiol. Sci.*, 3:765–771, 2004.

[50] M. S. Patterson, B. Chance, and B. C. Wilson. Time resolved reflectance and transmittance for the noninvasive measurement of tissue optical properties. *Appl. Opt.*, 28(12), 1989.

[51] M. S. Thompson, A. Johansson, T. Johansson, S. Andersson-Engels, S. Svanberg, N. Bendsoe, and K. Svanberg. Clinical system for interstitial photodynamic therapy with combined on-line dosimetry measurements. *Appl. Opt.*, 44(19), 2005.

[52] T. H. Foster, D. F. Hartley, M. G. Nichols, and R. Hilf. Fluence rate effects in photodynamic therapy of multiceli tumor spheroids. *Cancer Research*, 53:1249–1254, 1993.

[53] M.S. Patterson, B.C. Wilson, and R. Graff. In vivo tests of the concept of photodynamic threshold dose in normal rat liver photosensitized by aluminum chlorosulphonated phthalocyanine. *Photochem. Photobiol.*, 51:343–349, 1990.

[54] X. Xu, R. K. Wang, J. B. Elder, and V. V. Tuchin. Effect of dextran-induced changes in refractive index and aggregation of optical properties of whole blood. *Phys. Med. Biol.*, 48:1205–1221, 2003.

[55] A. M. K. Nilsson, G. W. Lucassen, W. Verkruysse, S. Andersson-Engels, and M. J. C. van Gemert. Changes in optical properties of human whole blood in vitro due to slow heating. *Photochem. Photobiol.*, 65(2):366–373, 1997.

[56] A. Jemal, T. Murray, A. Samuels, A. Ghafoor, E. Ward, and M. J. Thun. Cancer statistics 2003. *CA Cancer J. Clin.*, 53:5–26, 2003.

[57] American Cancer Society. What is prostate cancer . URL: http://www.cancer.org/Cancer/ProstateCancer/DetailedGuide/prostate-cancer-what-is-prostate-cancer.

[58] A. Johansson. *Spectroscopic Techniques for Photodynamic Therapy Dosimetry*. PhD thesis, Lund University, Faculty of Engineering, 2007.

[59] Thorlabs. FEL0700 specifications sheet . URL: http://www.thorlabs.com/Thorcat/7600/7675-S01.pdf.

[60] Thorlabs. DET100A specifications sheet . URL: http://www.thorlabs.com/Thorcat/13000/13056-S01.pdf.

[61] Oregon Medical Laser Center. Monte Carlo simulations
. URL: http://omlc.ogi.edu/software/mc/.

[62] P. R. Bargo, S. A. Prahl, and S. L. Jacques. Collection efficiency of a single optical fibre in turbid media. *Appl. Opt.*, 42(16):3187–3197, 2003.

[63] RefractiveIndex.INFO
. URL: http://refractiveindex.info/?group=GLASSES&material=F_SILICA.

[64] National Instruments. NI USB-6009 specifications sheet
. URL: http://sine.ni.com/ds/app/doc/p/id/ds-218/lang/en.

[65] Thorlabs. FB730-10 transmission data
. URL: http://www.thorlabs.com/NewGroupPage9.cfm?ObjectGroup_ID=1000.

[66] T. Svensson. *Pharmaceutical and biomedical applications of spectroscopy in the photon migration regime*. PhD thesis, Lund University, Faculty of Engineering, 2008.